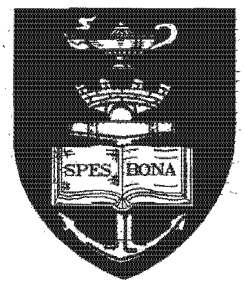

Geochemistry of Ferruginous Clogging of Karoo Wells

Sarah Jane Miller
B.Sc (Hons.) (Witwatersrand University)

Submitted in partial fulfillment of the requirements for the degree of

MASTER OF SCIENCE

in Environmental Geochemistry

Department of Geological Sciences
Faculty of Science
University of Cape Town

January, 2000

ABSTRACT

The main source of potable water in the Karoo is groundwater and thus any problems resulting from the abstraction of water or from difficulties in abstraction of the water are important. The iron clogging of screens, pumps and filter packs in supply wells is a world-wide problem and the consequences can be severe, leading to costly and harsh rehabilitation measures or even loss of the well. A study was undertaken in order to determine the chemistry and morphology of the precipitates found in relation to the water chemistry, in several wells in the Albertinia- Outshoorn-Calitzdorp area of South Africa.

A total of nine wells were sampled, one from Albertinia, one from Calitzdorp and the remaining seven wells were located in the Outshoorn area. One of the wells where no precipitation is evident was sampled for comparative purposes. Two water samples were taken at each of the sites: one was a 1 L unfiltered sample which was not preserved other than by refrigeration; the second sample was a 100 mL, filtered and preserved with 2 mL concentrated HCl per bottle, on site. Field measurements of electrical conductivity (EC), pH and temperature were made at the sampling site for all except one sample. Measurement of all the field parameters was repeated later in the laboratory. Dissolved oxygen was not measured due to failure of field equipment. In the laboratory a sample blank (sample 10) was made using one of the acid-washed bottles, by adding 2 mL of the conc. HCl used in the field to preserve the samples to distilled water from the laboratory. Where analytical methods allowed, the blank sample was analysed with the nine samples collected in the field.

There were 10 precipitate samples taken in total with more than one sample from selected wells. Samples of precipitate were collected at eight of the nine wells that were sampled for water. The samples were taken from either the clogged pipes or casings found on the surface or from the well itself (i.e. fresh) where possible. A sample was not obtained from well 9 as there was no precipitate available at the time of sampling however, the precipitate from well 9 had been previously sampled and this sample was used for the analyses. Fresh samples were stored in water from the well and dry precipitates were stored in airtight bottles.

The major and trace element chemistry of the water samples was determined. The mineralogy, morphology and chemistry of the precipitates were characterised.

The pH of the water samples ranged from 3.13 to 6.27 and the EC ranged from 230 to 2780 μS/cm for the samples where a precipitate is forming. The pH and EC of the sample that had no precipitate were 6.15 and 93 μS/cm respectively. The total Fe concentrations of the samples with detectable Fe ranged from 1.04 mg/L to 44.2 mg/L, with the Fe^{2+} species constituting at least 85 % of the iron species. The Fe concentration in sample 5 was below the detection limit of the colorimetric method but was determined by inductively coupled plasma atomic emission spectroscopy (ICP-AES) to contain 0.11 mg/L total iron. The low iron concentration could be the reason why a precipitate is not forming in this well. The iron speciation for this sample was not determined. The *pe* for the samples where iron was determined by colorimetry was calculated using the Fe^{2+}/Fe^{3+} redox couple. The *pe* ranged from 5.3 to 10.1 and the most acidic samples tended to have the highest *pe* values. The *pe*+pH values for all the samples were computed and the system appears to be poised at a *pe*+pH of 12.

The major ion chemistry of the samples reveals that Na^+ and Cl^- are the dominant ions in solution for all the samples with the exception of sample 8 which is dominated by Na^+ and SO_4^{2-}. The results of the ICP-MS semi-quantitative analysis shows that sample 5 has the lowest concentration of trace metals and that sample 8, in general, has the highest concentrations particularly Mn, B, Sr, Sn, Ba, W and Rb. The calculated saturation indices (SI) indicate that the waters (except 8) are supersaturated with respect to ferrihydrite and goethite. Some of the water samples are supersaturated with respect to a SO_4-phase namely jarosite. The SI indicate that ferrihydrite will form in preference to goethite in these samples and for goethite to form dissolution of the ferrihydrite would have to occur. Sample 8 is undersaturated with respect to ferrihydrite and supersaturated with respect to goethite and thus goethite is likely to form in preference to ferrihydrite for this water sample. Saturation indices for quartz indicate that all the waters are in equilibrium with this phase and are thus in equilibrium with the sandstones and quartzites that constitute the host rocks of the aquifer. The waters are not scaling as they are all undersaturated with respect to carbonate minerals (e.g. calcite). Most of the samples are suitable for domestic, irrigation and livestock use with minimal treatment required in those where Fe and trace metal concentrations exceed acceptable limits.

XRD analysis of the samples determined three groupings, 2 and 6-line ferrihydrite, goethite and group of samples with intermediate crystallinity. These groupings were confirmed with FT-IR. Samples 2B, 4, 7A, 7B, 7C and 9 are classed as ferrihydrites, the majority of which are well ordered (6-line) with samples 4 and 7C being poorly ordered (two-line). Samples 2A, 3 and 8 are identified as goethites. Samples 1A and 1B are a mixture of ferrihydrite and a smaller silicate component and sample 6 is a mixture of ferrihydrite with a trace amount of quartz. Sample 1A also contains a minor amount of lepidocrocite. The SEM images showed an acicular form for the goethites in general with sample 2A showing other morphological forms. The ferrihydrite samples had a spherical morphology with the two-line ferrihydrites displaying a less developed spherical nature. The examination of intermediate precipitates revealed a spherical morphology for these samples.

The precipitates are relatively pure with the Fe_2O_3 concentration ranging between 66 and 81 wt%. Samples 1A and 1B had lower Fe_2O_3 concentrations of 44 and 58 wt% respectively, which is due to dilution by the presence of a layer silicate phase. Samples 1A and 1B differ with respect to the rest of the samples in that they contain the largest concentrations of SiO_2, Al_2O_3 and K_2O out of all the precipitates. The XRD indicate that a layer silicate phase is present in these two samples which would account for the increased levels of SiO_2 and Al_2O_3. Samples 1A and 1B also have the highest concentrations of organic carbon.

Elevated SO_3 concentrations are noted in samples 2A and 8 in comparison to the other samples. These two samples had the highest concentrations of SO_4^{2-} in the water samples that may account for the higher concentrations of SO_3 in the precipitate. In general for all the samples, those with a high P_2O_5 tend to contain less SO_3. The samples with the low P_2O_5 tend to contain more SiO_2 that may be explained by the fact that silicate and phosphate compete for anionic sorption sites. The apparent sorption of silicate in preference to phosphate may be due to lower availability of PO_4^{3-} in these solutions.

The ferrihydrite samples contain more P_2O_5 than the more crystalline goethitic and intermediate precipitates. Samples 4 and 7C that have the highest P_2O_5 concentrations of all the samples and of the ferrihydrites. These two samples were identified as two-line ferrihydrite and are the most poorly crystalline samples of the ferrihydrites. The poorly crystalline ferrihydrites have greater surface areas than their crystalline counterparts and will

therefore have more sorption sites available for the sorption of PO_4^{3-}. This may explain the reason for the higher concentrations of P_2O_5 observed in the ferrihydrites in general.

Sample 8 has a low pH (3.13) and the iron oxide is expected to have a positive surface charge which anion adsorption. This sample has the highest concentrations of V, As, Se, Mo and U in the precipitate that is due to the precipitates greater anion sorption capacity in comparison with the other samples. The other samples tend to have higher concentrations of metals than sample 8 and are possibly removing these from solution.

Statistical correlation of the water and precipitate chemistry was undertaken and the results indicated no definitive correlations which may be used to predict the precipitate type that may form in the waters. The study of ferruginous clogging has however determined that ferrihydrite is the dominant phase followed by goethite and that most of the precipitates are poorly crystalline. The poor crystallinity of the samples suggests that mechanical methods of remediation as opposed to harsh chemical measures used currently might be fruitful. The study has also shown that the precipitates are scavenging small amounts of trace metals from the water and this may in fact be improving the quality of the water abstracted from the wells.

ACKNOWLEDGEMENTS

ESKOM and the *NRF* are acknowledged for funding that has made this course and my participation possible.

To *Prof. James Willis* and *Prof. Martin Fey*, my supervisors, thank you for your unbounded patience when answering my questions, your guidance in all matters, your humour especially in times of stress and the enthusiasm you show for geochemistry which has spurred my own interest in the subject. Thank you for a wonderful learning year.

I would like to thank *Jeff Jolly* of Groundwater Consulting Services for assisting with the inception of this project, his help in organising the field excursion and for his interest in the work being undertaken.

For helping with the acquisition of samples and for making the field excursion a memorable part of the thesis I wish to thank *Callie Calitz*, *Chris* and *Mariaan* of PumpCor, Riversdale. For their help in the acquisition of samples, thank you to *Deon Hasbrook* and *Johann Uys* of Overberg Water.

For their assistance with analyses, interest, humour and kindness throughout the year I wish to thank *Ernest Stout, Ivan Wilson, Neville Buchanan, Fran Pocock, Peter Abunda,* and *Leslie Petrik* in the Department of Geological Sciences.

Thank you to *Andreas Spath* for performing the ICP-MS analyses and *Patrick Sieas*, for performing the IC analyses and his help in the IC laboratory

Thank you to the *administration and technical staff* of the Department of Geological Sciences for all their assistance throughout the year.

To *Dane Gerneke* and *Mohammed Jaffer* of the Electron Microprobe Unit in the Department of Physics, thank you for your enthusiasm, time and for making the investigation of the morphology of iron precipitates an adventure that kept me coming back for more.

Thank you to *Meredith Timme* for your assistance with the making and analysing of samples by FT-IR.

To my classmates, *Steve McKeown*, *Gerry Papini*, *Anja Gassner*, *Mandla Mehlomakulu* and *Senzo Makhathini*, thank you for all the help, laughs, tears and friendship throughout this past year, it has been an experience I will never forget.

To *Marietta Echeverria* and *Richard O'Brien*, my fellow classmates, thank you especially, for your patience in the laboratory, your humour when I was losing mine, your assistance and company in the "wee" hours of the morning in the laboratory and computer room, and your good friendship this year.

To the past students who have helped us this year, thank you.

To my friends in Cape Town, especially *Alberto Tagliaro*, and in Johannesburg, thank you for not letting me take myself too seriously, for distracting me when I needed a break (before I did), for your friendship and support throughout the year, and for making this year a memorable one.

Thank you *Carole* for your help this year and for making me feel at home.

To *my family*, thank you for the support you give to all my endeavours, even when I am away from home, and thank you for confidence you have in my abilities.

TABLE OF CONTENTS

LIST OF FIGURES

LIST OF TABLES

INTRODUCTION

An important area for environmental geochemistry is the study of aquatic chemistry because the quality of water used for industrial and domestic purposes can impact on the infrastructure of industrial concerns and on water distribution systems. The impacts of poor water quality can result in increased costs due to remediation and maintenance expenses. Groundwater is a particularly important resource in South Africa that lies in a semi-arid region in which rainfall and waterbodies are unevenly distributed. With the need to augment the current supply of water with groundwater, comes the necessity to study the groundwater chemistry and the potential problems that may arise when the water is abstracted for use.

When a water well needs to be rehabilitated once or more within 15 years after it has been put into use, then well clogging is considered to be present (van Beek, 1984). The main causes of clogging are incrustation (usually iron) or biofouling of the screen and blockage of the gravel pack or aquifer around the well (Clark, 1988; Driscoll, 1986) (Figure 1). The well clogging is often characterised by a decrease in specific discharge and is indicated by an increase in drawdown (van Beek, 1984).

Figure 1 A clogged riser pipe showing the layering of precipitate inside the pipe

The problem of well clogging occurs worldwide even if the concentration of either oxygen or iron is extremely low in the extracted water (van Beek, 1984) and has been found to occur in wells supplying the Klein Karoo Rural Water Supply Scheme. This water supply scheme supplies the towns of Albertinia, Oudtshoorn and Calitzdorp and the clogging leads to an increase in the cost of maintenance of the wells. Private wells in the area also experience well clogging and this leads to increased maintenance costs for the farmers.

The main objective of this research was to determine the composition and morphology of precipitates and the composition of the water in each of the wells sampled. The second objective was to determine any relationships between the water and precipitate chemistry in order to obtain a greater understanding of the well clogging processes. A third objective was to ascertain if precipitation and precipitate type could be predicted. A fourth objective was to evaluate the water quality of the sampled wells. While this is not strictly part of the thesis it was done because the wells are part of the domestic water supply.

The research objectives were addressed by firstly undertaking a literature review of well clogging in both a global and local context. The local literature mainly takes the form of unpublished reports by groundwater consultants. Secondly, sampling of selected precipitates and water from the wells where precipitation is occurring was undertaken. These samples were analysed to obtain trace and major element compositions, and morphology and mineralogy of the precipitates. Thirdly, an attempt was made to correlate the water and precipitate chemistry in order to determine if precipitate type could be predicted. Water composition was then compared to South African water quality guidelines to assess the waters suitability for use.

CHAPTER 1 IRON OXIDE PRECIPITATION IN WELLS – A REVIEW

1.1 Introduction

Water wells deteriorate through years of use and require periodic maintenance (Clark, 1988). The main causes of the deterioration are encrustation or biofouling of the screen and blockage of the gravel pack or aquifer around the well (Clark, 1988; Driscoll, 1986), where reduced well performance with a gradual decrease in specific discharge is indicative of the deterioration (Clark, 1988). The cause of the encrustation is the change in the physical and chemical conditions in the groundwater between the body of the aquifer and the well that upsets the equilibrium (Clark, 1988; Driscoll, 1986).

Common encrusting materials are carbonates and ferric hydroxide, but the encrustation is often composed of several minerals, *e.g.* ferric hydroxide that often contains some manganese and carbonates (Clark, 1998; Driscoll, 1986). The encrustation and cementation by iron minerals can trap fine materials moving out of the aquifer and into the well during pumping. The entrapment of fines can exacerbate the clogging problem (Clark, 1988). Encrustation of a portion of the well screen can cause higher velocities through the non-incrusted portion of the screen (Driscoll, 1986; van Beek, 1984), which can cause sand grains, moved by the higher velocities, to erode and enlarge openings. The enlargement of the openings can lead to the ingress of sand into the well which can lead to increased pumping of sand (Driscoll, 1986).

Iron and manganese minerals exist in soils as insoluble forms of ferric oxide and manganese dioxide and the concentrations of these elements in groundwater are influenced by (Kothari, 1988): physical and chemical composition of the surrounding soils and rocks; hydrological conditions of the area; presence of microorganisms.

The chemical composition of the soil and rock and the influence of microbial activities on redox conditions, specifically reducing conditions, are the most important factors which determine the presence of iron and manganese in groundwater (Kothari, 1988). Iron exists in two oxidation states, namely Fe^{2+} (ferrous) and Fe^{3+} (ferric), while manganese exists as Mn^{2+}, Mn^{3+} or Mn^{4+}. Fe^{3+} and Mn^{4+} are less soluble in oxygenated water but in the absence of oxygen the reduced forms, Fe^{2+} and Mn^{2+}, are more soluble (Kothari, 1988). Water percolating through soil, which contains organic matter and aerobic organisms, becomes

depleted in oxygen and as Fe and Mn remain soluble under the reducing conditions they are transported to the groundwater. Thus groundwater usually contains higher concentrations of Fe and Mn than surface water (Kothari, 1988). When the groundwater is exposed to oxygen the soluble compounds of Fe and Mn form precipitates (Kothari, 1988). The solubility of iron is increased by chelation with organic matter (Carlson *et al.*, 1980). For the study area it has been shown that the precipitates are composed of iron oxides, and the focus of the literature review is to examine the chemical and physical factors that affect the precipitation of iron.

1.2 Redox reactions

Eh and pH are the master variables that control the speciation of multivalent elements (Patterson and Runnells, 1992). Microbes utilise oxygen as an electron acceptor during aerobic respiration, which involves the oxidation of organic matter. When the supply of oxygen is depleted other electron acceptors are used, *i.e.* Mn^{4+}, Fe^{3+}, NO_3^-, SO_4^{2-}, and CO_2. Microbial metabolism is highly redox sensitive with the functioning of microbes restricted to the Eh-pH range of the respiratory reaction they utilise (Patterson and Runnells, 1992). Figure 1.1 shows the Eh-pH diagram for the Fe-O-OH system. The reactions from which the diagram is derived are listed in Stumm and Morgan (1981).

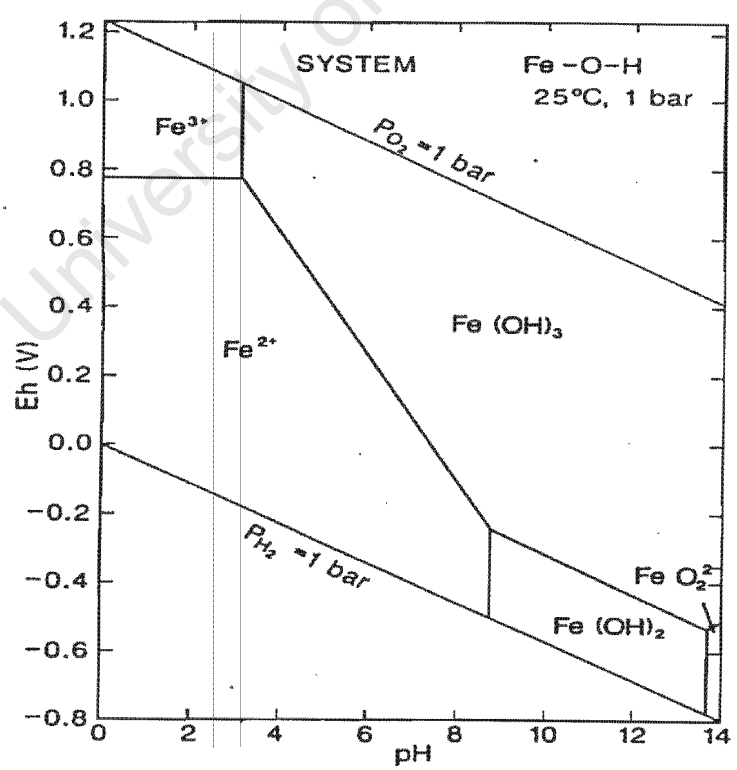

Figure 1.1. The Eh-pH stability diagram for the Fe-O-OH systems at 1 atm. and 25^0 C (Brookins, 1988).

The reduction of ferric oxyhydroxides is an important process in groundwater systems where these oxyhydroxides are present. Redox levels in groundwater are determined by the relative rates of introduction of oxygen by circulation and the consumption of oxygen by bacterially mediated decomposition of organic matter. The most important variables according to Drever (1997) are: oxygen content of the recharge water; distribution and reactivity of organic matter and other potential reductants in the aquifer; distribution of potential redox buffers in the aquifer; circulation rate of the groundwater.

Most groundwaters are close to the boundary between the Eh-pH fields of soluble (Fe^{2+}) and insoluble iron ($Fe(OH)_3$) (Clark, 1988) (Figure 1.1). The level of dissolved iron in groundwater is usually low (below 1 mg/*l* total iron) but can be increased considerably by slight changes in the water chemistry. An increase in acidity, caused by the dissolution of carbon dioxide (CO_2) or humic acids can increase the iron content of the groundwater. If there is de-oxygenation of the water due to decomposition of organic matter, a low pH can be accompanied by a negative Eh (redox potential) and the water could contain more iron in solution, especially if the water is percolating through ferruginous rocks or sediments (Clark, 1988).

The cause of the deposits found in water wells is a combination of the presence of oxygen from the atmosphere and soluble Fe from the groundwater, which react to form insoluble ferric oxyhydroxides in the well screen. Iron and oxygen concentrations are usually low in groundwater but through the action of pumping these reactants are transported to the screen (Ralph and Stevenson, 1995). Intermittent operation of the pump creates a temporary draw down effect close to the screen and atmospheric oxygen enters the area due to the reduced pressure (Ralph and Stevenson, 1995). Over-pumping of the well can also lead to the drop of the water level below the fracture system, which causes cascading of water within the well down the screens. The increased turbulence further aerates the water increasing the possibility of precipitation of ferric oxyhydroxides.

In the unconfined aquifer zone, the groundwater will be oxygenated by the solution of atmospheric oxygen during recharge and will have a positive Eh. The water will lie in the stability field of ferric hydroxide and the dissolved iron level will be low due to the insolubility of ferric hydroxide (Clark, 1988). In the confined aquifer, the oxygenation is low

and the water moves into the stability field of soluble ferrous iron. Wells are localised points where there is access of oxygen to the confined aquifers. The increase in Eh and pH, due to the exsolution of CO_2 can move the groundwater into the stability field of ferric hydroxide at the oxygen-water interface. The interface is at the screen and the formation of precipitate occurs immediately outside the screen. The chemical precipitation of ferric hydroxide is usually accompanied by biologically mediated precipitation (Clark, 1988).

The solid ferric hydroxide, resulting from the oxidation of soluble ferrous iron followed by precipitation, is precipitated as granules in iron bacterial sheaths. The filamentous colonies of bacteria and the ferruginous by-products can severely clog the screen of a well. The iron bacteria are widespread in iron-rich groundwaters and can tolerate a range of oxygen levels, but are most abundant where oxygen is freely available (Clark, 1988).

When Fe^{2+} in water wells is exposed to oxygenated conditions it is readily oxidised by molecular oxygen (Stumm and Morgan, 1981):

$$4Fe^{2+} + O_2 + 4H^+ \rightarrow 4Fe^{3+} + 2H_2O$$

The hydrolysis of the ferric iron forms poorly crystalline iron oxides that have low solubilities ($K_{sp} \approx 10^{-40}$):

$$5Fe^{3+} + 12H_2O \rightarrow Fe_5HO_8 \cdot 4H_2O + 15H^+$$

The Eh range in which the oxidation of iron occurs is from 0 to 400 mV and at a pH around 7.0. The Eh range within which bacterial iron oxidation takes place, decreases at higher pH values (Taylor *et al.*, 1997). The redox potential for Fe-compounds is greater than that for Mn-compounds. Mn occurs as hydrated Mn^{2+} and Fe is chelated to organic ligands in the aquatic environment (Carlson *et al.*, 1980).

The hydrolysis of Fe^{3+} proceeds through an intermediate Fe^{3+} hexaquo-cation $(Fe(OH_2)_6)^{3+}$ which undergoes deprotonation (Schwertmann and Taylor, 1989):

$$(Fe(OH_2)_6)^{3+} \rightarrow FeOOH + 3H_3O^+ + 3H_2O$$

The full hydrolysis leads to the formation of iron oxides and can be inhibited by low pH and/or the presence of ligands that replace the H_2O ligands of the aquo-cation (Schwertmann and Taylor, 1989).

1.3 Factors influencing precipitation

1.3.1 Water chemistry and well characteristics

Water quality and the surface characteristics of the screen determine the occurrence of encrustation and the rate at which encrustation occurs (Driscoll, 1986). The kind and amount of dissolved minerals and gases influences the tendency for mineral matter to be deposited and the rougher the surfaces of the well screen material the faster the rate of encrustation. With only a small portion of the total amount of dissolved minerals being deposited, severe clogging can occur (Driscoll, 1986). During pumping there are velocity-induced pressure changes which also disturb the chemical equilibrium of the groundwater and cause deposition of insoluble iron (Driscoll, 1986):

$$Fe(HCO_3)_2 \rightarrow Fe(OH)_2\downarrow + 2CO_2\uparrow$$

The solubility of ferrous hydroxide is less than 20 mg/*l* for this reaction. If there is aeration during pumping, additional ferric hydroxide precipitation occurs (Driscoll, 1986):

$$4Fe(OH)_2 + 2H_2O + O_2 \rightarrow 4Fe(OH)_3\downarrow$$

Oxidation of the iron hydroxides or an increase in pH leads to the formation of hydrated iron oxides. Thus ferric oxide is produced from the reaction of ferrous iron with oxygen (Driscoll, 1986):

$$2Fe^{2+} + 4HCO_3^- + H_2O + \tfrac{1}{2}O_2 \rightarrow Fe_2O_3 + 4CO_2 + 3H_2O$$

In an unconfined aquifer air can enter the void spaces in the cone of depression during pumping, and oxidise the iron in the films of water adhering to the voids (Driscoll, 1986; Ralph and Stevenson, 1995). If pumping is stopped and started intermittently, a coating of iron oxide can build up and gradually reduce the void space of the aquifer which in turn

reduces the storage capacity of the aquifer near the well (Driscoll, 1986).

1.3.2 Iron bacteria

Iron bacteria occur in wells open to the atmosphere when there is sufficient iron or manganese and soluble organic material, bicarbonate or carbon dioxide present in the groundwater (Driscoll, 1986). The bacteria assist in the transfer of electrons between oxygen and Fe^{2+} (Ralph and Stevenson, 1995). The iron bacteria enzymatically catalyse the oxidation of iron (and manganese) promoting the growth of thread-like slime from the energy produced (Driscoll, 1986; Tuhela *et al.*, 1992). The energy used is obtained by oxidising ferrous to ferric ions which is precipitated on or in the mucilaginous sheaths of the bacteria as hydrated ferric hydroxide. The precipitation of iron and the voluminous material of the bacterial growth leads to clogging of the wells (Driscoll, 1986).

According to Driscoll (1986), there are other forms of bacteria that cause the precipitation of iron through non-enzymatic means: increasing the pH of the water by the release of metabolic ammonia (alkaline), or by the removal of CO_2 from the water during photosynthesis; changing the redox potential through the release of oxygen; release of chelated iron by breaking the bond between iron and oxalate, citrate, humic acids or tannins.

Other bacteria reduce iron to a ferrous state under anaerobic conditions (Driscoll, 1986). Due to the presence of aerobic and anaerobic zones in the layers of iron encrustation, a wide variety of bacteria can be found (Tuhela *et al.*, 1992; Ralph and Stevenson, 1995). Iron bacteria such as *Gallionella* and *Leptothrix* are involved in the oxidation of iron (van Beek, 1984). During pumping the flow of suspended and soluble material to the well increases the nutrient supply to the micro-organisms making rapid growth of the bacteria and increased iron oxidation possible (van Beek, 1984).

Bacteria have excellent adhesion properties which enable them to live in the high flow velocity environment of the well (van Beek, 1984). Recent work on *Gallionella* has shown that it occurs as a free-swimming, flagellated cell and produces a stalk when exposed to ferrous iron (Tuhela *et al.*, 1993). *Thiobacillus ferrooxidans* and *Leptospirillum ferrooxidans* are limited to acid environments and their role in the oxidation of Fe^{2+} in groundwater wells is thus negligible due to the adverse pH conditions (Tuhela *et al.*, 1993). The influence of the iron bacteria on the oxidation of Fe^{2+} is unclear because as the pH increases the rate of purely

chemical Fe^{2+} oxidation increases 100-fold per unit rise in pH (Schwertmann and Taylor, 1989). The role of bacteria in iron precipitation is indirect in that they change iron speciation and saturation conditions by degrading the soluble organic-iron complex (Tuhela *et al.*, 1993). Very little energy is produced by the oxidation of iron resulting in a large amount of Fe^{2+} being converted to Fe^{3+} in order to sustain bacterial growth (Taylor *et al.*, 1997).

1.3.3 Reaction kinetics

Studies conducted by Tuhela *et al.* (1992) have shown that liquid media inoculated with samples from wells precipitated iron within 2 to 7 days of incubation. According to Driscoll (1986) and Ralph & Stevenson (1995), the growth rates of the bacteria can be extremely high such that a well screen is clogged rapidly, reducing the operational flow of wells below specifications within months of installation.

The rate of oxidation of Fe^{2+}, which is thermodynamically unstable at neutral pH in the presence of oxygen, depends on the temperature, pH, partial pressure of oxygen and the major anion present (Ralph and Stevenson, 1995). The rate of the purely chemical reaction between Fe^{2+} and O_2 is slow in water but is accelerated by iron bacteria which can result in a ten to hundred times increase in the rate of iron oxidation (Bao-rui, 1988). The rate of oxidation of Fe^{2+} in solutions increases a 100 fold for a unit increase in pH however the rate of oxidation of Fe^{2+} is very slow below pH 6. For a given pH, the rate of the oxidation reaction increases about 10 fold for a 15 ^{0}C increase in temperature (Stumm and Morgan, 1981). Abiotically the rate of reaction is too slow to explain the rapid clogging of wells that is often observed (Ralph and Stevenson, 1995; Schwertmann and Taylor, 1989). Ralph and Stevenson (1995) found that as the partial pressure of oxygen is reduced the biotic oxidation of iron in groundwater is significant in the deposition of iron oxides. Oxidation of iron may be biologically induced and rate of the reaction may be biologically controlled but the mineralogical fate of iron is controlled by geochemical parameters *e.g.* pH, $[SO_4]$ and $[HCO_3]$ whether the oxidation was by biotic or abiotic mechanisms (Bigham, 1994).

The physical and chemical factors which affect the removal of iron from groundwater are (Kothari, 1988): higher water temperature, increasing the rate of the oxidation reaction; detention time following oxidation, determines the completeness of the reaction; oxidation rates are slower at low pH values; oxidation will be faster with increasing dissolved oxygen concentration; the presence of chlorides, nitrates and phosphates alters the solubility of iron

and oxidation is accelerated by cations.

1.4 Properties of precipitates

1.4.1 Mineralogy

The phase of iron oxide that will precipitate from solution, and the stability of the phase, is dependant on the iron concentration in solution (Fe^{2+} and Fe^{3+}), pH, redox potential, concentration of complexing ligands (CO_3^{2-}, SO_4^{2-}, S^{2-}, etc.), partial pressure of CO_2 and O_2 in the solution, and the H_2O activity (Schwertmann and Taylor, 1989).

Ferrihydrite ($Fe(OH)_3$) is a poorly crystalline hydrous ferric oxide and is equivalent to amorphous $Fe(OH)_3$ in the older literature (Drever, 1997). From their studies, Tuhela *et al.* (1992) and Carlson *et al.* (1980) found that ferrihydrite is the dominant iron precipitate and that other ferric oxides or oxyhydroxides were not detected. Ferrihydrite is favoured over other iron oxide minerals if silicate, phosphate or organic matter are present (Tuhela *et al.*, 1992). Goethite is preferentially formed at a low rate of iron supply from either Fe^{2+} or Fe^{3+} ions in solution (Tuhela *et al.*, 1992). Goethite is the stable and widespread oxyhydroxide of iron and metastable iron oxides will convert via solution to goethite (Tuhela *et al.*, 1992). Ferrihydrite often occurs with goethite due to their simultaneous crystallisation or the transformation of ferrihydrite to goethite via solution (Carlson *et al.*, 1980). The transformation of ferrihydrite to goethite is inhibited by soil organic matter but proceeds once the ligands are oxidised (Carlson *et al.*, 1980). Organic matter may also inhibit the crystallisation of ferrihydrite (Carlson *et al.*, 1980) and this could be an important factor in the water well environment due to the presence of DOM (dissolved organic matter).

In a study by Vuorinen *et al.* (1988) ferrihydrite was formed instead of lepidocrocite due to a Si concentration greater than 4 mg/l in the groundwater. Iron oxides sorbed Ca^{2+}, Mg^{2+}, K^+ and Na^+ at pH values above 7 and sorbed Cu at low pH levels, while MnO_2 sorbed and scavenged heavy metals *i.e.* Ag, Sn, Ni, Co, Zn and Cu (Vuorinen *et al.*, 1988). Si inhibits the crystallisation of lepidocrocite and goethite in favour of ferrihydrite (Carlson and Schwertmann, 1987).

In a study in Finnish groundwater Carlson and Schwertmann (1987) found that there was Si bound to the Fe-OH functional groups at the oxide surface leading to Fe-O-Si bonds. The Si is

bound to the poorly ordered ferrihydrite. The effect of the Si bond to the Fe-OH functional groups is to lower the point of zero charge (pzc) by turning the Fe-OH proton accepting sites into Fe-O-Si-OH proton donating sites. The drop in pzc affects the flocculation behaviour of the precipitated iron oxides (Carlson and Schwertmann, 1987).

1.4.2 Morphology

The iron oxyhydroxides commonly found in groundwater wells are ferrihydrite and goethite and less commonly lepidocrocite. In previous work done on the precipitates in the study area ferrihydrite and goethite were identified as the dominant phases and thus the discussion will be limited to the three iron oxyhydroxides.

Ferric oxide is reddish brown, similar in colour to rust, while hydrated ferrous oxide is a black sludge (Driscoll, 1986; Ralph and Stevenson, 1995). The early chemical and biological precipitates of iron in groundwater wells are soft and powdery. As the deposits age with time they become more crystalline. The precipitates are then reddish-brown, hard and a mixture of ferric oxides and hydroxides which can cement a gravel pack till it is like concrete (Clark, 1988). The encrustation forms a hard, brittle deposit similar to the scale found in water pipes, but under different conditions can be a soft sludge or gelatinous material (Driscoll, 1986). The ochreous precipitates formed in water wells are amorphous and vary in their crystallinity but are usually poorly crystalline (Tuhela *et al.*, 1992). The crystallinity of the iron oxides influences the aggregation of the iron oxides and their ability to scavenge metal ions from the surrounding waters (Tuhela *et al.*, 1992).

Tuhela *et al.* (1992) found that poorly ordered ferrihydrites form aggregates more easily than the more ordered forms and have a smaller specific surface area. Tuhela *et al.* (1992) also concluded from their studies that ferrihydrite is more effective in adsorbing cations and anions than the more crystalline iron oxides. The variance in the ability of different iron oxides to adsorb ions from solution has relevance in the scavenging and retention of nutrient and toxic-metal ions, and in the estimation of mass balance and flux of major and minor elements to and from the water (Tuhela *et al.*, 1992).

The basic structural unit of the iron oxides is an octahedron where the iron atom is surrounded by 6 O ions (oxides or α-phases) or 3 O and 3 OH ions (oxyhydroxides or γ-phases) (Schwertmann and Fitzpatrick, 1992). The O and OH ions form either hexagonally close

packed (hcp) or cubic close packed (ccp) layers. The Fe^{3+} is in an octahedral position and by isomorphous substitution the site can be occupied by other trivalent ions such as Al^{3+}, Mn^{3+}, Cr^{3+} and Ni, Co, Cu, Zn and Ti without altering the structure (Schwertmann and Fitzpatrick, 1992). The various iron oxides have different arrangements of the basic $Fe(O,OH)_6$ octahedra (Figure 1.2).

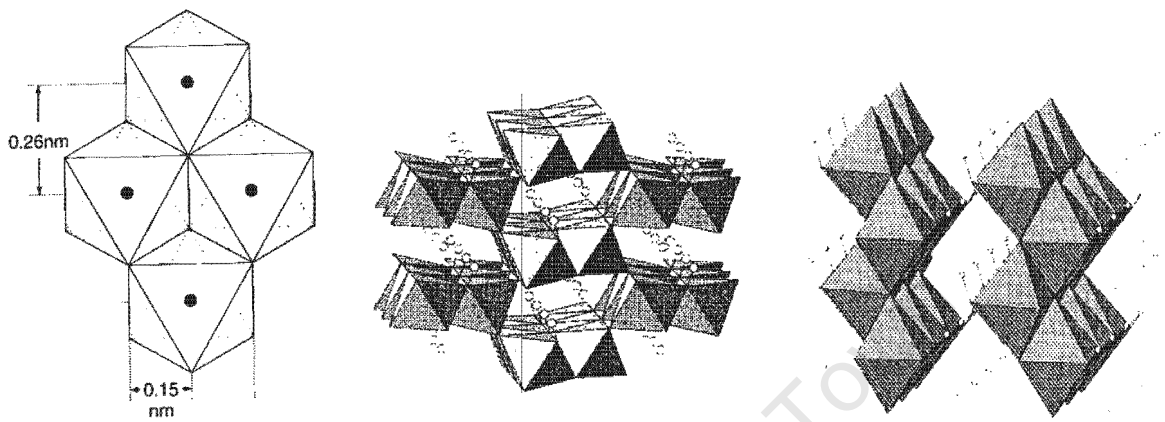

Ferrihydrite *Goethite* *Lepidocrocite*

Figure 1.2. Structure of iron oxide minerals (Cornell and Schwertmann, 1996).

1.4.2.1 Ferrihydrite ($Fe_5HO_8 \cdot 4H_2O$)

Ferrihydrite is often associated with goethite (α-FeOOH) and lepidocrocite (γ-FeOOH) but not with hematite (α-Fe_2O_3). The crystals are poorly ordered and about 2-5 ηm in size and the large surface area makes this iron phase highly reactive (Schwertmann and Fitzpatrick, 1992). Ferrihydrite is rusty, reddish-brown in colour (Bigham, 1994). Phosphate, arsenate, silicate, organics and heavy metals are often adsorbed on the surface of the ferrihydrite particles. Ferrihydrite is the least stable of the Fe^{3+} oxides with a solubility product of 10^{-38} to 10^{-39}. The rapid oxidation and hydrolysis of Fe^{2+} forms ferrihydrite. Higher oxidation rates and/or higher concentrations of nuclei and/or crystallisation inhibitors favour the precipitation of ferrihydrite over goethite or lepidocrocite (Schwertmann and Fitzpatrick, 1992). Humic compounds, silicate, phosphate and Mn-oxides stabilise ferrihydrite (Schwertmann and Fitzpatrick, 1992).

The transformation of ferrihydrite to goethite involves dissolution and recrystallisation during which Al or other elements can be incorporated into the goethite structure. The rate of the transformation is slow which explains the common association of ferrihydrite and goethite in nature (Schwertmann and Fitzpatrick, 1992). Ferrihydrite is similar in structure to hematite,

which consists of hcp O layers stacked perpendicularly to the z crystallographic axis with Fe^{3+} occupying two-thirds of the octahedral interstices and has no H bonds. The difference between ferrihydrite and hematite is that some of the Fe positions are vacant in ferrihydrite and H_2O molecules replace some O (and OH) (Schwertmann and Taylor, 1989).

1.4.2.2 Goethite (α-FeOOH)

Goethite is yellow-brown in colour and is the most stable of the Fe^{3+} oxides. It is the most common iron oxide in the surface environment in soils and sediments either as the only iron oxide or associated with one of the other forms (Schwertmann and Fitzpatrick, 1992). Goethite has a solubility product of 10^{-42} to 10^{-44}. Goethite is precipitated in favour of other iron oxides when organic compounds capable of complexing Fe, thus keeping the Fe^{3+} activity in solution low, are present (Schwertmann and Fitzpatrick, 1992). The substitution of Al for Fe in goethite has not been found in biotically produced goethite (Schwertmann and Fitzpatrick, 1992). Goethite is hexagonally close packed and consists of double chains of Fe-O-OH octahedra extended along the z crystallographic axis which are bound to neighbouring chains by Fe-O-Fe and H bonds (Schwertmann and Taylor, 1989). The specific area of goethite is higher than the less ordered iron oxides due possibly to the lesser aggregation of better ordered iron oxides (Carlson and Schwertmann, 1987).

1.4.2.3 Lepidocrocite (γ-FeOOH)

Lepidocrocite occurs less frequently than goethite, of which it is a polymorph, and is bright orange in colour (Schwertmann and Fitzpatrick, 1992). Lepidocrocite is often associated with goethite and ferrihydrite and is seldom associated with hematite. The occurrence of lepidocrocite indicates oxygen deficiency in some part of the system. It is metastable with respect to goethite and forms under conditions that kinetically favour its formation. Si inhibits the transformation of lepidocrocite to goethite in solution and high carbonate concentrations, which are pH and P_{CO2} dependent, suppress lepidocrocite formation and favour goethite formation. The suppression by carbonate is important when the precipitation of the iron oxide is biologically mediated (Schwertmann and Fitzpatrick, 1992). Lepidocrocite is cubic close packed and has the $FeO_3(OH)_3$ octahedra arranged in zigzag layers bound by H bonds which are slightly longer than the H bonds in goethite (Schwertmann and Taylor, 1989).

1.4.3 Adsorption of trace metals

In soils, in medium to alkaline pH and oxidising environments, amorphous or crystalline Fe solids are strong adsorbents or co-precipitating matrices (Bourg, 1995). In slightly reducing or

slightly oxidising environments, with a medium to acidic pH range, the iron oxyhydroxides are solubilised as Fe^{3+} is reduced. In a more alkaline environment this could result in the precipitation of carbonates which are less adsorbent than the oxides and hydroxides (Bourg, 1995). Iron oxides are known to act as sorbents for minor and major trace elements (Carlson *et al.*, 1980; Gann and Lopez, 1992).

Heavy metals are adsorbed by goethite in the order Cu>Pb>Zn>Cd>Co>Ni>Mn. The pH determines the extent of the adsorption, *i.e.* as the pH increases there is an increase in the amount of adsorption (Figure 1.3). Hydrolysed species are preferentially adsorbed over unhydrolysed species and thus as the pH increases the hydroxo-species, MOH^+, will be increasingly adsorbed over the M^+ species (Schwertmann and Taylor, 1989). Ion pairs can effect the adsorption rates as the MCl^+ species may be preferentially adsorbed over the M^{2+} species. Time also affects adsorption because time allows the diffusion of the metal into the micropores of the crystal.

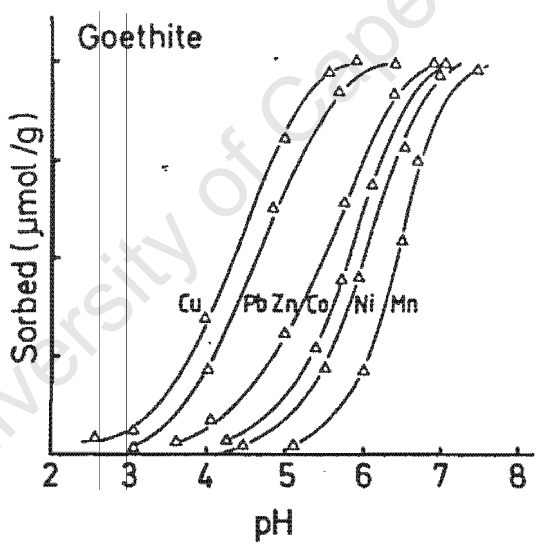

Figure 1.3. The effect of pH on the adsorption of heavy metals (Schwertmann and Taylor, 1989).

The specific adsorption of silicate, molybdate, arsenate, selenate, sulphate and organic anions compete with phosphate for available adsorption sites. Adsorption of a specific anion is controlled by pH as shown in Figure 1.4, where the adsorption of phosphate and selenite decrease with increasing pH and silicate and fluoride adsorption increase with pH and then decrease.

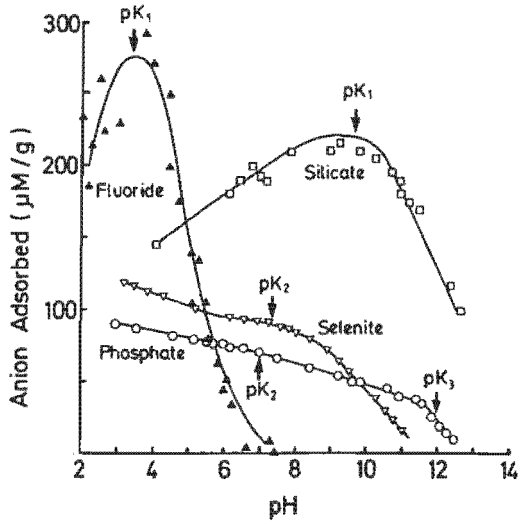

Figure 1.4. The effect of pH on the adsorption of some anions by goethite (Schwertmann and Taylor, 1989).

1.5 Consequences of precipitation

Biofouling due to the precipitation of iron oxide poses several problems in terms of water quality and performance to users of water supply and pumping wells (Tuhela *et al.*, 1993).

1.5.1 Screen blockage

The clogging of filter materials, screens, pumps and pipes can be extensive and is caused by the aggregation of iron oxides. The clogging can lead to corrosive conditions on metal structures immersed in contact with the water (Tuhela *et al.*, 1993; Tuhela *et al.*, 1992 and Carlson *et al.*, 1980) which can ultimately lead to failure of the well.

1.5.2 Pipes, sprinklers and drains

Iron precipitates can be deposited in the distribution system clogging the pipes (Kothari, 1988) and in drains draining fields with iron-rich water (Kuntze, 1982). Iron clogging and siltation often coincide which increase the difficulty of removal as the iron oxide cements the mineral grains which becomes harder with age and dehydration (Kuntze, 1982).

Clogging of nozzles and filters of drip-irrigation systems can occur with Fe^{2+} concentrations as low as 0.4 to 0.8 mg/*l* in a pH in the range of 4.0 to 7.2 (Kuntze, 1982). Clogging in pipes has been observed with Fe^{2+} concentrations as low as 0.2 to 0.3 mg/*l* and turbulent flow causes greater clogging hazards in pipes than slow flowing water (Kuntze, 1982).

1.5.3 Water quality

Iron can create serious aesthetic problems in drinking water supplies when the concentration exceeds 0.3 mg/*l* (Kothari, 1988), for example: the precipitation of iron gives a reddish or brown-black colour to water when exposed to air and this precipitate can stain household utensils, porcelain plumbing fixtures and clothes; the water can have a bitter metallic taste; softener efficiency can be reduced by becoming clogged with the iron precipitates; organisms using the iron as a food supply can die and slough off the pipes resulting in unpleasant odours and tastes (Kothari, 1988; Carlson *et al.*, 1980).

1.6 Conclusions

The dominant phases of iron oxides that are found to precipitate in groundwater wells are ferrihydrite and goethite. Lepidocrocite can occur in some wells where the Si concentration is not too high. The precipitation of the iron oxides is mainly abiotic and can be catalysed by iron bacteria such as *Gallionella* and *Leptothrix*, at neutral pH values. With increasing pH the role of the bacteria is diminished and chemical precipitation dominates.

The precipitates scavenge metals from the water and these metals are either adsorbed or incorporated into the structure of the iron oxide phase by isomorphous substitution for Fe. The presence of phosphates, silicates and other anions influences which phase will precipitate. The dominant factor, which causes the precipitation of the iron oxides, is the Eh-pH change at the boundary of the aquifer and the well that is exacerbated by pumping turbulence. The result of the precipitation of the iron oxides is the blockage of the well screen, gravel pack and conducting pipes, that if left unattended, can cause high maintenance costs.

CHAPTER 2 GEOCHEMISTRY OF GROUNDWATERS

2.1 Introduction

Groundwater and precipitate samples from nine water supply wells in the Klein Karoo area were collected on 25 and 26 of August 1999 in order to assess the relationship between the water chemistry and the precipitate found. For comparative purposes, a sample was taken from the well where precipitation has not occurred. The type of well ranged from privately owned wells to wells that are operated by municipalities for the supply of potable and irrigation water. The wells chosen were those where clogging was known to occur. The geological logs for all these wells were not available. The limiting of sampling to wells where the logs were available would have severely limited the study.

2.2 Sample collection

The wells were equipped with pumps and were purged before sampling until the EC was constant. Two samples were taken at each of the sites: one was 1 L, unfiltered, not preserved other than by refrigeration; the second sample was 100 mL, filtered and preserved with 2 mL conc. HCl per bottle, on site. Field measurements of EC, pH and temperature were made at the sampling site for all except one sample. Measurement of all the field parameters was repeated later in the laboratory. Dissolved oxygen was not measured due to failure of the relevant equipment (see Appendix A.6).

Samples were stored in a cooler box immediately after collection, and those collected on 25 August were placed in a fridge overnight. In the laboratory, all samples, both preserved and unpreserved, were kept in a fridge except when being used during analysis. During analysis, portions of sample were quickly withdrawn from the bottles in order to limit the contact of the samples with air. In the laboratory a sample blank (sample 10) was made using one of the acid-cleaned bottles, described in Appendix A.1. Two mL of the conc. HCl used in the field to preserve the samples was added to distilled water from the laboratory. Where analytical methods allowed, the blank sample was analysed with the nine samples collected in the field.

2.3 Site Description

Figures 2.1 to 2.4 show the locality of the wells. Samples 1, 3 and 4 were taken from different private wells on the farm Kruis Aar owned by Mr. S. Barnard (Figure 2.1). Sample 1 is located down hill of a farmhouse, sample 3 is adjacent to the farm dam and sample 4 is

located behind the hop plantation that is behind the fruitstall. Sample 2 was taken from a water supply well in Albertinia (Figure 2.2) and samples 5-8 were taken from supply wells in the Vermaaks River Valley (Figure 2.3). Sample 9 was taken from a water supply well in Calitzdorp (Figure 2.4).

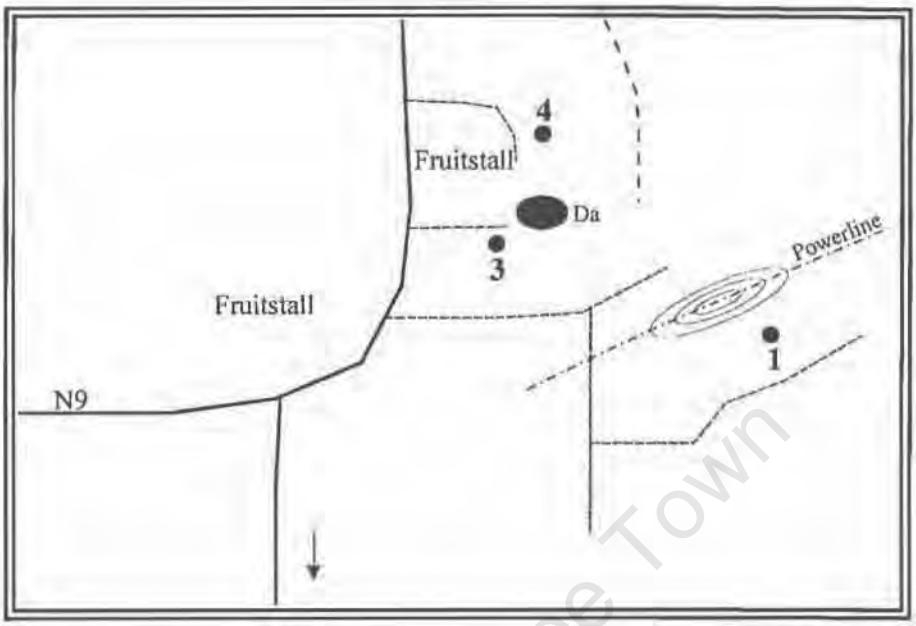

Figure 2.1. Schematic diagram of Kruis Aar sampling points

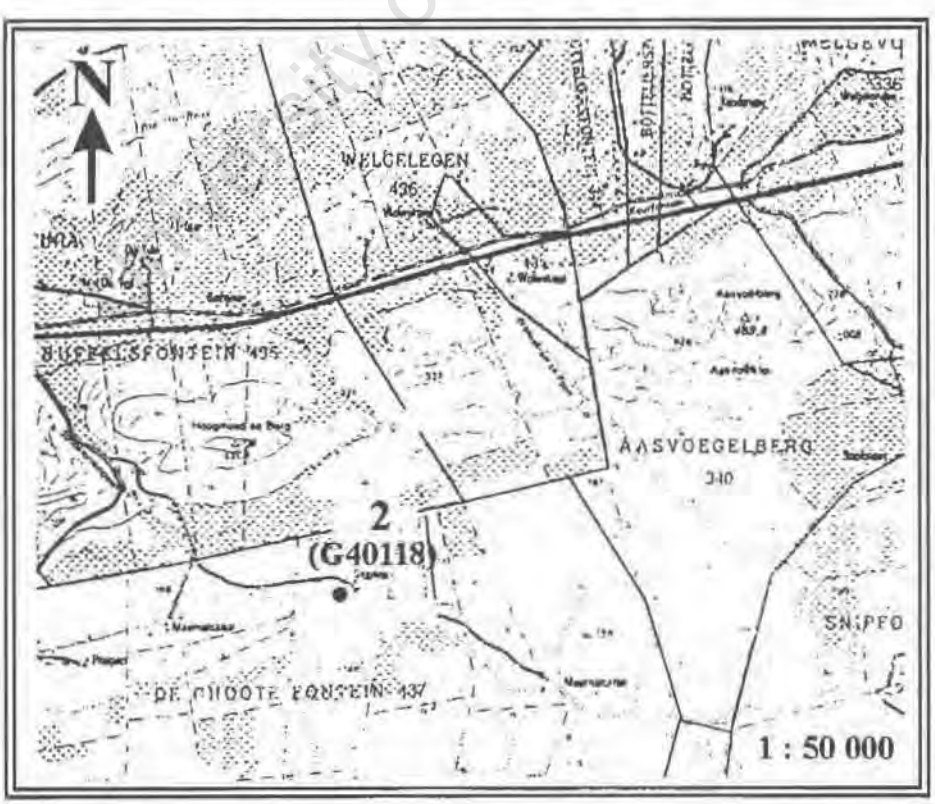

Figure 2.2. Map of sample site near Albertinia, sample 2

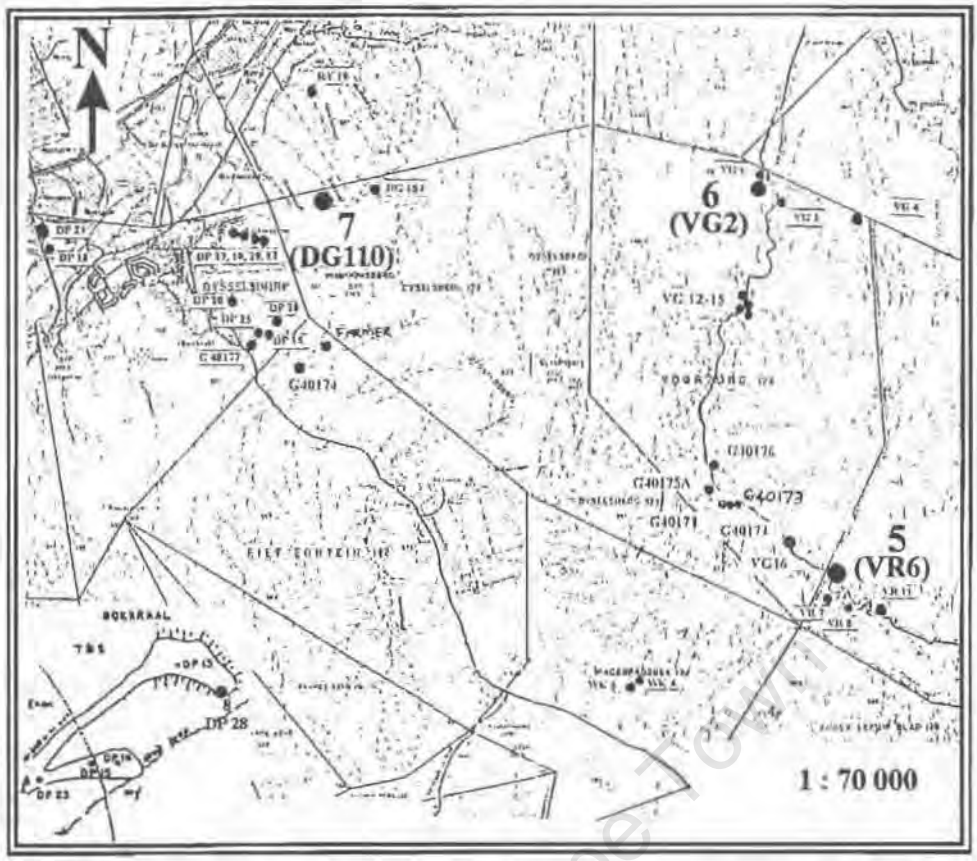

Figure 2.3. Map of Vermaaks River Valley sampling sites 5-8

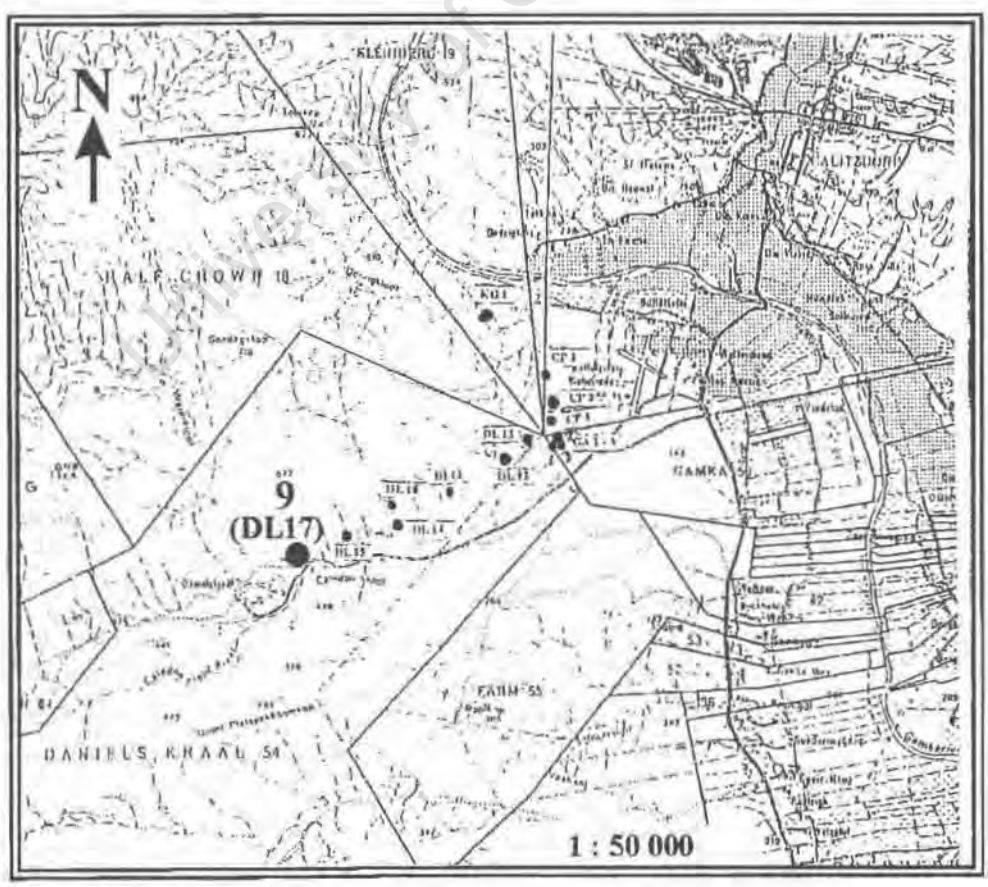

Figure 2.4. Map of sampling point 9 in Calitzdorp

2.3.1 Regional geology

2.3.1.1 Albertinia

The geology of the area is composed of massive light grey, quartzitic sandstones of the Skurweberg Formation of the Table Mountain Group. South of the Table Mountain Group rocks the quartzites are overlain by unconsolidated sandy soils of the Bredasdorp Group (GCS, 1996).

2.3.1.2 Outshoorn area

Samples 1, 3-8 come from the Outshoorn area where the geology is comprised of the lithologies of the Table Mountain Group (TMG). The TMG in the area is represented by the Baviaanskloof, Rietvlei, Skurweberg, Goudini Formations of the Nardouw Sub-group and the Cedarberg and Peninsula Formation's. The Baviaanskloof Formation is composed of micaceous, impure sandstone with subordinate shale, and the Rietvlei Formation is composed of feldspathic sandstone, siltstone and micaceous shale beds. The Skurweberg Formation underlies the Baviaanskloof and Rietvlei Formation's and is composed of quartzitic sandstone with thin lenticular conglomerate and grit beds and is in turn underlain by thinly bedded, quartzitic sandstone with thin shale beds, of the Goudini Formation. The Cedarberg Formation, comprised of massive shale/siltstone with thin sandstone lenses underlies the Nardouw Sub-group and is in turn underlain by the light-grey quartzitic sandstone with thin siltstone, shale and conglomerate beds, of the Peninsula Formation (Geological Survey, 1991).

2.3.1.3 Calitzdorp

The geology of the area is comprised of the Nardouw Sub-group of the Table Mountain Group and the Ceres Sub-group of the Bokkeveld Group. The Baviaanskloof and Skurweberg Formations represent the Nardouw sub-group in the area and are described in 2.3.1.2 above.

2.3.2 Well geology

The geological logs for all the wells that were sampled in this study could not be obtained. The geology of the logs that could be obtained are summarised below and copies of the logs are in Appendix C.2.

2.3.2.1 Sample 2 (Albertinia–G40118)

The well consists of calcareous sand up to 35 m below surface that is underlain by sandstone up to 139 m below surface. From ~90 m below surface the sandstone is fractured and shows iron staining on the joints. Below the sandstone is a micaceous sandy shale. The slotted casing was placed from 69-79 m and from 127-188 m below surface, which falls over the fractured sandstone and the shale of the Table Mountain Group (GCS, 1996).

2.3.2.2 Sample 7 (DG110)

From the surface to 216 m, the lithology is quartzite with shale bands of the Baviaanskloof Formation of the Table Mountain Group. The Baviaanskloof Formation is underlain by the Skurweberg Formation of the Table Mountain group that is composed of solid quartzite (Mulder, 1995).

2.3.2.3 Sample 9 (DL17)

From 0-28 m, the lithology is soft weathered sandstone that is underlain by quartzitic sandstone of the Baviaanskloof Formation of the Table Mountain Group. The Baviaanskloof Formation extends to a depth of 249 m and is shaley at 70, 128 and 150 m below surface (Mulder, 1995).

2.4 Previous Work

Previous work on the water chemistry was done in February 1999 by Fey et. al. at the University of Cape Town, for Groundwater Consulting Services (GCS). The four wells, DL17, DG110, DP28 AND VG2 were re-examined as part of the research.

Another study was done on the wells in Klein Karoo Rural Water Supply Scheme and focussed mainly on the microbiological and chemical issues. The study was done as a joint venture between GCS and the CSIR Groundwater Group (GWG) for the Department of Water Affairs and Forestry (DWAF) in 1998/9 (Engelbrecht and Jolly, 1999). A summary of the water data from previous work is tabulated in Appendix C.1.

2.5 Analytical methods

2.5.1 EC and pH

Field measurements were made on site using Corning sensors and were again measured in the laboratory using a Crison EC meter and a Metrohm pH meter. Details of apparatus used and the reproducibility of the method are given in Appendix A.1 and A.2.

2.5.2 Alkalinity and acidity

The alkalinity of the water samples was determined by potentiometric titration to a Bromcresol green endpoint of pH 4.5 using a Radiometer ABU80 auto burette and TTT85 titrator. The procedure involved determining the volume of 0.01M HCl required to titrate 10 mL of sample to the preselected endpoint. Titrations were carried out using 10 mL of unfiltered, unacidified sample. The alkalinity was computed and is expressed as mmoles/L HCO_3^-.

Total acidity for the two samples with pH values below 4.5 (as measured in the laboratory) was determined by titration to the phenolphthalein endpoint of pH 8.3. Acidity titrations were performed using 0.01M NaOH and 10 mL of unfiltered, unacidified sample. Repeat analyses were performed on each sample and on a blank of ultrapure water.

2.5.3 Major cations and anions

High performance ion chromatography (HPIC) was used to determine the major cations (Na^+, K^+, Mg^{2+}, Ca^{2+} and NH_4^+) and anions (F^-, Cl^-, NO_2^-, NO_3^-, Br^- and SO_4^{2-}) in the samples. A Dionex ion chromatograph in the Department of Geological Sciences at the University of Cape Town was used to perform the analyses on filtered and unacidified samples. The samples were diluted with distilled water to obtain EC values below 100 mS/m and then passed through a Dionex onguard–P filter, to remove all organics, before analysis. Details of the repeatability and accuracy of the results are discussed in Appendix A.9. The concentration of PO_4^{3-} was determined by the Ascorbic Acid 4500-P E colorimetric method from Standard Methods (1989) as detailed in Appendix A.16. For the very low PO_4^{3-} concentrations present in the samples, the concentration obtained by colorimetry is more accurate than the concentration as determined by HPIC. Results are reported in Table 2.1.

2.5.4 Trace elements

A Perkin-Elmer ELAN 6000 Inductively Coupled Plasma – Mass Spectrometer (ICP-MS) was used to determine the trace element composition of the samples and the blank. Al and Li were determined by ICP-MS. Trace element data are reported in Table 2.1. Field filtered and acidified samples were diluted with 2% HNO_3 to a total volume of 15 mL. An internal standard of 50 µl of 3 ppm Rhodium was then added to the sample. The internal standard was used to correct for drift and for calibration purposes. Initially semi-quantitative analysis (± 20 % error) was performed to determine the approximate concentration of all the elements in solution. Mn and Zn were found in higher concentrations than expected and were re-analysed by quantitative ICP-MS, together with Al and Si, to obtain accurate concentrations. The blank was analysed by ICP-MS for major and trace elements and by colorimetry to determine iron concentration. An assumption was made that all the elements present in sample 10 were present due to the HCl acid added and not from the distilled water. The results of the analyses have been subtracted from the sample results. The distilled water used for the preparation of sample 10 was not analysed separately. The details of analytical precision and accuracy are reported in Appendix A.10.

2.5.5 Iron

Total and ferrous iron (and ferric iron by difference) was determined by the 3500-Fe D-phenanthroline method as described in Standard Methods (1989), detailed in Appendix A.13. The absorbance values were obtained using a Sequoia-Turner model 340 spectrophotometer at a wavelength of 510 ηm after 10-15 minutes of colour development. Standards of known concentration were prepared and measured in the same way and a calibration curve was calculated. The colorimetric method allows both the redox species (Fe^{2+} and Fe^{3+}) to be determined individually together with the total Fe concentration. ICP-MS is not a very accurate method for the determination of total iron due to molecular and isobaric interferences (Spath, 1999).

2.5.6 Dissolved organic carbon (DOC)

DOC was determined by the CSIR in Stellenbosch using the Persulphate-Ultraviolet Oxidation Method detailed in Appendix A.8. DOC was determined in order to assess if it would be a significant nutrient source for oxidising bacteria in the wells.

2.6 Results and discussion

The results from all analyses are reported in Table 2.1.

2.6.1 pH and EC

The pH of the water samples ranges from 3.1 to 6.2. The waters are mostly slightly acidic with samples 8 being markedly acidic. The lab EC of the samples ranges from 11 (sample 5) to 302 mS/m (sample 2). The majority of the waters have a low salinity with sample 2 being very saline. The field and laboratory measurements of the EC and pH are similar except for sample 4, where the pH changed from 5.7 in the field to 3.9 in the laboratory, sample 7 whose EC changed from 17 mS/m to 24 mS/m, and sample 3 whose EC changed from 30mS/m to 43 mS/m. The more acidic pH values have important implications for metal solubility which will be addressed in Chapter 3 regarding the precipitates. The reason for the change in pH of sample 4 may be due to the hydrolysis of Fe or the high Al concentration in this sample.

2.6.2 Alkalinity and acidity

The samples with pH values above 4.5 were titrated to determine the alkalinity and the two samples with pH values below 4.5 were titrated to determine the acidity. In terms of alkalinity, the samples show very low acid neutralising capacity and in terms of acidity, sample 4 has the lowest and sample 8 has a much higher base neutralising capacity.

When acidity is positive a stronger acid anion than carbonic acid is present and is commonly sulphate. In acid water, aluminium species can contribute to the acidity because they are titratable with a base. Fe^{3+} behaves in an analogous manner to Al^{3+} and could thus contribute to the acidity (Drever, 1997).

2.6.3 Chemical composition

2.6.3.1 Iron species and pe

For all the waters sampled, ferrous (Fe^{2+}) iron constitutes the major component of the iron in solution with only a small proportion made up by ferric (Fe^{3+}) iron (Table 2.1). Sample 5 has a total iron concentration below the detection limit of the colorimetric method (10 µg/L). ICP-AES analysis of sample 5 gave a total iron concentration of 110 µg/L.

Table 2.1. Analytical data for all samples

Sample no.	1	2	3	4	5	6	7	8	9
Alternate name	Kruis Aar	Albertinia	Kruis Aar	Kruis Aar	VR 6	VG 2	DG 110	DP 28	DL 17
EC $(mS/m)_{field}$	56	n.d.	30	42	9	33	17	57	49
EC $(mS/m)_{lab}$	58	302	43	46	11	33	24	58	47
pH_{field}	5.21	n.d.	6.04	5.71	6.18	5.59	5.35	3.13	5.73
pH_{lab}	5.35	6.20	5.86	3.95	6.17	5.99	5.48	3.53	6.11
Major ions (mg/L)									
Cations (mg/L)									
Na^+	77.8	381.8	29.2	47.3	11.9	22.3	20.6	22.7	44.2
NH_4^+	0.0	0.0	0.0	0.0	0.0	0.0	0.0	0.35	0.50
K^+	2.0	7.5	3.9	2.9	0.76	7.1	1.4	3.9	14.8
Mg^{2+}	9.0	60.8	6.1	8.9	2.0	4.1	3.6	13.1	11.4
Ca^{2+}	9.4	72.5	5.2	9.7	5.1	17.0	5.4	22.8	27.4
Fe^{2+}	2.6	41.0	13.0	11.6	<0.01	0.90	8.5	14.6	3.3
Fe^{3+}	0.3	3.2	1.1	2.4	<0.01	0.14	3.2	0.81	0.25
Anions (mg/L)									
F^-	0.01	<0.01	0.09	6.6	<0.01	0.06	0.05	0.52	0.07
Cl^-	128.8	669.4	61.4	93.0	19.6	49.6	46.5	26.6	93.3
NO_2^-	<0.01	<0.01	<0.01	<0.01	<0.01	<0.01	<0.01	<0.01	<0.01
Br^-	<0.01	<0.01	<0.01	<0.01	<0.01	<0.01	<0.01	<0.01	<0.01
NO_3^-	0.37	<0.01	<0.01	<0.01	0.50	<0.01	<0.01	<0.01	<0.01
PO_4^{3-}	<0.01	<0.01	<0.01	<0.01	<0.01	<0.01	0.00	<0.01	<0.01
SO_4^{2-}	19.5	119.4	6.3	8.7	2.7	16.6	9.9	209.3	27.0
Alkalinity (mmoles/L)	0.09	1.02	0.46	n.d.	0.11	0.53	0.27	n.d.	0.75
Acidity (mmoles/L)	n.d.	n.d.	n.d.	0.72	n.d.	n.d.	n.d.	3.49	n.d.
DOC (mg/L)	<1.0	<1.0	<1.0	<1.0	<1.0	<1.0	<1.0	<1.0	<1.0
SAR $(mmol/L^{0.5})$	4.35	8.00	2.06	2.64	1.12	1.26	1.68	0.94	1.79
Trace elements (µg/L) semi-quantitative except for Al, Si, Mn and Zn									
Li	5.5	5.2	7.5	9.3	0.4	36	25	32	64
Be	0.5	0.2	<0.05	0.1	<0.05	0.4	0.2	37	0.1
B	32	133	20	18	6.1	14	14	14	75
Al	21	<0.05	54	234	22	<0.05	<0.05	5046	196
Si	4027	3301	4232	3886	3449	7490	3866	7359	5218
Sc	2.1	2.3	2.1	2.5	1.1	3.1	2.0	5.4	1.1
Ti	14	96	5.1	12	2.7	20	6.4	38	22
Cr	0.1	<0.05	<0.05	<0.05	<0.05	<0.05	<0.05	<0.05	<0.05
Mn	1400	1094	2908	3274	16	1727	3252	1941	925
Co	7.0	0.1	2.6	10	0.2	1.9	5.7	333	2.5

Table 2.1 continued...

Sample no.	1	2	3	4	5	6	7	8	9
Ni	11	2.1	5.6	14	1.6	10	9.7	653	5.5
Cu	28	<0.05	<0.05	11	24	2.0	2.4	34	15
Zn	385	<0.05	40	145	245	252	30	4016	97
Ga	0.1	0.1	0.2	0.3	<0.05	0.1	0.3	1.3	0.1
Ge	<0.05	0.3	<0.05	0.1	<0.05	0.1	0.3	0.5	0.1
As	<0.05	<0.05	<0.05	<0.05	<0.05	0.6	<0.05	7.5	<0.05
Se	0.6	7.3	0.4	1.3	<0.05	1.3	1.0	<0.05	<0.05
Rb	7.7	12	13	11	1.0	24	6.1	18	35
Sr	62	530	44	64	11	105	3.4	73	73
Cd	0.3	<0.05	0.2	1.6	<0.05	0.1	0.1	11	0.1
Sn	4.8	<0.05	<0.05	0.7	<0.05	12	<0.05	3.1	1.8
I	3.3	36	5.9	<0.05	<0.05	0.1	0.9	12	1.8
Cs	0.2	0.6	0.8	1.2	<0.05	1.8	0.4	2.7	2.0
Ba	59	199	50	30	5.2	77	7.3	34	113
La	0.2	<0.05	<0.05	<0.05	0.1	<0.05	<0.05	39	<0.05
Ce	0.2	0.1	0.2	<0.05	0.2	0.1	<0.05	133	0.1
Pr	<0.05	<0.05	<0.05	<0.05	<0.05	<0.05	<0.05	19	<0.05
Nd	0.1	<0.05	0.1	<0.05	0.1	<0.05	<0.05	95	0.1
Sm	<0.05	<0.05	<0.05	<0.05	<0.05	<0.05	<0.05	24	<0.05
Eu	<0.05	<0.05	<0.05	<0.05	<0.05	<0.05	<0.05	6.5	<0.05
Gd	<0.05	<0.05	<0.05	<0.05	<0.05	<0.05	<0.05	34	<0.05
Tb	<0.05	<0.05	<0.05	<0.05	<0.05	<0.05	<0.05	5.3	<0.05
Dy	<0.05	<0.05	<0.05	<0.05	<0.05	<0.05	<0.05	29	<0.05
Ho	<0.05	<0.05	<0.05	<0.05	<0.05	<0.05	<0.05	5.0	<0.05
Er	<0.05	<0.05	<0.05	<0.05	<0.05	<0.05	<0.05	13	<0.05
Tm	<0.05	<0.05	<0.05	<0.05	<0.05	<0.05	<0.05	1.6	<0.05
Yb	<0.05	<0.05	<0.05	<0.05	<0.05	<0.05	<0.05	9.7	<0.05
Lu	<0.05	<0.05	<0.05	<0.05	<0.05	<0.05	<0.05	1.3	<0.05
W	24	0.4	2.0	0.9	2.4	0.6	0.1	3.8	0.4
Tl	0.2	<0.05	0.2	0.3	<0.05	0.1	<0.05	1.5	0.1
Pb	2.5	<0.05	<0.05	<0.05	<0.05	0.8	0.5	59	<0.05
Th	<0.05	<0.05	<0.05	<0.05	<0.05	<0.05	<0.05	0.9	<0.05
U	0.2	0.1	0.3	0.5	0.4	0.7	0.2	843	0.5

Sample 5 has does not have an iron oxide clogging problem in the well which may be due to its very low total iron concentration. Sample 2 from Albertinia, has the highest iron concentration of all the samples with a Fe^{2+} concentration of 41.0 mg/L and a Fe^{3+} concentration of 3.09 mg/L. Sample 8 has the next highest concentrations of Fe^{2+} and Fe^{3+} (14.61 mg/L and 0.74 mg/L respectively). Sample 8 is the sample with the lowest pH and metals concentrations are expected to be higher in solution.

The higher concentrations of Fe^{2+} as compared with Fe^{3+} for each sample indicate that the iron in the aquifer is kept in the Fe^{2+} form due to reducing conditions present in the aquifer. The Fe^{3+} species may be present due to oxidation of the iron caused by turbulence in the well during pumping before sample collection.

The p*e* for the samples was calculated using the PHREEQC interface in the Aquachem modelling package using the redox couple, Fe^{2+}/Fe^{3+}. The p*e* for the ferrous-ferric system is defined as: $pe = \log K_{eq} + \log(a_{Fe}{}^{3+}/a_{Fe}{}^{2+})$ (Drever, 1997)

The values were modelled as DO measurements were not available due to malfunction of the equipment in the field. The Mn couple was not used in the calculations as the speciation for Mn had not been determined.

The modelled values obtained for p*e* are reported in Table 2.2. The iron species could not be determined for sample 5 and thus the p*e* for this sample could not be calculated. In Figure 2.5, the p*e* is plotted vs. $pH_{lab\ (and\ field)}$ for all the samples. Both the field and laboratory pH show a negative correlation with respect to p*e*. From Table 2.2, it can be noted that all the groundwaters appear to be poised at a p*e*+pH of 12.29 (12.36 using field data). According to Lindsay (1979) many systems such as soils show a constant value for p*e*+pH which reflects the characteristic redox status of the system, such that a change in either the p*e* or pH of the system results in a change in the other variable. This "poise" of the system in terms of redox suggest a control of the redox status by a specific set of redox equilibria e.g. Fe-mineral dissolution and oxidation in conjunction with the gaseous composition (O_2 and CO_2). The implication of this is that the groundwaters are chemically similar and that the pH could be used to obtain an estimate of the p*e* and hence the Fe^{2+}/Fe^{3+} ratio for groundwater in the system.

2.6.3.2 Major ion chemistry

The dominant major cationic species in solution for all the samples is Na^+, followed by Ca^{2+}, Mg^{2+} and K^+. In sample 3, the Ca-Mg dominance is reversed. The dominant anion for most of the samples, excluding sample 8, is Cl^-. In sample 8, $SO_4{}^{2-}$ is the dominant anion. The Aquachem modelling package was used to draw up a piper diagram for all the water samples

(Figure 2.6). Samples 1, 2, 4 and 8 fall into the $Cl+SO_4$ hydrochemical facies type whereas samples 3, 5 and 7 fall into the HCO_3-Ca+Mg type and samples 6 and 9 are classed as the $Cl+SO_4$-Na+K facies type.

Table 2.2. pH and p*e* values for samples containing iron

Sample no.	pH (field)	pH (lab)	p*e* values	p*e*+pH$_{(lab)}$
1	5.21	5.35	7.1	12.45
2	nd	6.20	5.3	11.50
3	6.04	5.86	5.9	11.76
4	5.71	3.95	8.9	12.85 (14.61)
6	5.59	5.99	5.9	11.89
7	5.35	5.48	7.3	12.78
8	3.13	3.53	10.1	13.63
9	5.73	6.11	5.4	11.51

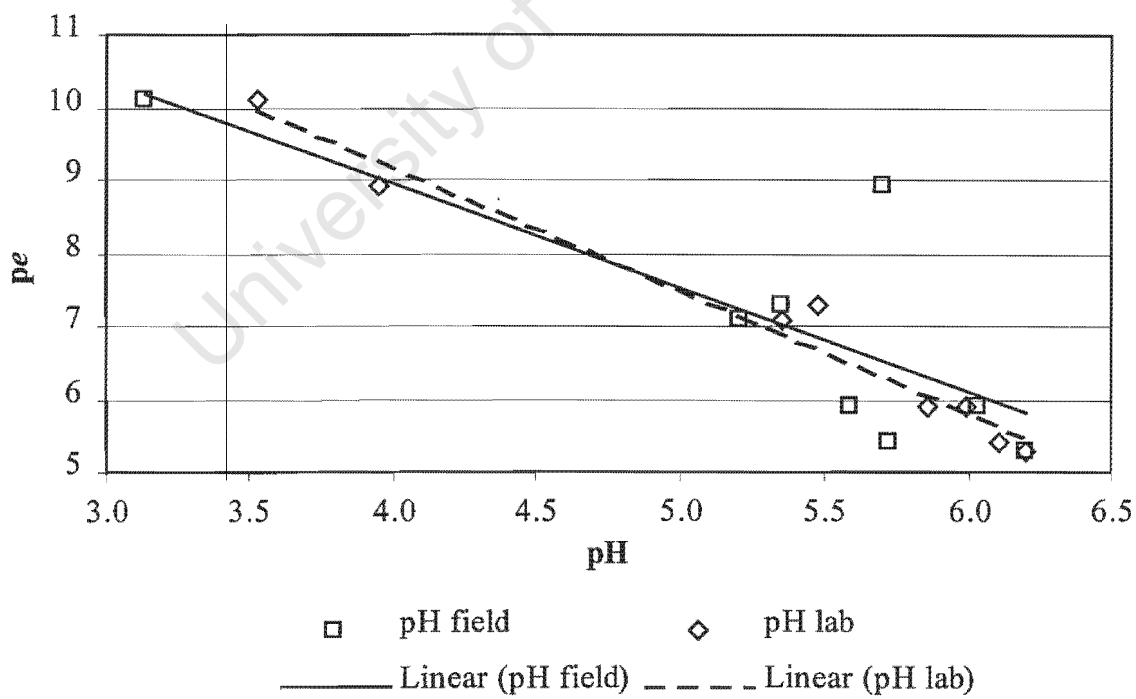

Figure 2.5. Calculated p*e* vs. pH for all samples

2.6.3.3 Trace element chemistry

The error on the values is 20 % by semi-quantitative analysis and all values reported are those after subtraction of the blank concentrations (sample 10). Silicon is the dominant trace metal in solution for all the samples followed by Mn (excluding 5 and 8). Sample 5 has the lowest concentrations of trace metals in general but this is expected as sample 5 has the lowest EC and highest pH out of all the samples. In samples 1, 5, 6 and 7 Zn is more dominant than Al, whereas in samples 3, 4, 8 and 9 Al is more dominant than Zn.

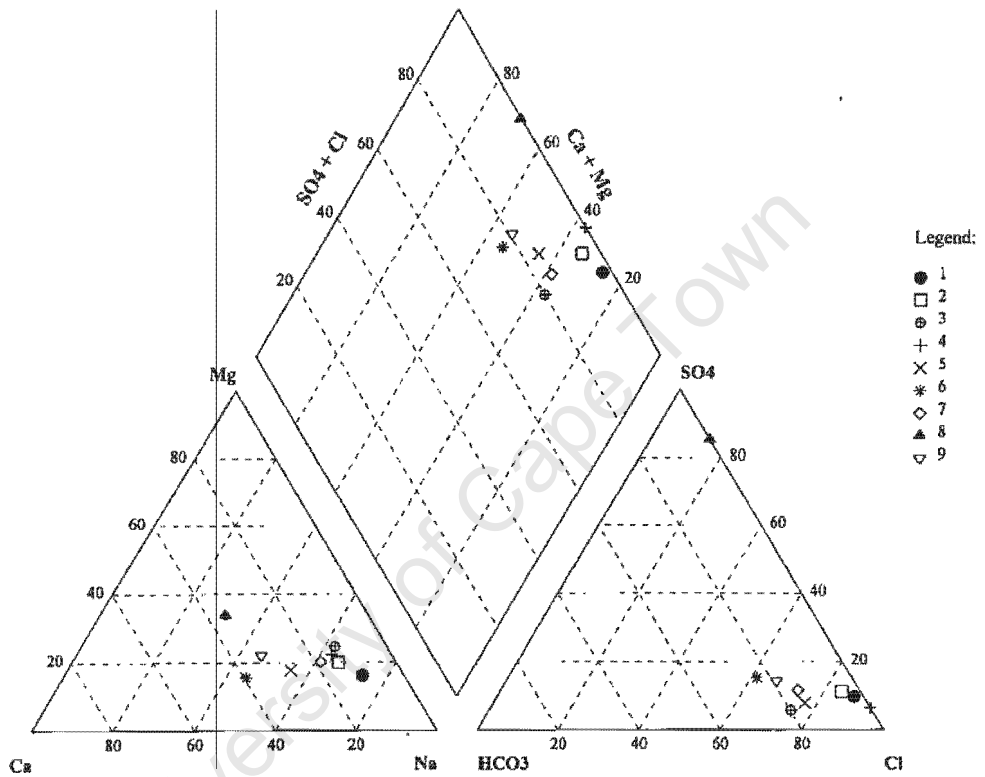

Figure 2.6. Piper diagram of all water samples, key indicates precipitate type

Sample 8 has by far the highest concentration of Al^{3+} (5.05 mg/L) and SO_4^{2-} (209 mg/L). Al^{3+} contributes to the acidity of the sample through the hydrolysis. Sample 4 has 0.23 mg/L of Al^{3+} which is higher than the other samples. The slightly elevated concentration of Al^{3+} in sample 4 could account for the acidic nature of the sample in the laboratory where hydrolysis of Al^{3+} generates H^+ ions contributing to the acidity in the sample. Sample 8 has in general the greatest concentration of trace metals in solution and this is possibly due to the markedly acidic nature of the sample with respect to the other samples.

2.6.4 *Speciation and saturation indices*

Modelling of the speciation and saturation indices for the water samples was performed using Aquachem with the PHREEQC database. For all the samples, the laboratory determined pH was used in the calculations of saturation indices. In addition, saturation indices for sample 4 were recalculated using the field pH due to the marked change in pH observed between the field and laboratory. Saturation indices were determined taking into consideration the calculated p*e* and both iron species. The SI is defined as:

$$SI = \log (IAP/K_{sp})$$

Where IAP is the ion activity product and K_{sp} is the solubility product. (Drever, 1997).

2.6.4.1 Iron minerals

The saturation indices (S.I.) of the iron minerals are listed in Table 2.3.

Table 2.3. Saturation indices of various iron minerals

Sample	Saturation indices		
No.	**Goethite**	**Fe $(OH)_3$ (a)**	**Jarosite**
1	6.66	0.77	-1.9
2	8.44	2.55	2.53
3	7.71	1.82	-0.92
4	4.92 (8.69)	-0.97 (2.80)	-3.48 (2.61)
6	6.94	1.04	-2.53
7	7.81	1.92	0.52
8	4.87	-1.02	0.38
9	7.31	1.42	-1.13

(a) = amorphous, SI's calculated using the field pH for sample 4 are in brackets

Figure 2.7 A show that sample 4 is supersaturated with respect to goethite, ferrihydrite and jarosite when the field pH is used but is only supersaturated with respect to goethite when the laboratory pH is used in the calculation. Figure 2.7A reveals that all the samples are supersaturated with respect to goethite. Sample 8 is undersaturated with the rest of the samples being supersaturated with respect to $Fe(OH)_3$. Samples 1, 3, 6 and 9 are undersaturated and sample 2 is supersaturated with respect to jarosite. Samples 7 and 8 are in equilibrium with jarosite. The p*e*+pH vs. SI graph (Figure 2.7 B) shows the same relationship

with the exception that the slope of the line is shallower.

The supersaturation of the samples with respect to goethite indicates that dissolution of the initial precipitate ($FeOH_3$) would have to occur in order for goethite to precipitate. The transformation of ferrihydrite to goethite is spontaneous because of the much lower stability of ferrihydrite. The transformation of ferrihydrite to goethite has been found to proceed via a dissolution-recrystallisation process, the rate of which may be slow resulting in the widespread association of ferrihydrite and goethite in nature (Schwertmann and Fitzpatrick, 1992). The dominance of ferrihydrite may be because rapid oxidation and hydrolysis of Fe^{2+} forms ferrihydrite preferentially to other iron oxides (Schwertmann and Fitzpatrick, 1992).

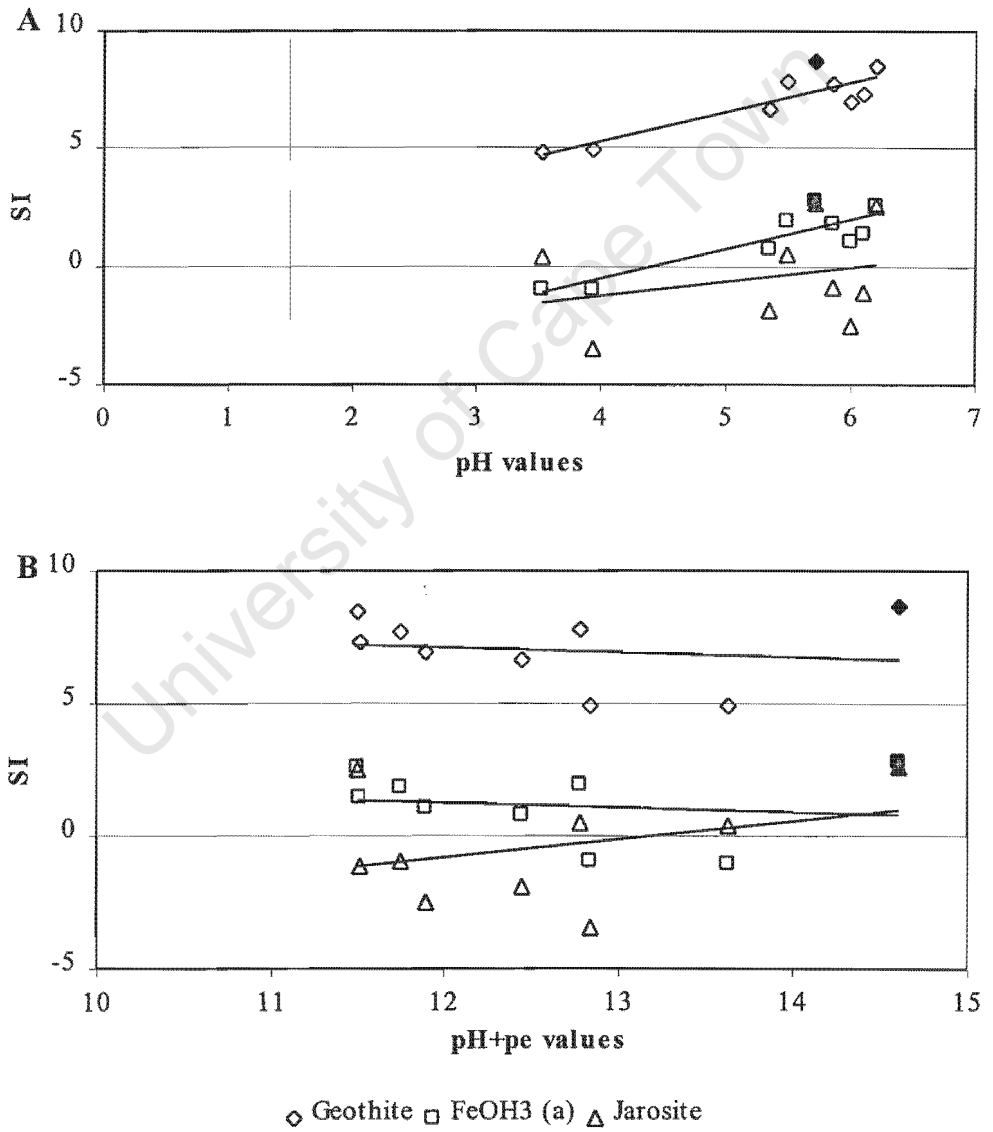

Figure 2.7. Saturation indices of jarosite, ferrihydrite and goethite vs. pH (A) and p*e*+pH (B). The solid points are the SI values for sample 4 calculated using the field pH.

When the iron in the aquifer water is exposed to oxygen through pumping the oxidation and hydrolysis could be rapid resulting in an initial precipitate of ferrihydrite. However, in the case of sample 8 the $Fe(OH)_3$ SI was negative so the formation of goethite directly without the transformation from ferrihydrite is more likely. Jarosite represents a SO_4-phase for the waters that may precipitate for samples 2, 4, 7 and 8. Other SO_4-phases may be more appropriate to consider but were not determined.

2.6.4.2 Other minerals

The saturation indices in Table 2.4 indicate all the waters are in equilibrium with quartz ($SI \leq \geq 0.5$) that suggests the aquifer host rocks are of a siliceous nature. Sample 2 is the only in equilibrium with siderite and this may be attributable to the higher alkalinity of this particular water with respect to the other samples.

Table 2.4. Saturation indices for other minerals

Sample no.	Quartz	Fluorite	Gypsum	Calcite	Siderite	Rhodochrosite
1	0.02	-6.4	-3.1	-4.3	-2.6	-2.7
2	-0.06	no SI	-1.8	-1.8	0.2	-1.1
3	0.05	-4.5	-3.7	-3.4	-0.7	-1.1
4	0.01	-0.6	-3.4	no SI	no SI	no SI
5	-0.04	no SI	-4.0	-3.6	no SI	-3.6
6	0.29	-4.0	-2.8	-2.7	-1.7	-1.2
7	0.01	-4.6	-3.5	-3.9	-1.5	-1.7
8	0.29	-7.1	-1.8	no SI	no SI	no SI
9	0.14	-4.2	-2.5	-2.2	-0.9	-1.2

2.6.5 Water quality

The water that was examined is used as potable water and for the irrigation of crops, namely hops and fruits, and possibly for livestock use. Potable water includes water that is used for drinking and bathing. The chemical composition of the water was compared to the available standards for these classes of water as defined by DWAF (1995) and DWAF (1993) (Figures 2.8 and 2.9). The guidelines are laid out in Table A.7 of Appendix A.17 and the values stipulated are those where there is no detrimental effect on human or animal health.

2.6.5.1 pH

Some of the waters fall between the lower limit of 6.0 pH and upper limit of 9.5 pH for domestic use with the exception of samples 1, 3, 4, 7 and 8. All the waters fall below the lower limit (pH 6.5) for irrigation water (Figure 2.8).

2.6.5.2 Major elements

The water samples are mostly below the specified DWAF ideal limits for water use in terms of domestic, irrigation and livestock use, for all the cations. Exceptions are sample 1, which has a Na^+ concentration of 78 mg/L, and is just above the limit for irrigation (70 mg/L).

Sample 2 has a Na^+ concentration of 382 mg/L that far exceeds the limits for domestic use (200 mg/L Na+) and irrigation water. The total iron concentrations of all the samples, except sample 5, are above the limit for domestic water, which is 1 mg/L (Figure 2.9). Samples 2, 3, 4, 7 and 8 are above the limits for total iron in irrigation water and in terms of livestock use, total iron concentrations above 10 mg/L can be harmful. The amelioration of the water through aeration should allow most of the iron in solution to precipitate out and thus reduce the concentrations in solution and the risk.

As for the cations, most of the samples have concentrations of the major anions below the limits as specified by DWAF (1995). Exceptions are samples 1 and 2, which have Cl^- concentrations of 129 mg/L and 669 mg/L respectively, which are above the limit for irrigation water which is set at 105 mg/L. Sample 2 is above domestic water limit set at 200 mg/L (Figure 2.8). The only sample that exceeds the domestic and livestock use limits set for F^- is sample 4 (6.6 mg/L).

2.6.5.3 Trace elements

Several trace elements were analysed for but do not have specified limits and are thus not discussed. The majority of the samples have concentrations below the limits specified for some of the trace elements. Sample 5 does not exceed any of the limits for trace elements for any of the water uses. Samples 4 and 9 exceed the domestic water limit for Al, which however does not have any expected health effects. All samples have Mn concentrations above the limits set for Mn with respect to both domestic and irrigation water.

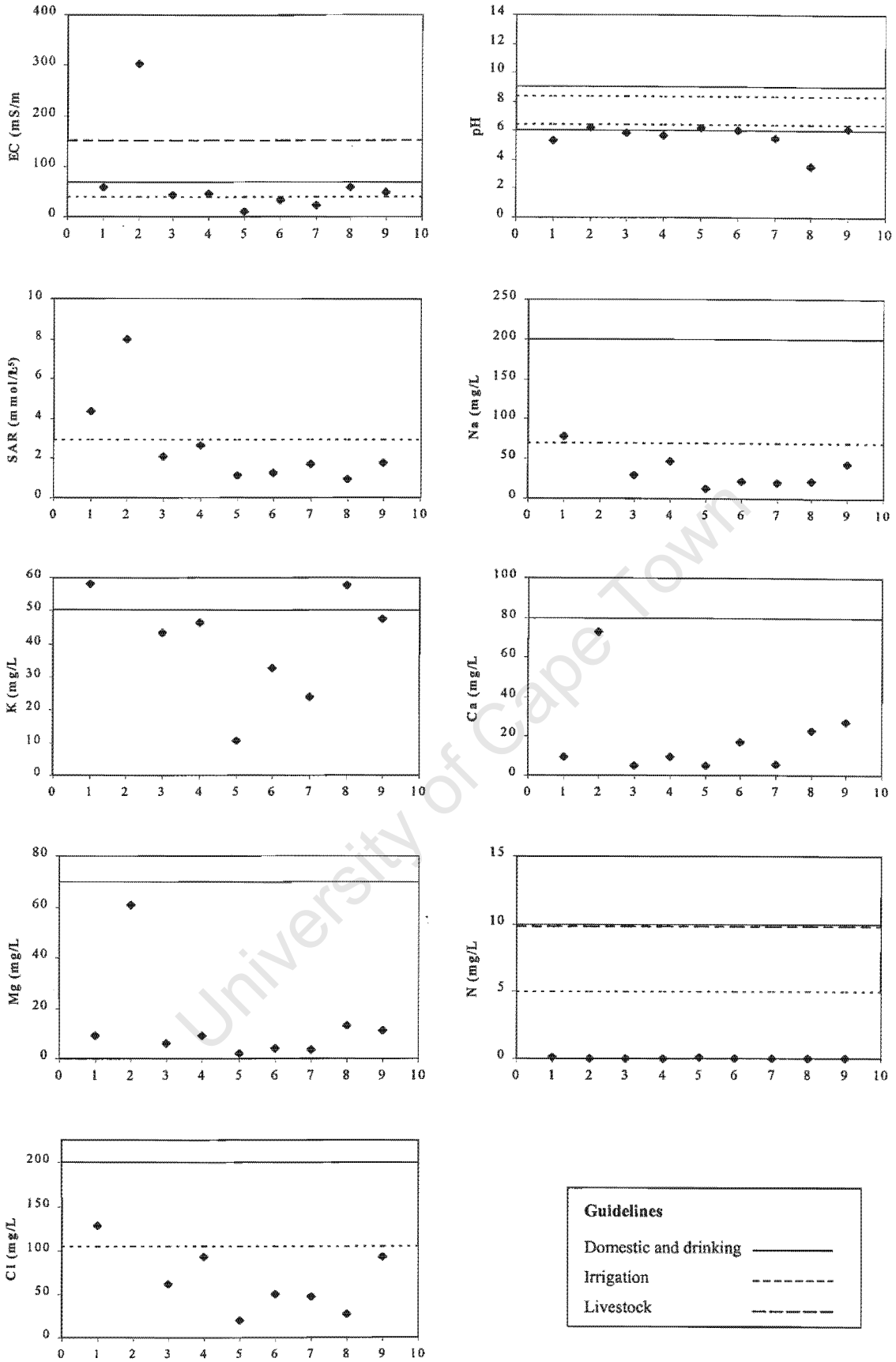

Figure 2.8. Comparison of sample parameters, EC, pH, SAR, Na^+, K^+, Ca^{2+}, Mg^{2+}, NO_2^- $+NO_3^-$ as N and Cl^- with the DWAF water quality guidelines (horizontal scale is sample no.)

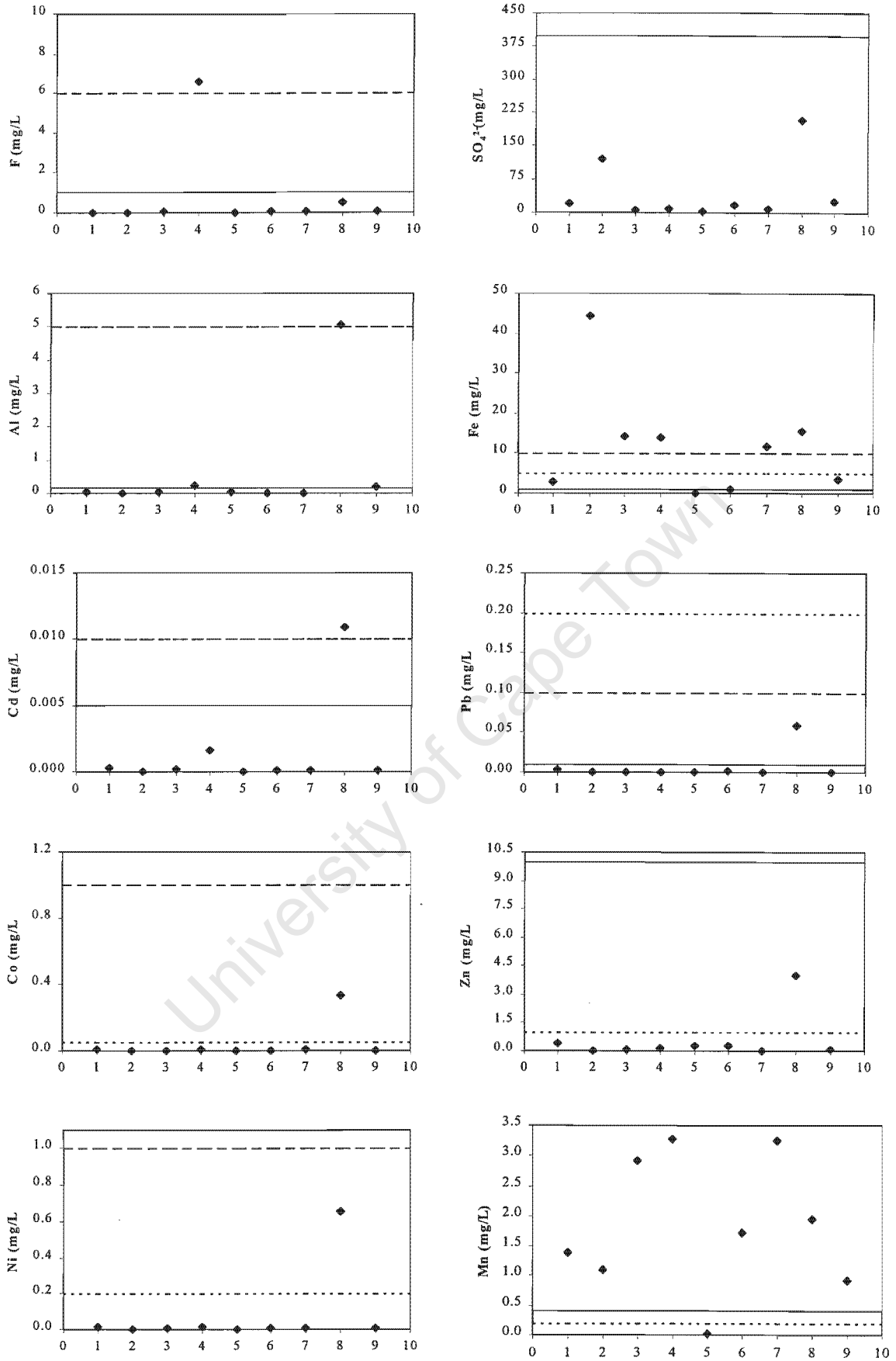

Figure 2.9. Comparison of sample parameters, F^-, SO_4^{2-}, Al, Fe, Cd, Pb, Co, Zn, Mn and Ni with DWAF water quality guidelines (horizontal scale is sample no.)

Sample 8 has an Al concentration (5.1 mg/L) above the domestic and just above livestock use limits. The Cd concentration found in sample 8 (0.011 mg/L), is above the limits for domestic and irrigation and livestock water use. The Co concentration in the sample 8, with a concentration of 0.3 mg/L, exceeds the limit of 0.05 mg/L for irrigation use and the toxic threshold of 0.1 mg/L for plants. The limit for Zn is exceeded only by sample 8, with respect to irrigation water, with a sample concentration of 4.0 mg/L. The Ni concentration of 0.65 mg/L in sample 8 is above the limit set for irrigation (0.2 mg/L) and close to the limit for livestock use (1.0 mg/L).

2.6.5.4 Sodium adsorption ratio (SAR)

The SAR is an index of the potential of a given irrigation water to induce sodic soil conditions (DWAF, 1993). The SAR and the EC values should be looked at together in order to assess whether a particular water is suitable for irrigation. Waters with a high SAR and low EC can promote soil dispersion and structural breakdown resulting in the plugging of surface pores. The plugging of the pores results in a decrease of infiltration and can lead to decreased crop production (Ayers and Westcot, 1985). Samples 3 to 9 have SAR values below 3 $mmol/L^{0.5}$ which is the concentration below which Na should not accumulate to toxic levels in the soil (DWAF, 1993). Sample 1 has a SAR of 4.4 $mmol/L^{0.5}$ and sample 2 has a SAR of 8.0 $mmol/L^{0.5}$ which according to DWAF (1993) should be applied only to soil, thereby limiting the Na uptake to that through the roots. The SAR was calculated for all the samples using the HPIC results and then plotted on the graph of SAR vs. EC (Figure 2.10), to determine the suitability of the water. Sample 5 will promote soil dispersion that may lead to reduce infiltration problems if used for irrigation over a period time. Sample 2 will not cause a reduction in the infiltration rate of water and samples 1, 3, 4 and 6 to 9 may cause a slight reduction in infiltration rate if used for long term irrigation.

When the water quality variables EC and Na concentration are plotted on a Wilcox diagram the following observations can be made in terms of the effect on plants if the waters are used for irrigation (Figure 2.11). Sample 2 presents a medium Na hazard and very high salinity hazard to plants. The remainder of the samples will only pose a low Na with samples 5 and 7 also posing only a low salinity hazard and samples 1, 3, 4, 6, 8 and 9 posing a medium salinity hazard.

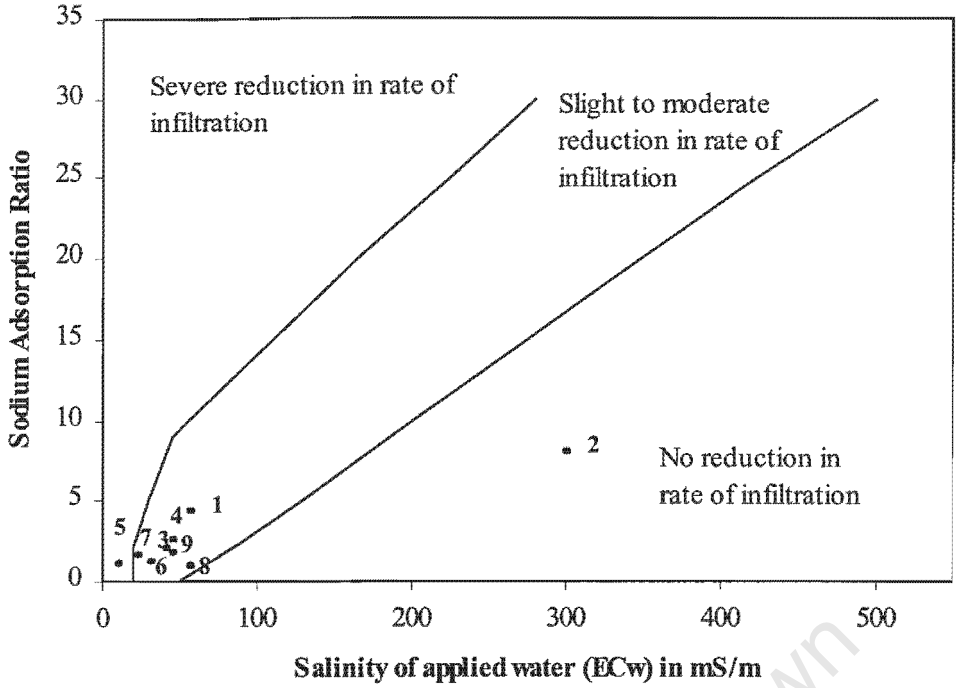

Figure 2.10. SAR vs. EC for all water samples showing classification of water based on its potential to cause soil dispersion (Ayers and Westcot, 1985)

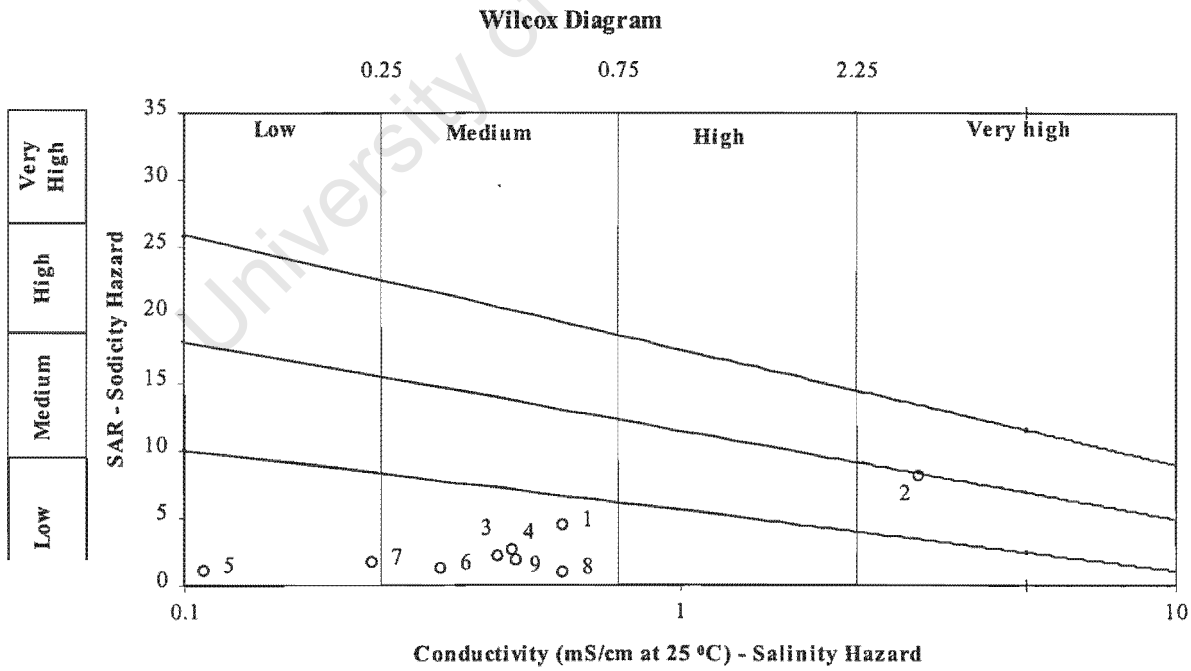

Figure 2.11. Wilcox diagram indicating severity of salinity and sodicity hazard to plants (Lloyd and Heathcote, 1985)

2.6.5.5 Scaling or corrosive potential

The water used privately and in the Klein Karoo water scheme, is abstracted and transported along pipes, some of which may be concrete. The water is subsequently used in homes and for irrigation. The scaling or corrosive potential of the water is important to consider as this property will affect the water distribution and irrigation pipes, and geysers and boilers used. Scaling is the deposition of a precipitate of calcium carbonate onto water conveying equipment. An ideal precipitation potential for $CaCO_3$ is 4 mg/L as this provides a thin protective coating of calcium carbonate on the inside of metal and concrete piping and protects against corrosion and aggression (Snoeynik and Jenkins, 1980). The saturation indices determined for calcite (Table 2.4) are all negative which indicates that precipitation of the Ca-carbonate will not occur and thus the waters are corrosive. The SI's for the iron minerals are positive and the deposition of iron precipitates may lead to clogging of distribution pipes as has already been observed in the riser pipes and well screens of most of these wells (except 5).

Corrosion is defined as the removal of metal from the fabric of well installations and water distribution systems (Lloyd and Heathcote, 1985). In groundwater situations ferric hydroxide may precipitate which restricts the corrosion rate because it forms a tenacious coating. When well casings are exposed to the atmosphere, oxide films develop on the metal surface. When the metal is immersed in a corrosively active water, like that of the wells in the Klein Karoo, anodic areas develop at the point where the oxide film is weak while cathodic areas occur where the oxide film is thicker. The ferric hydroxides deposit on the cathodic areas and metal is removed from the metal at the anodic areas (Lloyd and Heathcote, 1985). This corrosion can occur on metal pumps that are immersed in corrosive water. It is thus prudent to avoid using metal well screens and pipes if possible in the waters where this is likely to occur and in the Klein Karoo PVC is used in place of metal. Stainless steel is less subject to corrosion than other metals but in reducing waters, its potential to corrode can increase (Lloyd and Heathcote, 1985).

2.6.5.6 Overall assessment of water quality

Samples 5 – 8 are used as domestic water supply for the communities of Dysseldorp and Outshoorn and are treated before use. The treatment of this water includes aeration of the sample and then settling of the colloidal matter in settling tanks. The water is then put through sand-bed filters, sanitised and the pH is adjusted and then distributed to the community. The

aeration and pH adjustment of the water causes Fe to drop out of solution and in doing so probably removes most of the trace metals, which will co-precipitate or be scavenged by the Fe-precipitate. The scavenging and co-precipitation of trace metals is especially relevant to sample 8 that has high trace metal concentrations.

2.6.6 Influence of geology on the chemistry of the water

The bulk chemistry of the aquifer host rocks is unquantified and thus comparisons between the water chemistry and geology can only be qualitative. The geology of the sampling sites comprises predominantly sandstones and quartzites with minor shale and siltstone lenses. The waters of all the wells are in equilibrium with quartz (Table 2.4), which confirms the geology of the aquifer. The source of Fe in the waters may be the sandstone/quartzites or the shale and siltstone.

2.7 Conclusions

From the chemical analysis of the water samples, the following conclusions can be made. All the wells in which precipitation of iron oxyhydroxides is occurring have total iron concentrations that range from 1.04 to 44.2 mg/L. The well in which no precipitation has been found, has a total iron concentration of 0.11 mg/L. Ferrous iron is the dominant iron species in the waters. The *pe* values calculated using the Fe^{2+}/Fe^{3+} redox pair gave values ranging from 5.3 to 10.1 where the most acidic sample, 8, had the highest *pe* value. The reason for the high *pe* value corresponding to the most acidic sample is not clear and further investigation of this needs to be undertaken. The system appears to be poised at a *pe*+pH of 12 and implies that the pe and Fe^{2+}/Fe^{3+} ratio can be estimated from the pH of water in this particular aquifer system.

The results of major ion analyses reveal Na^+ and Cl^- to be the dominant ions in solution for most of the samples with sample 8 being dominated by Na^+ and SO_4^{2-}. The trace metal analyses show that sample 5 has the lowest concentrations of trace metals with respect to all the waters and sample 8 has in general the highest concentrations of trace metals especially Mn, B, Sr, Sn, Ba, W and Rb. The calculated saturation indices for the waters indicate that the waters (except 8) are supersaturated with respect to ferrihydrite and goethite and some are supersaturated with respect to a SO_4-phase, jarosite. These waters will form ferrihydrite in preference to goethite and for goethite to precipitate the ferrihydrite would have to undergo dissolution. Sample 8 is undersaturated with respect to ferrihydrite and may form goethite

directly. The saturation indices further show that the waters are in equilibrium with the sandstones and quartzites that constitute the host rocks for the aquifer and that these waters are not scaling but corrosive. The corrosivity of the waters is due to the low SI for $CaCO_3$ and due to the possibility of corrosive cells being formed on metal containing pipes by localised precipitation of iron oxyhydroxides.

In terms of domestic water use, most of the waters are suitable for direct use without the need for treatment. Samples 1, 3, 4, 7 and 8 require pH adjustment before use for domestic and irrigation use. The pH adjustment in conjunction with aeration should cause precipitation of the Fe remaining in solution for those samples where the Fe levels are considered too high. Sample 8 may require additional treatment prior to use to ensure the removal of the elevated concentrations of Al, Pb, Cd, Co, Zn and Ni and sample 4's F^- concentration needs to be lowered prior to use.

Samples 1, 3, 4, 6, 8, and 9 are suitable for irrigation use as the potential for soil dispersion and the Na and salinity hazards with respect to plants, are moderate. Monitoring of the soil and suitable crop selection will need to be performed. Sample 5 poses no hazard to plants but will cause a severe reduction in infiltration due to soil dispersion and thus may not be suitable for irrigation use. Sample 2 will not cause soil dispersion but poses a moderate hazard in terms of Na and a high hazard in terms of salinity to plants and is only be suitable for salt tolerant crops. Sample 7 is very suitable for irrigation use due to only moderate soil dispersion potential and no hazard to plants.

The majority of the waters are suitable for livestock watering if the Fe concentrations are reduced for samples 2 to 4, 7 and 8 by treatment. The concentration of Al and Cd in sample 8 will have to be reduced before this water is usable for livestock watering.

CHAPTER 3 GEOCHEMISTRY OF PRECIPITATES

3.1 Introduction

Ferrihydrite formation is a typical phenomenon wherever Fe^{2+} containing spring and groundwater appear at or near the aerated surface. Under these conditions, Fe^{2+} is abiotically, and sometimes biotically, oxidised at a very high rate preventing the formation of more crystalline oxides (Cornell and Schwertmann, 1996). In the Klein Karoo, some groundwater wells have been found to precipitate iron oxyhydroxides on the screens, riser pipes and pumps of the wells. The mineralogy of the precipitate that forms has to date not been fully investigated. One objective of this study was therefore to characterise the precipitates as fully as possible using a variety of methods. A second objective was to relate, if possible, the composition of the precipitates to the groundwater composition and overall geochemistry of the aquifer.

3.2 Sample collection

Samples of precipitate were collected at eight of the nine wells that were sampled for water. The samples were taken from either the clogged pipes or casings found on the surface or from the well itself (i.e. fresh) where possible (Table 3.1). A sample was not obtained from well 9 as there was no precipitate available at the time of sampling however, the precipitate from well 9 had been previously sampled and this sample was used for the analyses. Fresh samples were stored in water from the well and dry precipitates were stored in airtight bottles.

3.3 Analytical methods

3.3.1 X-ray powder diffraction (XRD)

The mineralogy of the precipitates was determined using X-ray diffraction. A portion of the sample was ground using an agate mortar and pestle and pressed into an aluminium frame that was placed in the Phillips PW3890 X-ray diffractometer fitted with a Cu X-ray tube (Cu Kα = 1.542 Å) for analysis. The instrument was set to scan over a 2θ range from 5° to 75°, continuously in 0.05^0 steps of 2.8 sec duration. Further details are in Appendix B.3.

Table 3.1. Source and description of precipitate samples (numbers refer to wells providing water samples in Chapter 3)

Sample no.	No. of samples	Details of samples	Colour*
1	2 (1A and 1B)	A- Fresh sample at 20 m from surface along riser pipes;	A- Dark brown 10YR 3/3;
		B- Fresh sample from near the pump.	B- Dark brown 7.5YR 3/4.
2	2 (2A and 2B)	A- From steel casing on the surface;	A- Strong brown 7.5YR 4/6;
		B- Fresh sample of tank sludge.	B- Strong brown 7.5YR 5/8.
3	1	Sample from pipes on surface.	Dark reddish brown 5YR 3/4.
4	1	Fresh sample from pipes.	Brownish yellow 10YR 6/8.
5	0	No precipitation occurring.	–
6	1	Sample from pipes on surface.	Dark reddish brown 5YR 3/4.
7	3 (7A, 7B and 7C)	A- Fresh sample of dislodged precipitate from pipes;	A- Strong brown 7.5YR 5/8;
		B- Fresh sample of hard precipitate dislodged during cleaning of pipes;	B- Strong brown 7.5YR 4/6;
		C- Fresh sample of soft precipitate from end of transmission pipe.	C- Yellowish brown 10YR 5/8.
8	1	Sample from pipes at DWAF workshop combined with previous sample taken.	Strong brown 7.5YR 4/6.
9	0	No precipitate available, sample at UCT used.	Strong brown 7.5YR 5/8.

* Determined using a Munsell® Soil Color Chart (1992)

3.3.2 *Fourier transform infrared spectrometry (FT-IR)*

Samples were air–dried and finely powdered using an agate mortar and pestle. Approximately 2 mg of sample was weighed out and mixed with 200 mg of oven-dried (110 ^{0}C) KBr. The sample–KBr mixture was then ground in an agate mortar and pestle to a fine powder and pressed in a dye under 10 tonne pressure for 1 minute. The discs were analysed with a Paragon FT-IR spectrometer over a range of 400 to 4000 cm^{-1}, at a step rate of 4 scans per 4.0 cm^{-1}. Details are provided in Appendix B.5.

3.3.3 *Scanning electron microscopy with energy dispersive X-ray spectrometry (SEM-EDS)*

Precipitate samples were vacuum–air–dried in a dessicator overnight and then mounted using a carbon–based glue onto metal stubs and viewed with a Lecia Stereoscan SEM. Energy dispersive spectrometry (EDS) was used to obtain spot semi-quantitative chemical analyses of

3.4 Previous Work

Previous work on the precipitates and water chemistry was done in February 1999 by Fey et. al. at the University of Cape Town, for Groundwater Consulting Services (GCS). Table 3.2 gives a summary of the findings. The four wells, DL17, DG110, DP28 and VG2 were re-examined as part of the research.

Table 3.2. Summary of February 1999 study (Fey et al., 1999)

Sample	DL17	DG110	DP28	VG2
Morphology (SEM)	Irregular spherical particles, aggregated	Irregular, large angular and small spherical particles	Small needle-like structures, aggregated	Irregular spherical particles, aggregated
Particle size	~200nm–1μm	Bimodal, 100μm and 1 μm	0μm and <200nm	~200nm-1μm
Elemental composition (EDS)				
Major	Fe, O	Fe, C, O	Fe, C, O	Fe
Minor	Si, Ca, Cl	Si, P	S	O, P, Si
Trace	P		Si	S
Mineralogy (XRD)	Poorly crystalline ferrihydrite	Amorphous	Goethite	Poorly crystalline ferrihydrite
Saturation indices				
Ferrihydrite	2.90	2.53	-0.172	1.69
Goethite	7.29	6.92	4.22	6.08
Natrojarosite	4.55	5.46	4.81	1.43
Manganite	14.5	12.6	6.51	15.0

3.5 Results and discussion

3.5.1 Mineralogy

3.5.1.1 XRD data

The following section presents the results of the XRD identification that was used to obtain the mineralogy of the samples. No attempt was made to go into the detail on the significance of the diffractograms. The XRD patterns for the precipitates have been grouped on their broad similarities in Figures 3.1 and 3.2. The precipitates showing mainly two broad halos at about 2.53 and 1.47 Å in Figure 3.1, are similar to the two-line ferrihydrite of Cornell and Schwertmann (1996). Precipitates (2B, 7A, 7B and 9) show evidence of the more crystalline 6-line ferrihydrite in the form of additional broad reflections at 2.24 and 1.72 Å, whereas precipitates (4 and 7C) are the less crystalline two-line ferrihydrite.

In Figure 3.2, three precipitates (2A, 3 and 8) appear to consist almost entirely of goethite (main reflections at 4.18 and 2.45 Å) with little indication of other phases being present. In samples 1A, 1B and 6, there is some evidence of crystallinity but this is superimposed on the broad halos characteristic of ferrihydrite, which are evident in all the patterns in Figure 3.1. In samples 1B and 6 the more crystalline material consists mainly of goethite with strongest peaks at 4.18 and 2.45 Å whereas in sample 1A it would appear to be made up mostly of a phyllosilicate compound (strong reflection for randomly orientated clay at 4.5 Å). A similar, though smaller, amount of silicate clay (4.5 Å) appears to be evident in the pattern for sample 1B together with a trace amount of lepidocrocite. All three of these precipitates (1A,1B, & 6) appear to contain traces of quartz (3.33 Å).

Based on XRD evidence, three groups of precipitate may be recognised: **I** those consisting almost entirely of ferrihydrite (Figure 3.1); **II** those consisting mainly of goethite and **III** precipitates of intermediate mineralogical composition (Figure 3.2). It should be noted, however, that sample 1A is perhaps more appropriately classified in group **I** but with a silicate clay impurity. The mineralogical identifications for each sample are summarised in Table 3.3.

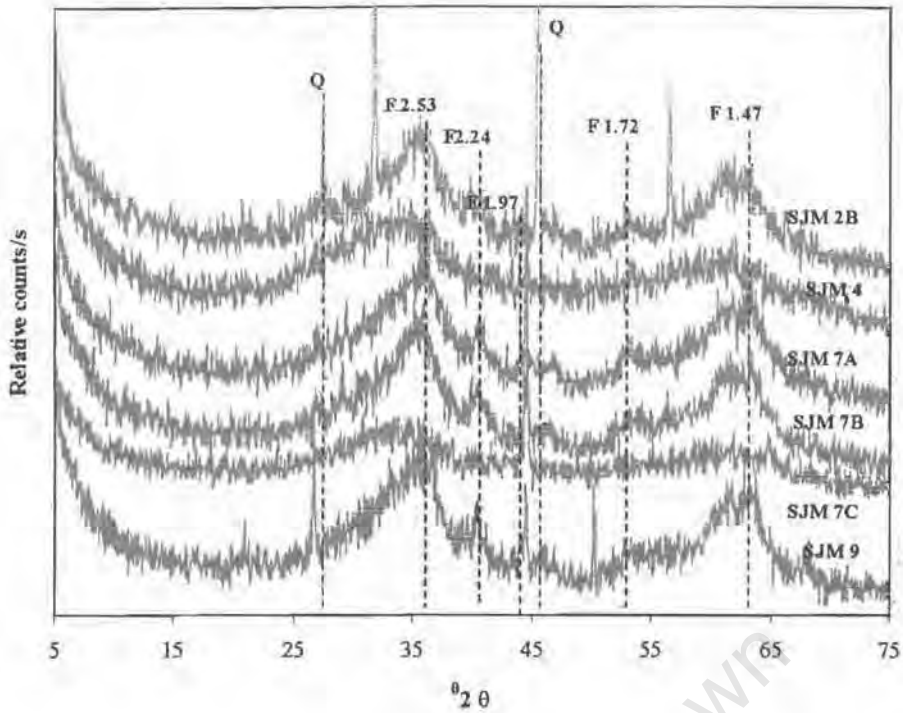

Figure 3.1. XRD diffractograms of the more poorly crystalline precipitates (**Q:** quartz, **F:** ferrihydrite, **G:** goethite and **K:** kaolinite).

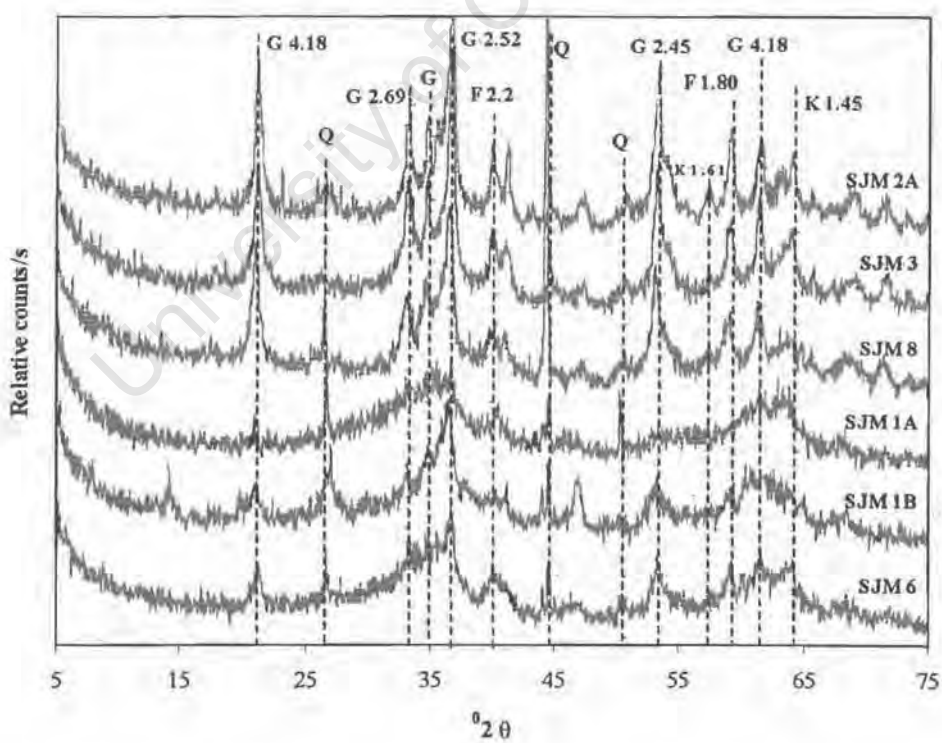

Figure 3.2. XRD diffractograms of more crystalline precipitates consisting of predominantly goethite (2B, 4, 7A) and ferrihydrite and goethite and/or a silicate component (7B, 7C, 9) precipitates (**Q:** quartz and **F:** ferrihydrite)

Table 3.3. Classification of precipitates according to mineralogy

Precipitate sample number	Precipitate type
1A	Mixture of ferrihydrite and a silicate component
1B	Mixture of ferrihydrite and goethite, with a smaller silicate component and trace lepidocrocite.
2A	Goethite
2B	Ferrihydrite (well ordered)
3	Goethite
4	Ferrihydrite (poorly ordered)
6	Mixture of ferrihydrite and goethite with trace quartz
7A	Ferrihydrite (well ordered)
7B	Ferrihydrite (well ordered)
7C	Ferrihydrite (poorly ordered)
8	Goethite
9	Ferrihydrite (well ordered) and trace quartz

Samples 2A and 2B should be the same as they are from the same well but 2A is a goethite and 2B is a well-ordered ferihydrite. Sample 2B was a sample of the tank sludge and was thus a relatively fresh precipitate whereas 2A was from the well casing and may have formed under different conditions (over a longer period of time allowing the precipitate to 'age' to goethite).

3.5.1.2 Infrared spectra

An initial visual assessment of the spectra obtained by FT-IR (Figure 3.3) appeared to confirm the groupings made using XRD and the spectra have been grouped accordingly. The FT-IR spectra do not provide much more than some of the mineralogical information supplied by XRD. In Figure 3.3 A, the broad intense band 940 cm^{-1} is probably diagnostic for ferrihydrite containing a Si impurity (Cornell and Schwertmann, 1996), while in Figure 3.3 B, the bands at 882 and 796 cm^{-1}, correspond with the δ-OH and γ-OH bands diagnostic for goethite (Cornell and Schwertmann, 1996). In Figure 3.3 C, the spectra for precipitates 1A and 1B display a significant absence in the 1000 cm^{-1} region suggesting Si-O stretching vibrations (Klute, 1986) in confirmation of the XRD identification of the silicate clay component in these samples.

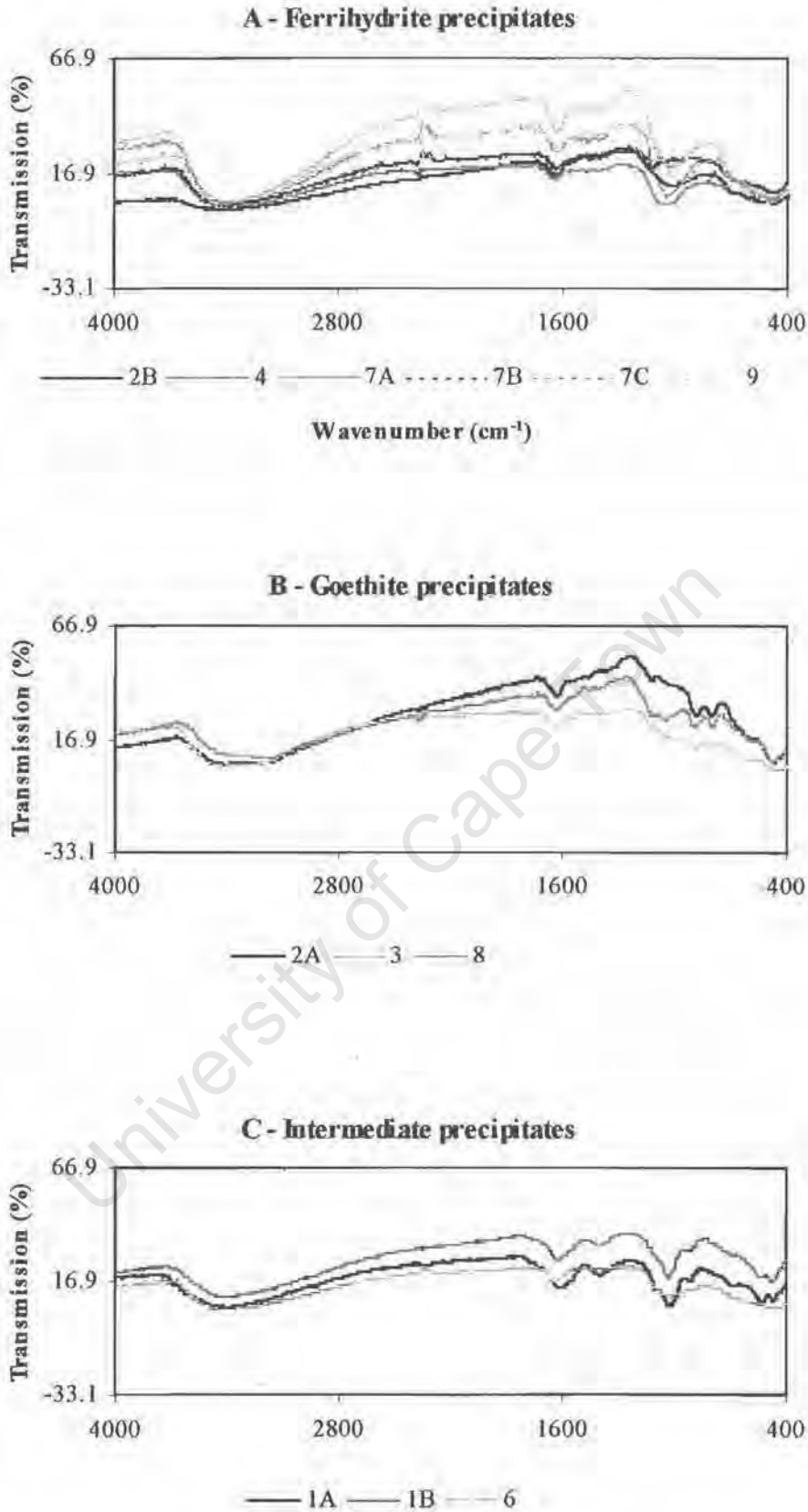

Figure 3.3. Infrared spectra for the three precipitate groupings based on XRD patterns (spectra in 3.3A correspond to precipitates in Figure 3.1; 3.3B and C correspond to precipitates in Figure 3.2A and B respectively).

3.5.2 *Morphology*

The morphology of the precipitates was examined by SEM for all samples and by TEM for selected samples. Typical morphologies for synthetic iron oxides are listed for reference purposes in Table 3.4. Note that the SEM images are represented at a variety of scales, shown by the bar scales at the bottom of the images.

Table 3.4. Typical morphology of iron oxyhydroxides*

Oxide	Principal morphology	Other morphologies
Goethite	Acicular (spiked)	Stars (twins), hexagons, bipyramids, cubes, thin rods
Lepidocrocite	Laths	Tablets, plates, diamonds, cubes
Akaganéite	Somatoids, rods	Stars, crosses (twins), hexagons, prisms
Schwertmannite	"hedge-hog" aggregates	
δ-FeOOH	Plates	Thin, rolled films
Feroxyhyte	Plates	Needles
Ferrihydrite	Spheres	
Hematite	Hexagonal plates, rhombohedra	Spindles, rods, ellipsoids, cubes, discs, spheres, double ellipsoids, stars, bipyramids
Table 4.3 continued		
Magnetite	Octahedra	Intergrown octahedra (twins), rhombic dodecahedra, cubes, spheres, bullets
Maghemite	Laths or cubes	Plates, spindles
FeO	Cubes	Irregular pieces
$Fe(OH)_2$	Hexagonal plates	

- from Cornell and Schwertmann (1996)

3.5.2.1 Ferrihydrite sample morphology

Figure 3.4 A, B and C show the typical morphology of samples 2B, 7A and 9 respectively, which is separate spheres that range in size from <1 μm to 1μm in diameter. In natural environments, the precipitate particle size is usually <0.1 μm due to the presence of impurities. The unexpected larger diameter observed by SEM for these precipitates is possibly due to aggregation of smaller particles that could not be distinguished at the magnification used for the examination. The morphology of these precipitate samples is consistent with the description in Table 3.4. SEM images of samples 4 and 7C show the same spherical structure but particles appear to be flatter (Figure 3.5 A and B). These two samples were determined by XRD analysis to be poorly ordered ferrihydrite and this could explain the less spherical nature of these two samples. The EDS spectra (not shown) for 4 and 7C show minor P in the precipitate and this may be influencing the structure of the precipitate.

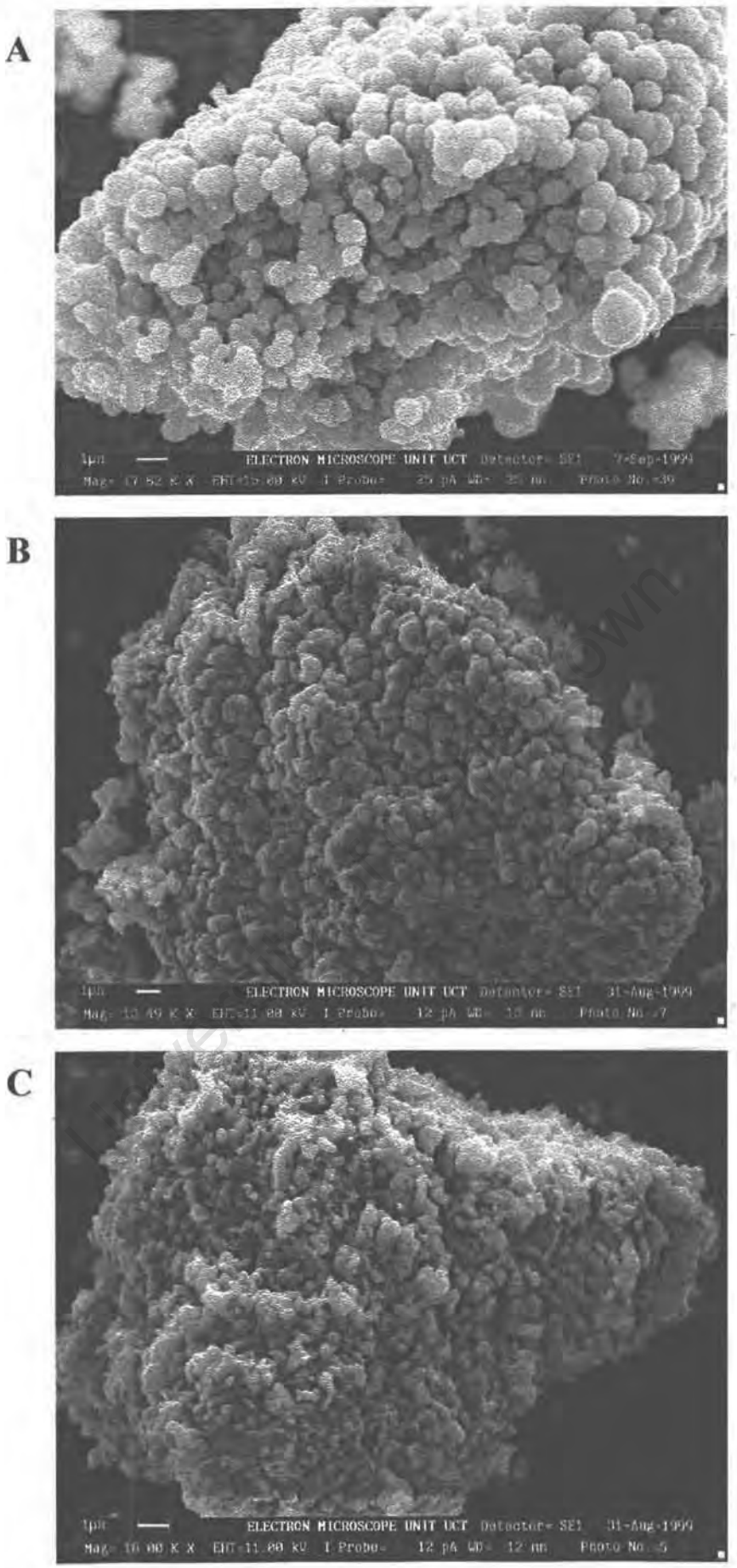

Figure 3.4. Typical morphology of ferrihydrite samples. **A** – 2B; **B** – 7A; **C** – 9.

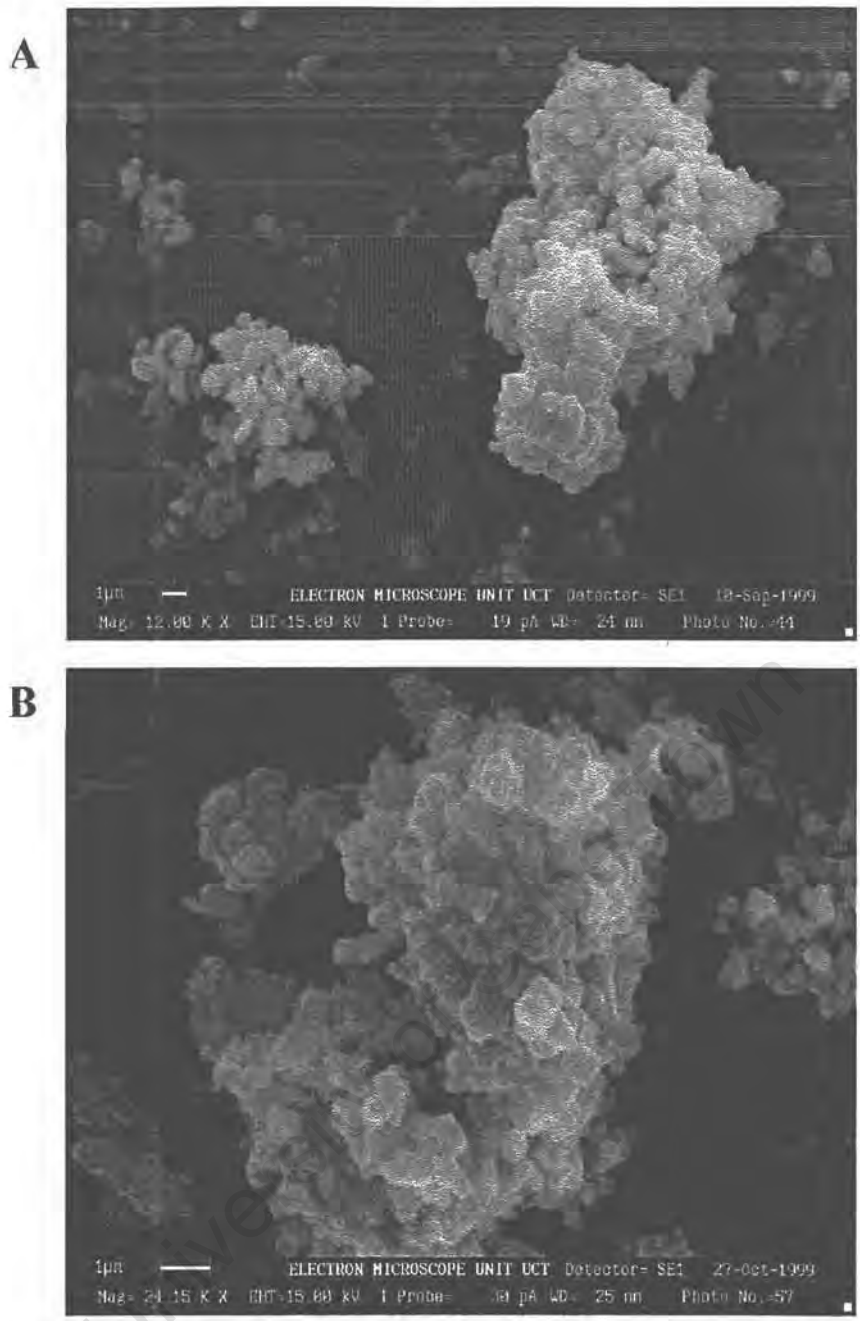

Figure 3.5. SEM images showing the typical morphology of samples 4 (**A**) and 7C (**B**)

Samples 9 and 7C were also viewed by TEM. Figure 3.6 A shows the typical morphology observed a high magnification for sample 7C which is round spheres that are approximately 200 ηm in diameter and are aggregated together. Figure 3.6 B shows the high magnification morphology for sample 9, which is a spherical structure as found in sample 7C with the diameter of the spheres ranging in size from 100 ηm to 200 ηm. The diffraction pattern (not shown) for sample 9, using TEM, indicated a mixture of poorly crystalline and crystalline phases. This is consistent with the XRD results that identified a mixture of ferrihydrite and quartz phases for sample 9.

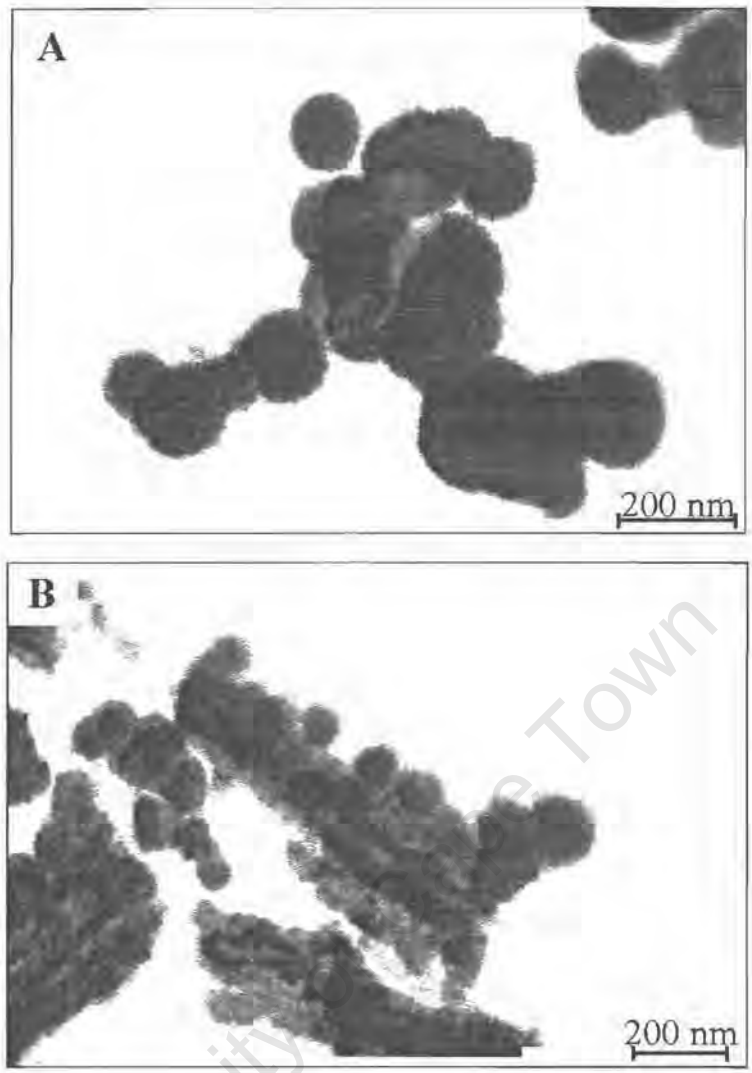

Figure 3.6. TEM images of samples 7C (**A**) and 9 (**B**) showing the spherical morphology

3.5.2.2 Goethite sample morphology

The samples that were classed as being predominantly goethite by XRD show numerous morphological configurations. Figure 3.7 A and B show the typical acicular morphologies of samples 2A and 8 respectively. The acicular crystals in both samples appear to form elongated and botriodal particle aggregates. Sample 2A had several forms of precipitate other than the acicular morphology. In Figure 3.8 A, the acicular particles display a "hedge-hog" morphology closely resembling the schwertmannite of Cornell and Schwertmann (1996, Figure 3.22). However the EDS spectra (not shown) of the sample did not show any S in this precipitate and the XRD analysis did not identify schwertmannite as a possible phase and thus this precipitate may not be schwertmannite. Other interesting morphological variations of sample 2A are shown in Figures 3.8 B and C.

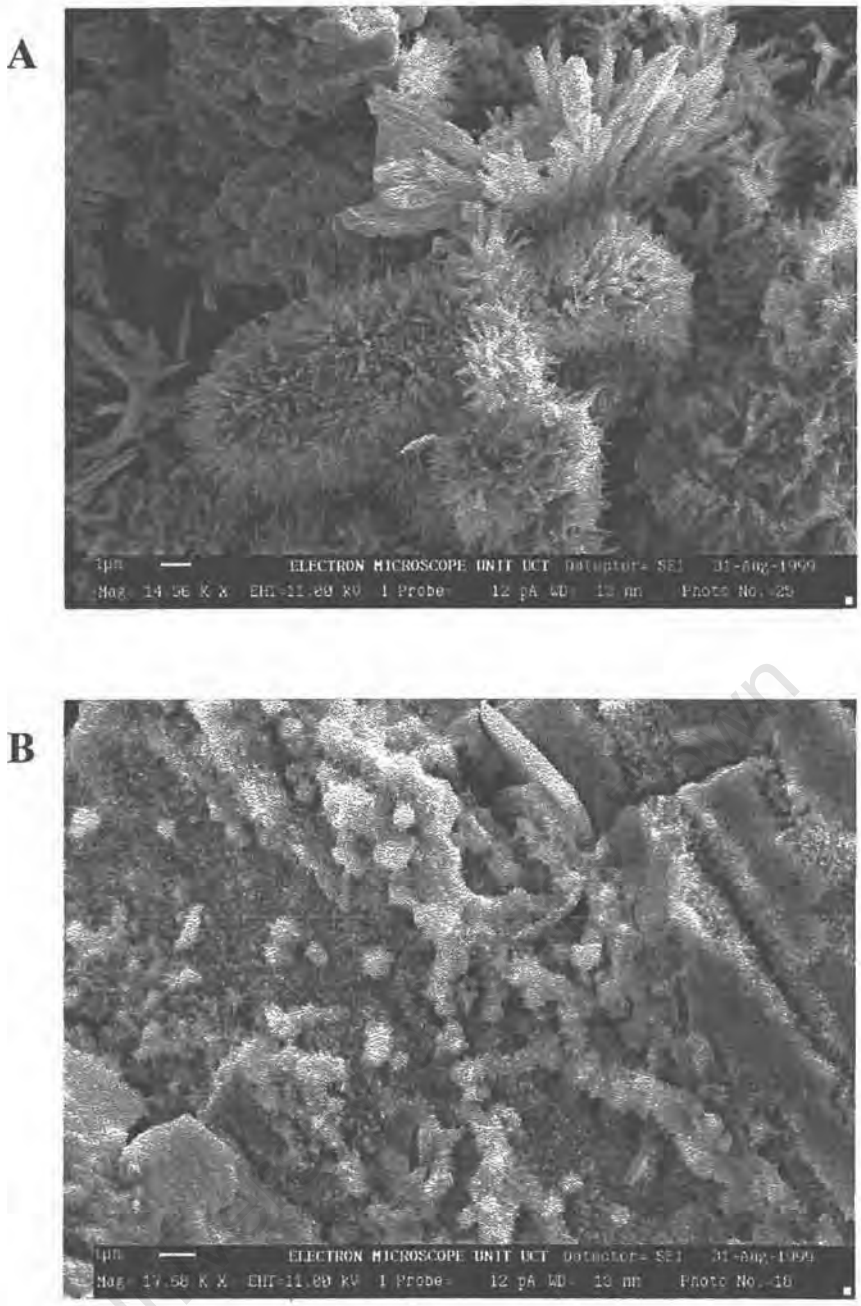

Figure 3.7. SEM images showing the acicular morphologies of goethite samples 2A (**A**) and 8 (**B**)

Figures 3.9 A and B indicate the possible involvement of bacteria in the precipitation of the goethite by acting as nucleation sites. Figure 3.9 A shows rounded particles with a hollow structure that reveals layering. The goethite may have precipitated on a round bacterial particle that subsequently disintegrated (no C other than that due to the C-coating was detected). In Figure 3.9 B the elongated rods resemble bacterial rods (pers. Comm. D. Gerneke) upon which the goethite appears to have precipitated.

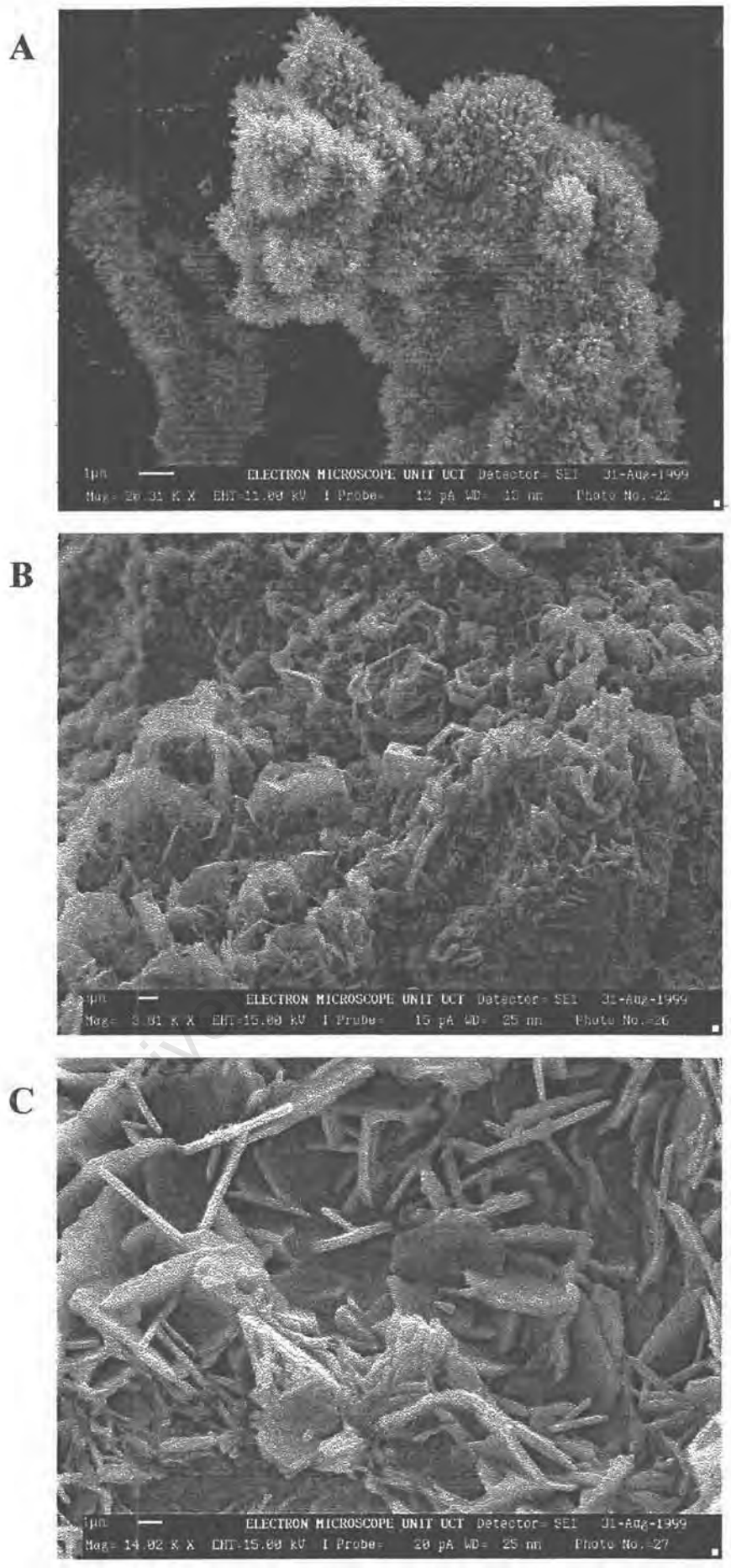

Figure 3.8. SEM images of sample 2A (**A, B and C**) showing interesting morphology

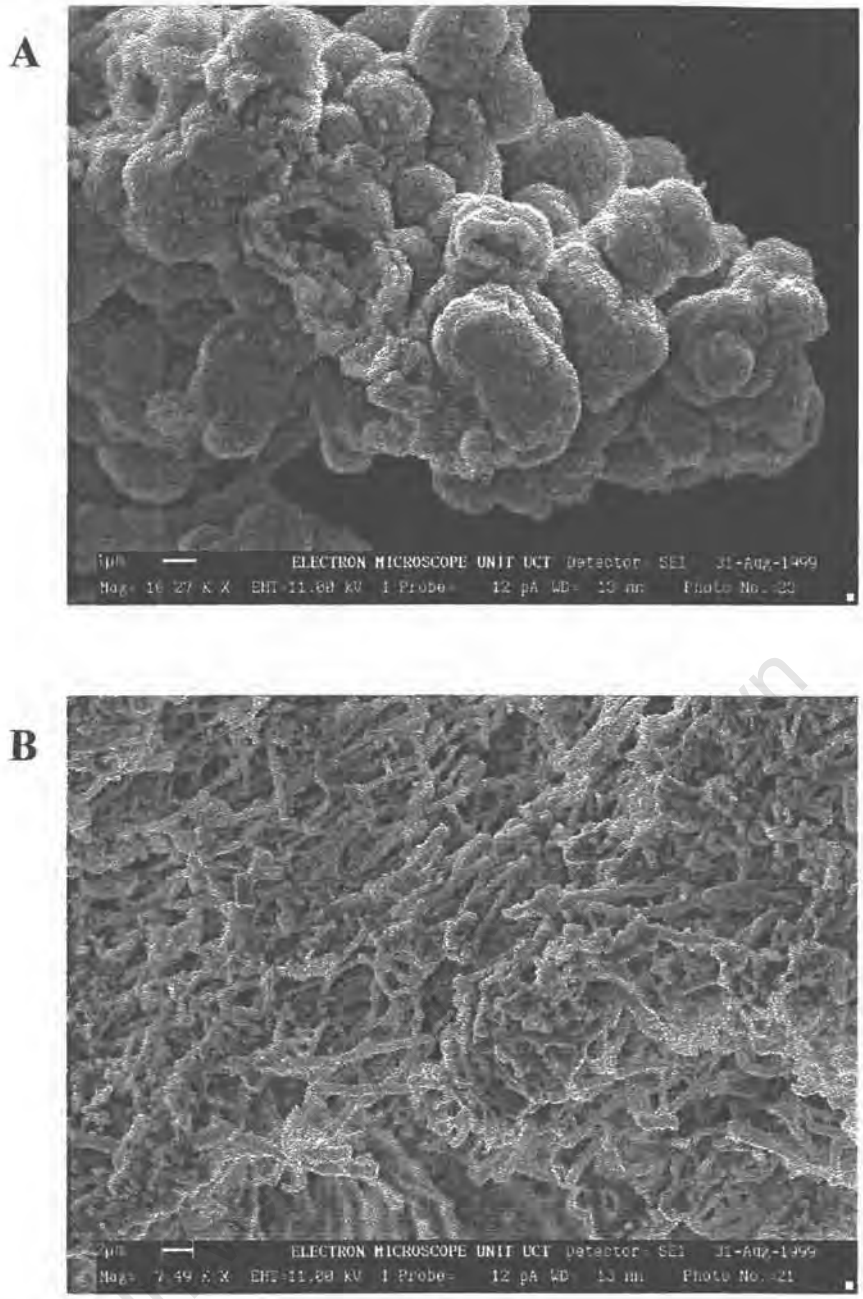

Figure 3.9. SEM images of samples 2A (**A**) and 8 (**B**) showing a hollow sphere and rod shaped particles that may indicate bacterial involvement in iron oxyhydroxide precipitation

Figure 3.10 shows the morphology of sample 3, which are rounded particles aggregated together. This may indicate that the sample is more poorly crystalline than samples 2A and 8 or that the magnification was not high enough to distinguish individual particles of goethite.

The TEM images of sample 8 show aggregates of particles and a hexagonal-shaped particle (Figure 3.11). The particles resemble those found in Cornell and Schwertmann (1996, Figure 3.9) for goethite which is consistent with the XRD identification of this sample. The diffraction pattern for sample 8 under TEM showed the sample to be a crystalline phase, which is expected for goethite.

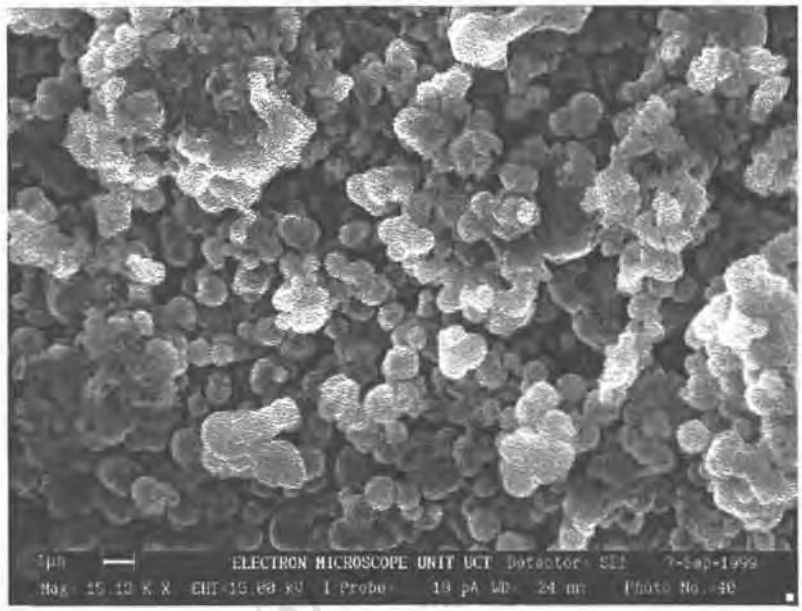

Figure 3.10. SEM images of sample 3 showing the typical morphology of the precipitate

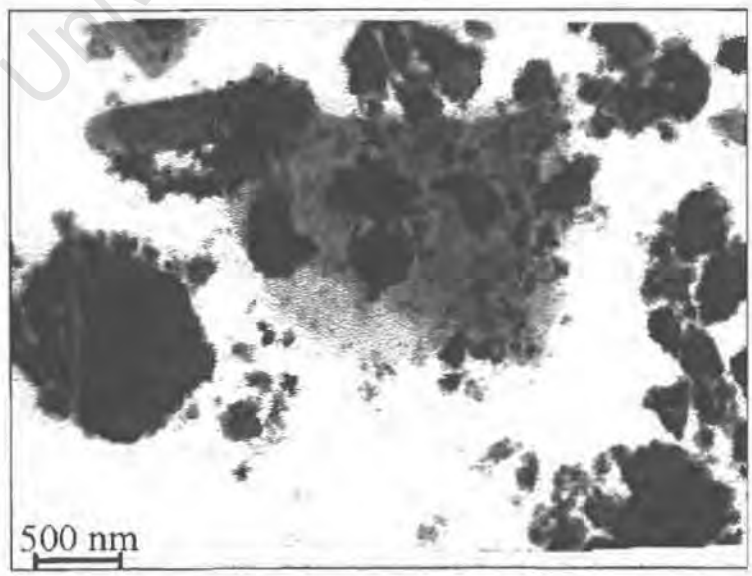

Figure 3.11. TEM image of sample 8 showing the morphology at high magnification

3.5.2.3 Sample morphology of intermediate precipitates

Sample 1A consists of flake-like particles being sub-micron in size, which are aggregated together in a porous structure (Figure 3.12 A). Sample 1B displays more rounded spheres of precipitate than sample 1A, which appear to have grown together. (Figure 3.12 B). Figure 3.12 C, shows a well developed spherical structure for sample 6 with the particles aggregating together. The spherical morphology observed for these precipitates is typical for ferrihydrites (Cornell and Schwertmann, 1996) and consistent with the XRD identification of these samples. The EDS spectra (not shown) of samples 1A and 1B show that they are iron oxides with minor Si and Al. The presence of Si and Al is consistent with the identification of an alumino-silicate phase, in the two samples, by XRD. The EDS (not shown) of sample 6 indicated the presence of minor Si that was also identified by XRD. Sample 6 was also examined by TEM and Figures 3.13 A and B show the fine particles forming aggregates and rounded particles that resemble the TEM images for ferrihydrite in Cornell and Schwertmann (1996, Figure 4.23b). Needle-like morphology is also visible in Figure 3.13 B (marked by the circle) which resembles that found in Cornell and Schwertmann (1996, Figure 4.9c) for goethite. The diffraction pattern (not shown) under TEM indicated that this precipitate is poorly crystalline. The two different TEM morphological features and the poorly crystalline nature indicated by the diffraction pattern are consistent with the XRD findings for this sample.

3.5.2.4 Effect of morphology on clogging

Goethite has a surface area range of 8-200 m^2g^{-1} and ferrihydrite 200-400 m^2g^{-1}. High surface areas (80-150 m^2g^{-1}) are reported for goethites formed by oxidation of Fe^{2+} systems at pH 6-7 and room temperature. Data concerning the surface area of schwertmannite is limited. Due to poor crystallinity, the surface areas are high and range from 125-255 m^2g^{-1} (Cornell and Schwertmann, 1996). The differences in surface area have important implications in terms of both the ability to block the well and to scavenge trace metals from solution. Ferrihydrite has a higher surface area in general when compared with goethite and thus it will form a larger bulk, porous precipitate as observed in the SEM analysis of the precipitates. Thus, the ferrihydrite precipitates will possibly clog the wells at a faster rate than the goethite precipitates. However, the goethite will be more crystalline and may thus be harder to remove than the loosely aggregated ferrihydrite. Goethite would thus require more severe physical and chemical remediation methods than the wells clogged with ferrihydrite, which could possibly be removed by mechanical means alone.

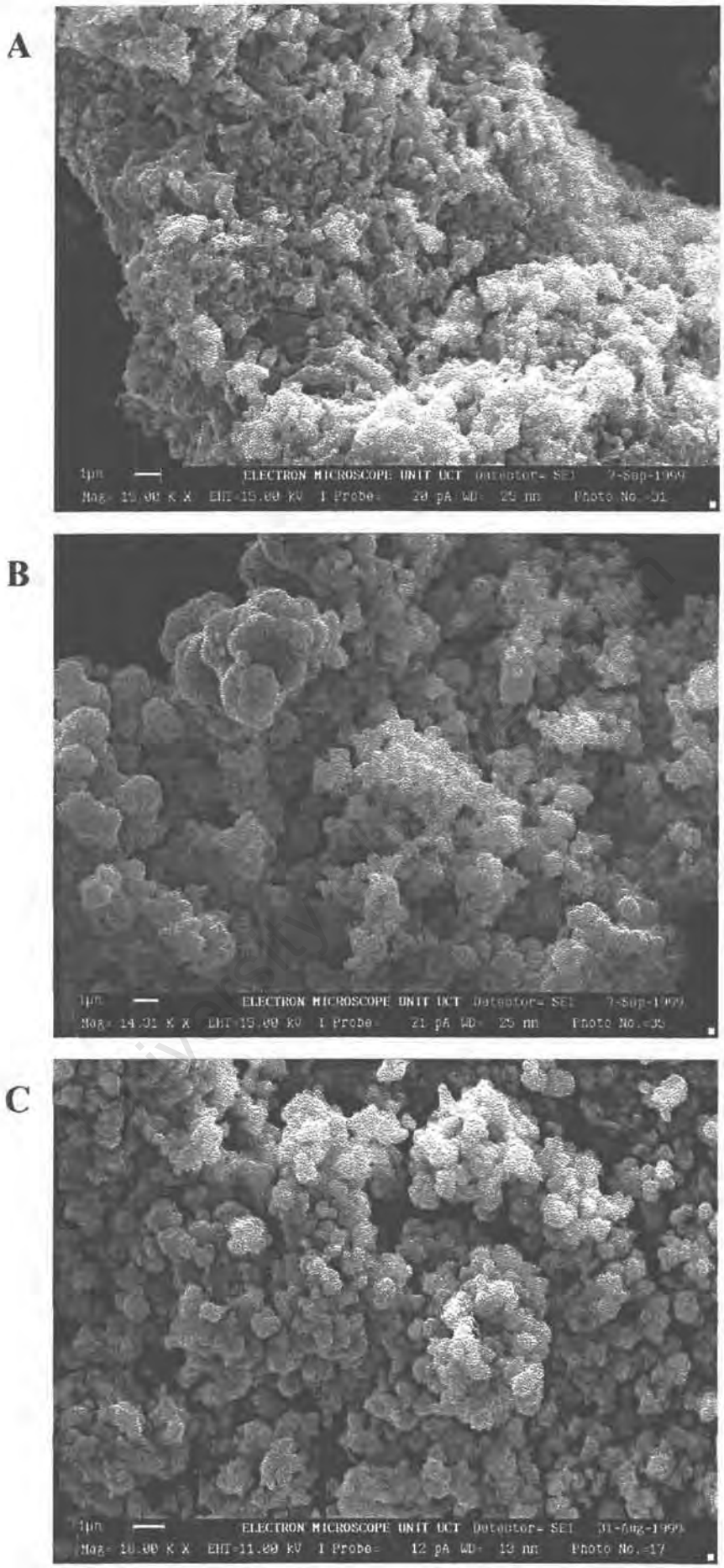

Figure 3.12. SEM images of samples 1A (**A**), 1B (**B**) and 6 (**C**) showing the morphology

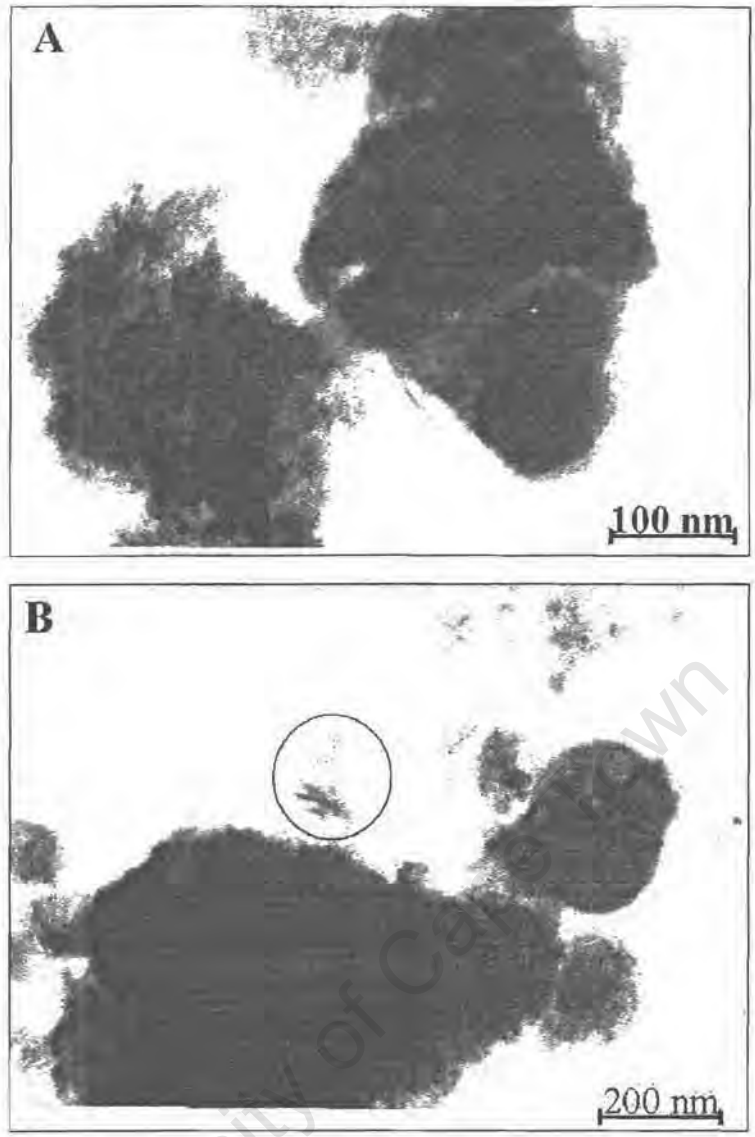

Figure 3.13. TEM images of sample 6 (**A** and **B**) showing morphological characteristics. The circle marks the needle-like morphology

3.5.3 Bulk composition

3.5.3.1 Organic carbon

Table 3.5 lists the results of the organic carbon analysis. The organic carbon content of the precipitates ranged from 0.16 to 9.04 %. In a study on iron oxides in Finnish water treatment facilities by Carlson and Schwertmann (1987) the oxides were found to contain between 0.8 and 11.2 % total organic carbon. The authors found that the concentration depended on the concentration of organic C in the water and the intensity of bioproduction (algae) in the treatment plant (Carlson and Schwertmann, 1987). In general the precipitates of intermediate crystallinity have a higher organic carbon content on average (4.80 %) with the goethite precipitates containing 1.04 % and ferrihydrite precipitates containing 0.89 %. This may

indicate that the precipitation for the intermediate precipitates involves a larger number of bacteria than for the precipitation of goethite and ferrihydrite.

Table 3.5. Organic carbon data for precipitate samples

Precipitate	Sample number	% Organic Carbon
Intermediate	1A	9.04
	1B	4.40
	6	0.95
Goethite	2A	1.26
	3	0.55
	8	1.30
Ferrihydrite	4	0.98
	7A	0.50
	7B	0.41
	7C	0.16
	9	0.53

3.5.3.2 Major and trace element composition

The XRF analysis of the precipitate confirmed the iron-rich nature of the precipitates with the Fe_2O_3 concentrations ranging from 44 to 81 wt%. This concentration range is higher than that found for iron oxides in Finnish water treatment facilities which had a range of between 26 and 43 wt% Fe (Carlson and Schwertmann, 1987). The two samples with the lowest Fe_2O_3 concentrations (1A and 1B) are the samples that have the highest SiO_2, Al_2O_3 and K_2O concentrations (Table 3.6). The presence of SiO_2, Al_2O_3 and K_2O indicates contamination of the sample with K-aluminosilicate which confirms the XRD findings. The contamination is higher in 1A, which has the lowest Fe_2O_3 concentration. These samples do not have the highest Al, Si and K values for the water samples which suggest that the aluminosilicate is incorporated into the precipitate and is not formed in the well. The other samples have Fe_2O_3 concentrations between 66 and 81 wt%.

Sample 7B has the highest concentration of MnO followed by 7A. The water sample for well 7has one of the highest Mn concentrations and it is expected that all the samples from this well would have high Mn. However, 7C has one of the lowest concentrations of MnO. The reason for this discrepancy could be that 7C was taken from the well screen at the end of the distribution pipes where flow is rapid and may be too great for adsorption to occur. Samples 7A and 7B come from the distribution pipes where water may lay stagnant for periods of time thus allowing for Mn to be adsorbed.

Table 3.6. Major element data for the precipitates (wt%.)

	Intermediate			*Goethite*			*Ferrihydrite*				
Sample no.	**1A**	**1B**	**6**	**2A**	**3**	**8**	**4**	**7A**	**7B**	**7C**	**9**
SiO_2	14.93	14.99	3.56	2.07	2.53	2.51	1.27	3.21	5.03	1.39	9.47
TiO_2	0.209	0.148	0.013	0.009	0.008	0.056	0.029	0.029	0.044	0.009	0.058
Al_2O_3	9.49	4.67	0.22	0.22	0.12	1.65	0.73	0.43	0.66	0.23	0.90
Fe_2O_3	44.07	57.54	75.86	77.24	80.77	68.12	66.40	73.33	68.92	67.63	69.20
MnO	0.063	0.074	0.247	0.105	0.050	0.011	0.057	0.630	1.463	0.054	0.077
MgO	0.24	0.21	0.06	0.27	0.03	0.15	0.11	0.06	0.12	0.05	0.19
CaO	0.077	0.038	0.205	0.561	0.013	0.000	0.070	0.013	0.014	0.038	0.680
Na_2O	<0.2	<0.2	<0.2	<0.2	<0.2	<0.2	<0.2	<0.2	<0.2	<0.2	<0.2
K_2O	0.726	0.346	0.033	0.008	0.010	0.258	0.119	0.032	0.049	0.008	0.214
P_2O_5	0.09	0.05	5.69	0.04	2.76	0.86	15.06	4.20	3.88	11.65	1.05
SO_3	<0.1	0.00	1.75	3.82	0.64	4.18	0.46	0.67	0.90	0.56	0.56

The P_2O_5 concentrations for the samples range from 0.04 to 15 wt% with the majority of the samples with a concentration below 6 wt%. Samples 4 and 7C, ferrihydrite, have the highest concentrations of P_2O_3. These minerals could be an iron-phosphate phase, e.g. strengite [$Fe(PO_4)\cdot 2H_2O$] which would need to be confirmed by further work. All the water samples had PO_4^{3-} concentrations below the detection limit for the colourimetric method used.

SO_3 concentrations for the samples are generally below 1 wt% with the exception of samples 6, 2A and 8. 2A and 8 have much higher SO_3 values than the other samples and have the highest concentrations of SO_4^{2-} in the water samples. The SO_3 is either adsorbed onto the

surface of the precipitates or incorporated in the structure. Samples 2A and 8 displayed some characteristics of schwertmannite when examined using SEM and thus the SO_3 is probably part of the precipitate structure, though further work would need to be done to confirm this.

Three of the samples, 6, 7A and 7B have exceptionally high MnO values when compared to the rest of the samples. The concentration in the precipitate does not appear to correlate to the concentration in water or to the concentration of Fe_2O_3 in the precipitate which would be expected as Mn and Fe are known to co-precipitate in nature.

Table 3.7. Trace element data for precipitates (ppm)

	Intermediate			*Goethite*			*Ferrihydrite*				
Sample no.	**1A**	**1B**	**6**	**2A**	**3**	**8**	**4**	**7A**	**7B**	**7C**	**9**
Sc	8.07	7.35	<0.6	<0.6	<0.59	2.77	<0.59	0.68	<0.59	<0.58	0.95
V	180.08	62.4	<3.29	<3.26	<3.29	313.73	<3.17	<3.18	<3.17	<3.12	<3.18
Cr	89.87	55.09	75.05	293.15	20.8	102.31	29.77	79.06	32.54	46.84	40.62
Mn	319.79	403.69	1608.9	634.09	240.76	11.97	334.22	3981.93	10272.1	317.73	434.45
Co	6.24	6.04	16.7	20.33	<5.6	<5.05	<5.22	14.88	34.25	<5.17	<5.3
Ni	14.66	4.41	85.29	131.35	<5.4	<4.55	8.11	<4.94	<4.71	<4.52	<4.65
Cu	23.6	878.39	43.52	171.59	48.3	20.99	2011.25	44.46	46.81	121.35	81.87
Zn	32.86	48.73	946.94	420.16	3620.24	260.8	637.52	132.27	49.69	87.84	864.17
As	70.76	85.28	75.82	35.91	<3.89	798.61	34.39	37.55	40.07	60.69	61.06
Se	4.86	<3.78	<4.77	<4.9	<5.08	709.38	8.51	<4.72	<4.74	<4.5	<4.65
Br	197.36	154.82	<5.72	18.1	<6.03	16.24	<5.17	20.79	27.68	<5.34	<5.56
Rb	58.63	27.80	2.48	<1.95	<2.01	10.61	4.83	<1.89	3.10	<1.88	7.84
Sr	17.02	9.10	25.92	29.37	4.10	6.95	14.52	2.95	3.44	<1.72	81.60
Y	13.11	10.44	<1.89	4.69	2.77	2.78	15.78	<1.83	2.31	3.61	4.23
Zr	57.51	112.40	4.21	<1.75	4.36	22.06	32.83	15.14	14.95	2.83	28.25
Nb	5.26	3.55	<1.58	<1.6	<1.64	<1.51	6.07	<1.54	<1.57	<1.51	<1.55
Mo	2.12	1.83	13.39	18.57	<1.73	3.08	<1.58	2.26	<1.66	<1.6	24.45
Ba	214.17	120.79	423.47	25.59	48.65	38.99	148.3	28.07	59.69	62.91	312.24
Pb	35.3	1718.9	139.7	15.2	25.2	754.4	283.4	129.6	178.0	381.7	270.0
Bi	<8.75	14.19	<14.66	<15.05	<15.64	<14.02	<13.28	<14.49	<14.56	<13.78	<14.31
Th	8.67	6.85	<4.16	<4.14	<4.25	129.33	<3.86	<4.03	<4.08	<4.02	<4.06
U	5.94	11.62	<4.02	4.53	6.46	20.50	25.32	4.54	7.94	5.21	<3.94

When looking at the trace metals there does not appear to be any particular group of precipitates, which show higher or lower concentrations of trace metals in general. Samples 1A and 1B that are thought to be contaminated with a K-aluminosilicate had the highest levels of Sc, Br, Rb and Y which may be related to the presence of the aluminosilicate.

Sample 8 is an exceptional sample in many respects. It is the most acidic water and warmest sample (26 ^{0}C) with a wide range of dissolved trace metals above the average levels for the other water samples. Sample 8 also has unique precipitate trace chemistry when compared with that of the other precipitates. The precipitate from well 8 contains the highest concentrations for V, Mn, As, Se, Th and U, and the second highest concentration of Pb out of all the samples. When comparing the water samples, 8 was also found to contain the highest levels of As, Pb, Th and U but contained no Se and V and only a moderate amount of Mn.

3.5.4 Influence of chemistry on mineralogy and morphology

Both adsorbed and incorporated foreign ions can alter the relative free energies and growth rates of different crystal faces that will in turn modify the crystal habit. That is low levels of impurities can enhance growth of a particular face whereas higher levels block growth. The variations in growth rates result in a distorted morphology and particularly in natural environments there is no distinct morphology by which an iron oxide can be identified (Cornell and Schwertmann, 1996). Sample 2A showed the most variations in morphology and both 2A and 8 had a tendency to resemble schwertmannite although the XRD analysis of the samples did not detect any schwertmannite phase. These two samples also contained the largest amounts of SO_3, with sample 8 having the second highest concentration, with respect to the other samples. The SO_3 in the samples either is adsorbed onto the structure or is part of the structure, which was not determined during this study.

For goethite conditions of rapid growth and/or the presence of impurities, long, thin needles with a high aspect ratio form. The aspect ratio is the ratio of crystal length to width (Cornell and Schwertmann, 1996). Samples 2A and 8 may have formed under such conditions resulting in the acicular morphology observed whereas sample 3 may have formed under different conditions. High levels of silicate species strongly modify the morphology of goethite grown from ferrihydrite at pH 12, which is altered due to retardation of growth. Silica species however do not alter goethite morphology in acid or neutral media and thus should not influence the goethite of the wells in this study (Cornell and Schwertmann, 1996).

3.5.5 *Correlation between water and precipitate chemistry*

Statistical treatment of the water and precipitate chemistry was undertaken to ascertain if there were any significant correlations which would enable prediction of the precipitate type to be made based on the water chemistry encountered. If prediction of the precipitate type could be made then the maintenance programme and procedure could be designed specifically for each well and thus make for a more efficient and cost effective maintenance programme. In Figure 2.6 no clustering of the waters based on the class of precipitate was evident.

To determine if there was any correlation between the pH of the water and the trace and major elements in the precipitate in relation to the concentration of the metal in the water graphs of the ratio of $E_{solution}/E_{solid}$, where E = element, vs. pH (both field and lab values were used) were plotted. This did not show any significant trend for most of the elements due to the lack of data distributed across the pH range.

Statistical correlations were determined for Fe_2O_3, Al_2O_3 and Organic C vs. trace and major element composition of the water and precipitate samples. Spearman rank order correlations were determined where a significant relationship gave an R-value = >0.5 and a p-value = <0.05. A matrix plot was then examined to ascertain if the relationships were real or if there was a few outliers determining the relationship. In most of the correlation graphs, this was the case with the exception of SiO_2 and Al_2O_3 vs., Fe_2O_3. The lack of significant correlations is mainly due to the small number of samples (n = 11) and a lack of distribution of data across the concentration ranges for the elements being correlated.

From the previous chapter, it was determined that most of the water samples are supersaturated with respect to ferrihydrite with the exclusion of sample 8. This sample is supersaturated with respect to goethite but has lower saturation indices when compared to the other samples. According to the Gay-Lussac-Ostwald (GLO) Step Rule which states in terms of solubility that, if the initial state of a soil is such that several solid phases can potentially form with a given ion, the solid phase that forms first will be the one for which the activity ratio is nearest to the activity ratio of the soil followed by formation of the solid phases in decreasing order of activity ratio (Sposito, 1989), we thus expect ferrihydrite to be the first phase formed. In the case of sample 8 goethite would thus preferentially form which was observed.

3.6 Conclusions

The precipitates are relatively pure with the Fe_2O_3 concentration ranging between 66 and 81 wt%. Samples 1A and 1B had lower Fe_2O_3 concentrations of 44 and 58 wt% respectively that was due to dilution by the presence of a layer silicate phase. The majority of the precipitates are ferrihydrite with the development of relatively crystalline goethite in some of the samples. In most cases the waters follows GLO step rule resulting in an initial precipitate of ferrihydrite which may transform to goethite except for sample 8 where the saturation indices indicate that the sample will form goethite in the first phase of crystallisation. The goethite precipitates were all scrapings from pipes that had been on surface for a period of time and the significance of this in terms of precipitate type is unknown. Sample 1A contained some lepidocrocite but it is unclear why is has only developed in this well at this site.

Samples 1A and 1B are different to the rest of the samples in that they contain the most SiO_2, Al_2O_3 and K_2O out of all the precipitates. The XRD indicates that a layer silicate phase is present which would account for the increased levels of SiO_2 and Al_2O_3. Samples 1A and 1B also have the highest concentrations of organic carbon. Samples 1A and1B are different to the other samples because they were removed from the exterior of the riser pipes and not from the interior as with other samples. There was thus more opportunity for entrapment of aluminosilicates and organic matter in the precipitate due to input into the well from the surface environment.

From Table 3.5, elevated SO_3 concentrations are noted in samples 2A and 8 with respect to the other samples. These two samples had the highest concentrations of SO_4^{2-} in the water samples which may account for the higher concentrations of SO_3 and although the Fe^{3+} complexes more strongly with PO_4^{3-} than with SO_4^{2-} (McBride, 1994), the high concentration of SO_4^{2-} could compete with the PO_4^{3-} and thus occupy more of the sorption sites. In general for all the samples, those with a high P_2O_5 tend to contain less SO_3. The samples with the low P_2O_5 tend to contain more SiO_2 that may be explained by the fact that silicate and phosphate compete for the same sites. The apparent sorption of silicate in preference to phosphate may be due to lower availability of PO_4^{3-} in these solutions.

The ferrihydrite samples contain more P_2O_5 than the crystalline goethitic and intermediate precipitates. Samples 4 and 7C that have the highest P_2O_5 concentrations of all the samples and out of the ferrihydrites. These two samples were identified as two-line ferrihydrite and are the most poorly crystalline samples of the ferrihydrites. The poorly crystalline ferrihydrites have greater surface areas than their crystalline counterparts and will therefore have more sorption sites available for the sorption of PO_4^{3-}. This explains the reason for the higher concentrations observed in the ferrihydrites in general. Whether the high sorption of PO_4^{3-} inhibits the transformation to the more ordered 6-line ferrihydrite is unknown.

Adsorption of metals from solution onto oxide surface is known to occur and affects trace metal transport in many natural systems (Benjamin and Leckie, 1981). The adsorption of metals onto the iron oxide surface is due to the positive or negative charge that develops on the surface created by the adsorption or desorption of H^+ or OH^-. The charge therefore varies with the concentration of H^+ and OH^- ions in solution (pH) (Schwertmann and Taylor, 1989). Arsenic and selenium both occur in solution as anions or as neutral species. Under oxidising conditions the As is present as arsenic acid and arsenate (AsO_4^{3-}). For Se the dominant form under oxidising conditions is selenate (SeO_4^{2-}). Arsenate species are strongly adsorbed at near-neutral pH onto iron oxyhydroxides whereas selenate is only weakly adsorbed (Drever, 1997). Vanadium, molybdenum and uranium also occur as anions in solutions (Fairbridge, 1972). Sample 8 has a low pH (3.13) and the iron oxide is expected to be positively charged which increases the sorption sites available for anion adsorption. The sample has the highest concentrations of V, As, Se, Mo and U in the precipitate that is due to its greater anion sorption capacity in comparison with the other samples. The other samples tend to have higher concentrations of metals than sample 8 and are thus removing these from solution. The iron oxides precipitating in these water supply wells are thus filtering the water before its abstraction, which is improving the wells water quality.

CHAPTER 4 CONCLUSIONS AND RECOMMENDATIONS

4.1 Conclusions

The groundwater from the wells in which precipitation of iron oxyhydroxides is occurring have total iron concentrations that range from 1.04 to 44.2 mg/L. The well in which precipitation has not been found has a total iron concentration of 0.11 mg/L in the water. Ferrous iron constitutes greater than 85% of the iron species in the waters. The *pe* values calculated using the Fe^{2+}/Fe^{3+} redox couple, ranged from 5.3 to 10.1 where the most acidic samples tended to have the highest *pe* values.

The results of major ion analyses reveal Na^+ and Cl^- to be the dominant ions in solution for all the samples, with the exception of sample 8 that is dominated by Na^+ and SO_4^{2-}. The trace metal analyses show that sample 5 has the lowest concentrations of trace and sample 8 has in general the highest concentrations of trace metals namely, Mn, B, Sr, Sn, Ba, W and Rb. Saturation indices for the waters indicate that the waters (except 8) are supersaturated with respect to ferrihydrite and goethite and some are supersaturated with respect to a SO_4-phase, jarosite. These waters will form ferrihydrite in preference to goethite and for goethite to precipitate ferrihydrite undergoes dissolution followed by precipitation. Sample 8 is undersaturated with respect to ferrihydrite and may form goethite directly. The saturation indices further show that the waters are in equilibrium with the sandstones and quartzites that constitute the host rocks in the aquifer. The saturation indices for carbonate minerals indicate that these waters are not scaling but corrosive.

In terms of domestic water use, most of the waters are suitable for direct use without treatment. Samples 1, 3, 4, 7 and 8 require pH adjustment before use for domestic and irrigation use. The pH adjustment in conjunction with aeration should cause precipitation of the Fe remaining in solution for those samples where the Fe levels are high. Sample 8 may require additional treatment before use to ensure the removal of the elevated concentrations of trace metals. The F^- concentration in sample 4 needs to be lowered before use. Samples 1, 3, 4, 5, 6, 7, 8, and 9 are suitable for irrigation use with minor treatment to remove Fe and other trace metals. Sample 2 may only be suitable for salt tolerant crops. The majority of the waters are suitable for livestock watering, if the Fe concentrations are reduced for samples with concentrations above acceptable limits.

The XRD examination of the precipitates suggested that the majority are ferrihydrite, while the development of relatively crystalline goethite is apparent in some of the samples. Some of the samples contained a minor, layer silicate phase and sample 1A had minor lepidocrocite. The XRF results show that the precipitates are relatively pure iron oxide with the Fe_2O_3 content ranging between 66 and 81 wt%. Samples 1A and 1B had lower Fe_2O_3 concentrations of 44 and 58 wt% respectively. The XRD indicate that a layer silicate phase is present which would account for the increased levels of SiO_2 and Al_2O_3 in samples 1A and 1B. Sample 1A and 1B have the highest concentrations of organic carbon. Elevated SO_3 concentrations are noted in samples 2A and 8 relative to the other samples. These two samples had the highest concentrations of SO_4^{2-} in the water samples that may account for the higher concentrations of SO_3 in the precipitates. The ferrihydrite samples contain more P_2O_5 than the crystalline goethitic and intermediate precipitates. The two two-line ferrihydrites have the highest P_2O_5 concentrations.

Sample 8 has the highest concentrations of V, As, Se, Mo and U in the precipitate that is due to its greater anion sorption capacity, which is a result of the low pH of the water in this well. The other samples tend to have higher concentrations of metals than sample 8. The iron oxides precipitating in these water supply wells appear to be 'filtering' metals from the water before its abstraction, which is reflected in the elevated trace metal concentrations in some of the precipitates. The 'filtering' of the water is probably improving the water quality of the wells.

The objectives of the study were to:

- Determine the composition of the waters in the wells.
- Determine the composition and morphology of the precipitates.
- Determine any relationships between the water and precipitate chemistry in order to gain a greater understanding of the clogging process.
- Ascertain if precipitation and precipitate type could be predicted.
- Assess water quality in terms of domestic and livestock use.

The composition of the waters and the composition and morphology of the precipitates was successfully achieved using various analytical techniques. However, the identification of the

precipitate type could be enhanced with the use of differential and thermal gravimetric analysis (DGA/TGA). Relationships between the water and precipitate chemistry were determined on a basic level but the study was not able to correlate the water and precipitate chemistry definitively. Sampling of a larger number of wells with a wider range in chemistry and pH, both with precipitation and without, and sampling of fresh precipitates from all the wells may enable correlations to be made. This could enable the prediction of precipitate type and how often and what maintenance procedures need to be undertaken, from the water chemistry. The assessment of water quality with regards to use as a domestic, irrigation and livestock watering supply was achieved.

4.2 Recommendations

Further work needs to be done on the following aspects of this study. The kinetics of each specific well clogging needs to be determined i.e. how long does it take to reduce the specific yield of the well by a standard percentage. Investigation into how the S and P are held in the precipitate, in the structure or adsorbed onto the surface, needs to be examined to determine how this will influence the precipitate type and structure. The aquifer and well geology needs to be quantified and bulk chemistry of the rocks in the area needs to be determined. This will help to gain an understanding of the source of the trace metals in the waters and to be able to allow for correlation of Fe concentration and rock type.

REFERENCES

Armstrong, W.B. (1978) Redox potential measurement as an indication of biochemical well plugging. *Ground Water*, **16**, no. 6, pp. 446-447.

Ayers, R.S. and Westcot, D.W. (1985) *Water Quality for Agriculture*. FAO irrigation and drainage paper, **29**. Rome.

Bao-rui, Y. (1988) Investigation into mechanisms of microbial effects on iron and manganese transformations in artificially recharged groundwater. *Water Science and Technology*, **20**, no. 3, pp. 47-53.

Bau, M., Usui, A., Pracejus, B., Mita, N., Kanai, Y., Irber, W. and Dulski, P. (1998) Geochemistry of low-temperature water-rock interaction: evidence from natural waters, andesite, and iron-oxyhydroxide precipitates at Nishiki-numa iron-spring, Hokkaido, Japan. *Chemical Geology*, **151**, pp. 293-307.

Bigham, J.M. (1994) Mineralogy of ochre deposits. pp. 10-12. ***In:*** D.W. Bowles and J.L. Jambor (eds.) *The Environmental Geochemistry of Sulfide Mine-Wastes*. Mineralogical Association of Canada.

Bourg, A.C.M. (1995) Speciation of heavy metals in soils and groundwater and implications for their natural and provoked mobility. pp. 19-31. ***In:*** W. Salomons, U. Förstner and P. Mader (eds.) *Heavy Metals: Problems and Solutions*. Springer-Verlag, Berlin.

Brookins, D.G. (1988) *Eh-pH Diagrams for Geochemistry*. Springer-Verlag, Berlin.

Carlson, L. and Schwertmann, U. (1987) Iron and manganese oxides in Finnish ground water treatment plants. *Water Research*, **21**, no. 2, pp. 165-170.

Carlson, L., Vuorinen, A., Lahermo, P. and Tuovinen, O.H. (1980) Mineralogical, geochemical, and microbiological aspects of iron deposition from groundwater. pp. 355-364. ***In:*** P.A. Trudinger, M.R. Walter and B.J. Ralph (eds.) *Biochemistry of Ancient and Modern Environments*. Australian Academy of Science, Canberra City.

Clark, L. (1988) *The Field Guide to Water Wells and Boreholes*. John Wiley and Sons, Chichester.

Cornell, R.M. and Schwertmann, U. (1996) *Iron Oxides: Structure, Properties, Reactions, Occurrences and Uses*. VCH Publishers, New York.

Department of Water Affairs and Forestry (1995) *Draft of South African Water Quality Guidelines* (2nd Ed.), Volume 1: Domestic Use. Pretoria.

Department of Water Affairs and Forestry (1995) *Draft of South African Water Quality Guidelines* (2nd Ed.), Volume 5: Agricultural Use - Irrigation. Pretoria.

Drever, J.I. (1997) *The Geochemistry of Natural Waters: Surface and Groundwater Environments*, 3rd edition. Prentice-Hall, Inc., New Jersey.

Driscoll, F.G. (1986) *Groundwater and Wells*, 2nd edition. St. Paul Minnesota, Johnson Division.

Engelbrecht, P. and Jolly, J. (1999) *Iron Precipitation in Boreholes in the Klein Karoo.* Unpublished internal Groundwater Consulting Services report, Cape Town.

Faure, G. (1991) *Principles and Applications of Geochemistry*, 2nd edition. Prentice-Hall, Inc., New Jersey.

Fey, M.V., Petrik, L. and Azzie, B.A. (1999) *Preliminary Chemical and Mineralogical Assessment of Brothel Waters and Precipitates.* Unpublished report, University of Cape Town

Gann, A. and López, C. (1992) Complex Fe-Mn oxide coatings on boulders in a tropical river. pp. 557-560. ***In:*** Y.K. Kharaka and A.S. Maest (eds.) *Water-Rock Interaction*, Vol. 1. A.A. Balkema, Rotterdam.

GCS (1996) *Albertinia: Groundwater Supply Project, Phase II Investigation.* Unpublished Groundwater Consulting Services Report, no. 95-W06-04.Rep2.

Geological Survey (1991) 3320 LADISMITH, 1:250 000 geological series map. The Government Printer, Pretoria.

Herbert, R.B. (1996) Metal retention by iron oxide precipitation from acidic ground water in Dalarna, Sweden. *Applied Geochemistry*, **11**, pp. 229-235.

Kennedy, J.A. and Powell, H.K.J. (1986) Colorimetric determination of aluminium (III) with chrome azurol S and the reactivity of hydrolysed aluminium species. *Analytica Chimica Acta*, **184**, pp. 329-333.

Korhonen, L. (1988) Iron bacteria in the artificially charged groundwater of Kuopio. *Water Science and Technology*, **20**, no. 3, pp. 221-222.

Kothari, N. (1988) Groundwater, iron and manganese: an unwelcome trio. *Water/Engineering & Management*, **135**, no. 2, pp. 25-26.

Kuntze, H. (1982) *Iron Clogging in Soils and Pipes: Analysis and Treatment.* Verlag Paul Parey, Berlin.

Laberty, C. and Navrotsky, A. (1998) Energetics of stable and metastable low-temperature iron oxides and oxyhydroxides. *Geochimica Et Cosmochimica Acta*, **62**, iss. 17, pp. 2905-2913.

Lanyon, R. (1996) *Chemical Analysis of Water Samples from the Rietvlei and Diep River, Cape Town.* Unpublished MSc. Report, University of Cape Town.

Lind, C.J. and Anderson, L.D. (1992) Trace metal scavenging by precipitating Mn and Fe oxides. pp. 397-402. ***In:*** Y.K. Kharaka and A.S. Maest (eds.) *Water-Rock Interaction*, Vol. 1. A.A. Balkema, Rotterdam.

Lindsay, W.L. (1979) *Chemical Equilibria in Soils.* John Wiley and Sons, New York.

Lloyd, J.W. and Heathcote, J.A. (1985) *Natural Inorganic Hydrochemistry in Relation to Groundwater – An Introduction*. Clarendon Press, Oxford.

McBride, M.B. (1994) *Environmental Chemistry of Soils*. Oxford University Press, New York.

Mulder, M.P. (1995) *Grondwatervoorsiening vir Klein Karoo Landelike Waterskema*, Vol. 2. Unpublished Department of Water Affairs and Forestry report, Cape Town.

Munsell (1992) *Munsell® Soil Color Chart*. Revised edition, Macbeth, New York.

Murray, K. and Wade, P. (1996) Checking anion–cation charge balance of water quality analyses: limitations of the traditional method for non-potable waters. *Water SA*, **22**, pp. 27-32.

Patterson, C.G. and Runnells, D.D. (1992) Dissolved gases in ground water as indicators of redox conditions. pp. 517-519. ***In:*** Y.K. Kharaka and A.S. Maest (eds.) *Water-Rock Interaction*, Vol. 1. A.A. Balkema, Rotterdam.

Pitkänen, P., Pirhonen, V. and Snellman, M. (1988) Geochemical modelling of water-rock interaction in deep groundwater. *Water Science and Technology*, **20**, no. 3, pp. 245-246.

Ralph, D.E. and Stevenson, J.M. (1995) The role of bacteria in well clogging. *Water Research*, **29**, no. 1, pp. 365-369.

Schwertmann, U. and Fitzpatrick, R.W. (1992) Iron minerals in surface environments. pp. 7-30. ***In:*** H.C.W. Skinner and R.W. Fitzpatrick (eds.) *Biomineralization: Processes of Iron and Manganese – Modern and Ancient Environments*. Catena Verlag.

Schwertmann, U. and Taylor, R.M. (1989) Iron oxides. ***In:*** J.B. Dixon and S.B. Weed (eds.) *Minerals in soil environments* (2nd edition). Soil Science Society of America, USA. pp. 379-438.

Skinner, H.C.W. and Fitzpatrick, R.W. (1992) Iron and manganese biomineralisation. pp. 1-6. ***In:*** H.C.W. Skinner and R.W. Fitzpatrick (eds.) *Biomineralization: Processes of Iron and Manganese – Modern and Ancient Environments*. Catena Verlag.

Snoeyink, V.L. and Jenkins, D. (1980) *Water Chemistry*. John Wiley and Sons Inc., USA.

Spath, A. (1999) Inductively coupled plasma mass spectrometry (ICP-MS). Env. Geochem. MSc. lecture notes.

Standard Methods (1989) *Standard Methods for the Examination of Waste and Wastewater*. 17th Ed., American public Health Association, Washington D.C.

Stumm and Morgan (1981) *Aquatic Chemistry*. John Wiley and Sons Inc., USA.

Taylor, S.W., Lange, C.R. and Lesold, E.A. (1997) Biofouling of contaminated ground-water recovery wells: characterisation of microorganisms. *Ground Water*, **35**, no. 6, pp. 973-980.

Tuhela, L., Carlson, L. and Tuovinen, O.H. (1992) Ferrihydrite in water wells and bacterial enrichment cultures. *Water Research*, **26**, no. 9, pp. 1159-1162.

Tuhela, L., Smith, S.A. and Tuovinen, O.H. (1993) Microbiological analysis of iron-related biofouling in water wells and a flow-cell apparatus for field and laboratory investigations. *Ground Water*, **31**, no. 6, pp. 982-988.

Van Beek, C.G.E.M. (1984) Restoring well yield in the Netherlands. *Journal of the American Waste Water Association*, October 1994, pp. 66-72.

Vuorinen, A., Carlson, L., Seppänen, H. and Hatva, T. (1988) Chemical, mineralogical and microbiological factors affecting the precipitation of Fe and Mn from groundwater. *Water Science and Technology*, **20**, no. 3, pp. 249.

Vuorinen, A., Lahermo, P. and Hatva, T. (1988) The effect of fluorine on the precipitation of hydrous iron oxides from groundwater using re-infiltration. *Water Science and Technology*, **20**, no. 3, pp. 247.

Weisner, M.R., Grant, M.C. and Hutchins, S.R. (1996) Reduced permeability in groundwater remediation systems: role of mobilized colloids and injected chemicals. *Environmental Science and Technology*, **30**, iss. 11, pp. 3184-3191.

APPENDIX A

Analytical methods used for water samples

A. 1 Introduction

Two samples were taken at each of the sites, one was a 1 L sample which was not filtered and not preserved other than by refrigeration. The second sample was 100 mL and was filtered at the site and preserved with 2 mL conc. HCl per 100 mL bottle. The acid was added to the sample in the bottle and was done in order to preserve the metals in solution. HCl was used as this is specified in Standard Methods (1989) as the preservation technique for ferrous iron and is less oxidising than HNO_3 which is the commonly used acid for preservation. The sample bottles were all acid washed with conc. HCl and soaked in distilled water overnight. The bottles were then rinsed three times with distilled water and left to dry prior to sampling.

Field filtering of the samples was done using a vessel with a hand pump. A 0.45 μm filter pore size was used to remove silt, clay, bacteria and iron and manganese oxyhydroxides as recommended by Weaver (1992). It was recognised that this pore size may not remove all colloidal material from the sample and that what is then operationally defined as dissolved may in fact not be entirely correct. Laboratory filtering was done using a syringe and filter casing with a 0.45 μm pore size Millipore® filter.

In this thesis, the term filtered refers to filtering, in the field or laboratory, through a 0.45 μm pore size filter unless otherwise specified.

A. 2 Electrical conductivity (EC)

Field measurements of EC were determined using a Corning sensor with a range of 0-199.9 mS/m with varying resolutions as listed in Table A-1. A two point calibration was performed each day (in free air = 0.00 mS/m and with a 141.3 mS/m standard). The meter shows a temperature compensated reading and displays the temperature of the sample, which was recorded. The temperature range of the probe is –0.5 °C to 100 °C with a resolution of 0.1 °C A third party collected one of the samples and the EC reading was determined in the laboratory for this sample.

Table A–1. Resolution of Corning EC sensor for various EC ranges

Range	Resolution
0 – 1.999 mS/m	0.01μS
2.0 – 19.99 mS/m	0.1μS
20.0 – 199.9 mS/m	1μS
200 – 1999 mS/m	0.01mS

EC was measured for all samples in the laboratory using a CRISON microCM 2201 conductivity meter, three days after collection. The meter comprises a conductivity cell (cell constant: C = 1.02 cm^{-1}) and a temperature probe. The temperature probe provides for

automatic temperature compensation to 25 °C. An electrical conductivity standard (143.3 mS/m at 25 °C) was measured prior to analysis at room temperature (16 °C). Sample repeats of the EC were performed and the results used for the dilutions for ion chromatography. A RSD of 5% is considered to show good repeatability. For the purposes of this study 10% was considered to show relatively good repeatability. All the samples in Table A–2 show good repeatability for the laboratory EC values except for sample 5. The low salinity of sample 5 is the cause of the high deviation.

Table A–2. EC field and laboratory (29/8/99) data in mS/m

Sample no.	Reading 1	Reading 2	Average	% RSD	Field EC
1	53.0	63.5	58.3	9	55.6
2	278	326	302	8	—
3	39.7	47.0	43.4	8	30.2
4	43.8	49.1	46.5	6	41.8
5	9.3	12.2	10.7	13	9.40
6	32.5	32.8	32.7	0.5	32.7
7	23.0	24.8	23.9	4	17.0
8	56.4	58.7	57.6	2	56.7
9	46.4	48.5	47.5	2	49.3

(RSD – relative standard deviation)

A. 3 pH measurements

Field measurements of pH were determined using a Corning pH sensor with a range of 0-14 pH and a resolution of 0.01 pH. A two point calibration was performed each day (pH 7 buffer and pH 4 buffer). A third party collected one of the samples and the pH reading was done in the laboratory.

pH for all samples was measured in the laboratory using a Metrohm 691 combined electrode pH meter, consisting of indicator and reference electrodes, three days after collection. Calibration of the pH electrode was done prior to measurement using pH 4.00 and pH 7.00 buffer solutions. Analysis and calibration were done at room temperature (16 °C). Table A-3 shows that there is good repeatability of the laboratory data.

Table A–3. pH field and laboratory (29/8/99) data

Sample no.	Reading 1	Reading 2	Average	% RSD	Field pH
1	5.47	5.23	5.35	2.24	5.21
2	6.25	6.15	6.20	0.81	—
3	5.90	5.81	5.86	0.77	6.04
4	3.94	3.95	3.95	0.13	5.71
5	6.26	6.07	6.17	1.54	6.18
6	5.97	6.01	5.99	0.33	5.59
7	5.45	5.51	5.48	0.55	5.35
8	3.53	3.52	3.53	0.14	3.13
9	6.03	6.19	6.11	1.31	5.73

(RSD – relative standard deviation)

A. 4 Sodium adsorption ratio (SAR)

SAR is the ratio of the concentration of sodium (Na^+) and competing exchange cations (Ca^{2+}, Mg^{2+} and K^+) in solution. The K^+ ion rarely occupies a significant fraction on the exchange sites and is thus not considered in the equation (McBride, 1994). The SAR was determined for each sample using the IC analyses and the formula

$$SAR = \frac{[Na^+]}{\sqrt{([Ca^{2+}] + [Mg^{2+}]) / 2}}$$

Where all solution concentrations are expressed in units of millimoles (milliequivalents) per litre according to McBride (1994).

A. 5 Alkalinity measurements

The alkalinity of water is its acid-neutralising capacity (Standard Methods, 2320 pg. 2-25). This was determined by potentiometric titration to a Bromcresol green endpoint of pH 4.5 using a Radiometer ABU80 auto burette and TTT85 titrator. The procedure involved the determining the volume of 0.01*M* HCl required to titrate 10 mL of sample to the preselected endpoint. Titrations were carried out using 10 mL of filtered, unacidified sample. The result was then computed using the following formula to determine the alkalinity expressed as mmoles/L:

$$\text{Total Alkalinity (in mmoles}_c\text{/L)} = \frac{\text{mL of HCl x normality of acid x 1000}}{\text{mL sample}}$$

HCO_3^- is the dominant carbonate species in the pH range 6.4 – 10.33 (Drever, 1997). All the samples except for sample 8 were below 6.4, which would mean that the dominant species would be H_2CO_3. This species has no charge and would thus not be involved in the alkalinity titration reaction.

A. 6 Redox potential

An attempt was made to measure DO in the field as an indicator of the redox potential of the waters. However, the probe membrane was not functional after the first reading was taken and thus no further readings were done. Calculation of the p*e* was modelled using the redox pair Fe^{2+}/Fe^{3+} in the Aquachem package.

A. 7 Acidity measurements

In samples containing only carbon dioxide-bicarbonates-carbonates, titration to pH 8.3 at 25 °C corresponds to stoichiometric neutralisation of carbonic acid to bicarbonate (Standard Methods, 1989). The value obtained is for total acidity. Acidity titrations were performed using 0.01 *M* NaOH and 10 mL of sample. Acidity titrations were performed on the samples whose pH was below 4 (as measured in the laboratory) and a repeat was performed on each sample and a blank. The blank was 10 mL of ultrapure water.

$$\text{Acidity (mmoles}_c\text{/L)} = \frac{\text{(ml NaOH titrant used x normality of NaOH) x 1000}}{\text{ml sample}}$$

A. 8 Dissolved Organic Carbon (DOC) concentrations

100 mL unfiltered and unacidified samples were submitted to the analytical services laboratory of the CSIR in Stellenbosch for analysis.

A. 8.1 Principle

An automated Persulphate-Ultraviolet Oxidation Method was used for the determination of DOC (pers. comm. M. Louw). The method is applicable to the determination of DOC over the range 0.1 to 20.0 mg/L as C with a detection limit of 1 mg/L. Organic carbon is oxidised to carbon dioxide by persulphate in the presence of ultraviolet light. The CO_2 produced then diffuses across a gas permeable membrane and is measured by the decrease in absorbance of a phenolphthalein solution. Inorganic carbon is removed by acidifying the sample to pH 2 or less to convert the inorganic species to CO_2, and then purging the sample with a purified gas (N_2) to strip off the CO_2.

A. 8.2 Results

A standard curve is produced and the absorbance values are converted to a DOC value in mg/L.

A. 9 Major cation and anion concentrations

Cation and anion concentrations in the water samples were determined by high performance ion chromatography (HPIC) using a Dionex ion chromatograph in the Department of Geological Sciences at the University of Cape Town. Filtered and unacidified samples were diluted with distilled water to obtain EC values below 100 µS/cm. Samples were then passed through a Dionex onguard–P filter prior to analysis, which contains a polyvinylpyrrolidone (PVP) polymer designed to remove the phenolic fraction of humic acids, tannic acids, lignins, anthocyanins and azo dyes. Anions are separated on a HPIC–AS4A anion exchange column with an eluant comprising 1.8 mM Na_2CO_3 and 1.7 mM $NaHCO_3$ and cations are separated on a HPIC–CS12A cation exchange column using a 22 mM methanesulfonic acid eluant. HPIC determines the concentration of uncomplexed, freely available ions in solution and thus ion pairs can interfere with the determination of the ions present.

In order to check the quality of the analytical data the ionic charge balance for each sample was calculated according to Murray and Wade (1996).

$$\text{Ionic Balance} = \frac{\text{Sum of Cations} - \text{Sum of Anions}}{\text{Sum of Cations} + \text{Sum of Anions}} \times 100$$

For the calculation the equivalent weight of the ions is used where:

Equivalent Weight = Atomic Weight / Valence (as meq/L)

Solutions are electrically neutral, as the charge attributable with the anions is equivalent to the charge attributable to the cations. If the charges do not balance then there is a problem with the analysis or an ion has not been accounted for. All but one of the samples has an excess of cations and sample 5 has the greatest charge imbalance. The imbalance in sample 5 is due to the low ionic strength and exaggerated percentage differences are the result of slight

differences in ion concentrations. The charge balances are generally acceptable for the samples.

Table A–4. Charge balance for all samples

Sample number	1	2	3	4	5	6	7	8	9
Element (mmol$_c$/L)									
Li^+	0.00	0.00	0.00	0.00	0.00	0.01	0.00	0.00	0.01
Na^+	3.39	16.61	1.27	2.06	0.52	0.97	0.90	0.99	1.92
NH_4^+	0.00	0.00	0.00	0.00	0.00	0.00	0.00	0.02	0.03
K^+	0.05	0.19	0.10	0.07	0.02	0.18	0.04	0.10	0.38
Mg^{2+}	0.74	5.00	0.50	0.73	0.17	0.33	0.30	1.08	0.93
Ca^{2+}	0.47	3.62	0.26	0.48	0.26	0.85	0.27	1.14	1.37
Fe^{2+}	0.09	1.47	0.47	0.41	0.00	0.03	0.31	0.52	0.12
Fe^{3+}	0.02	0.17	0.06	0.13	0.00	0.01	0.17	0.04	0.01
Al^{3+}	0.00	0.00	0.01	0.03	0.00	0.00	0.00	0.56	0.02
Total cations	*4.76*	*27.05*	*2.66*	*3.91*	*0.96*	*2.37*	*1.98*	*4.45*	*4.79*
F^-	0.00	0.00	0.00	0.35	0.00	0.00	0.00	0.03	0.00
Cl^-	3.63	18.88	1.73	2.62	0.55	1.40	1.31	0.75	2.63
NO_2^-	0.00	0.00	0.00	0.00	0.00	0.00	0.00	0.00	0.00
Br^-	0.00	0.00	0.00	0.00	0.00	0.00	0.00	0.00	0.00
NO_3^-	0.01	0.00	0.00	0.00	0.01	0.00	0.00	0.00	0.00
PO_4^{3-}	0.00	0.00	0.00	0.00	0.00	0.00	0.00	0.00	0.00
SO_4^{2-}	0.41	2.49	0.13	0.18	0.06	0.35	0.21	4.36	0.56
Alkalinity	0.09	1.02	0.46	0.00	0.11	0.53	0.27	0.00	0.75
Total anions	*4.14*	*22.39*	*2.33*	*3.15*	*0.73*	*2.28*	*1.79*	*5.13*	*3.94*
Total cations - Total anions	0.62	4.66	0.34	0.76	0.23	0.10	0.19	-0.68	0.85
Total ions	8.90	49.44	4.99	7.06	1.69	4.65	3.77	9.59	8.73
Cation excess (expressed as %)	**7.02**	**9.42**	**6.72**	**10.80**	**13.47**	**2.11**	**4.96**	**-7.11**	**9.69**

A. 10 Trace element concentrations

The concentrations of the trace metals in the water samples were determined using an ELAN 6000 Inductively Coupled Plasma – Mass Spectrometer (ICP-MS). Field filtered and acidified samples were diluted by a 1:1 ratio of sample to 2% HNO_3 to a total volume of 15 mL. An internal standard of 50 µl of 3 ppm Rhodium was then added to the sample. This is to correct for drift and for calibration purposes. Samples were shaken to ensure proper mixing prior to analysis. With every set of samples analysed, a standard (with certified concentrations of ions) and a blank (pure HNO_3) are analysed. In ion chromatography the lower detection limit for most ionic species is in the ppb. (µg/L) range (Lanyon, 1996) and the percentage error on the data for a semi-quantitative scan is approximately 20% (pers. comm. A. Spath).

ICP-MS determines the total concentration of ions in solution thus any colloidal material left in solution will be ionised and contribute to the concentration determined. As previously stated in section A. 1, an operational definition of dissolved was chosen and colloidal matter smaller than 0.45 µm may affect the results obtained.

A. 11 Silica concentrations

Silica concentrations were determined by quantitative ICP-MS. For quantitative ICP-MS standards of known concentration are made and a calibration curve is constructed. The samples were prepared for analysis as described in section A.9. For some of the samples the dilution factor was increased from 10 to 100 times.

A. 12 Aluminium concentrations

Quantitative ICP-MS and ICP-AES determined aluminium concentrations for all samples and the blank (10). For quantitative ICP-MS standards of known concentration are made and a calibration curve is set up. The samples were prepared for analysis as described in section A.9. For some of the samples the dilution factor was increased from 10 to 100 times. The Namakwa Sands laboratory, Saldahna Bay, performed the ICP-AES analyses. 20 mL of each sample was submitted for analysis. The analysis was performed as an analytical check on the results obtained by quantitative ICP-MS. From the comparison of the data in Table A-5 a good consistency between the two sets of results can be noted and thus the ICP-MS results are acceptable.

Table A–5. ICP-MS and ICP-AES Al data

Sample no.	ICP-AES	ICP-MS
1	<0.1	0.07
2	<0.1	0.01
3	0.11	0.10
4	0.31	0.29
5	<0.1	0.07
6	<0.1	0.02
7	<0.1	0.01
8	3.1	2.55
9	0.14	0.13
10	<0.1	0.05

A. 13 Iron concentrations

Total and ferrous iron (and ferric iron by difference) was determined by the 3500-Fe D-phenanthroline method as described in Standard Methods. Dissolved iron is defined as that passing through a 0.45 μm filter but colloidal iron may be included (Standard Methods, 1989). Sample that was field filtered and acidified was reduced to ferrous iron using 1 mL concentrated (conc.) HCl and 0.5 mL hydroxylamine HCl by boiling. Ammonium acetate (5 mL) and 2 mL phenanthroline were then added and the absorbance was read in the Sequoia-Turner model 340 (1 cm pathlength) at a wavelength of 510 ηm after 10-15 minutes of colour development. Standards of known concentration were prepared and measured in the same way and a calibration curve was produced. The concentration was then converted to mg Fe/L by the following formula:

$$\text{mg Fe/L} = \frac{\mu\text{g Fe}}{\text{mL sample}}$$

This gives the total dissolved iron concentration in the sample. Ferrous iron was determined by adding 10 mL phenanthroline and 5 mL ammonium acetate to a portion of the field filtered and acidified sample. The concentration in mg/L was calculated using the formula above. The ferric iron concentration was calculated by difference. The lower limit of detection for this method is 0.01 mg/L.

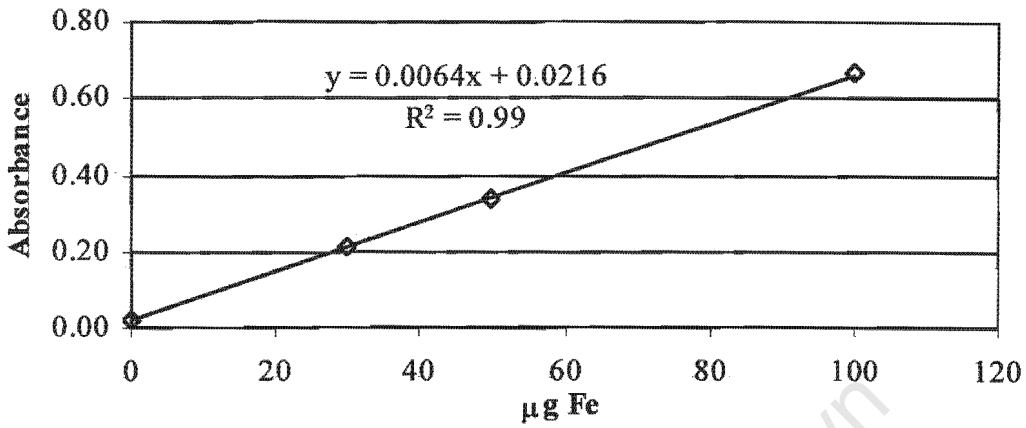

Figure A–1. Calibration curve for iron determination

Samples were also submitted to the Namakwa Sands laboratory for ICP-AES analysis to check the values obtained for total iron concentration as determined by colourimetry. The results from both analytical techniques are tabulated in Table A-7 below. From Table A-6 it can be noted that the two different methods for the total iron concentrations give comparable results.

Table A–6. Colorimetric and ICP-AES data for iron

Sample no.	ICP-AES	Colorimetry
1	3.2	2.9
2	46.6	44.2
3	15.3	14.1
4	12.8	14.0
5	0.11	bdl
6	0.58	1.0
7	14.5	11.7
8	8.3	15.4
9	1.8	3.5
10	<0.1	bdl

Bdl – below detection limit

A. 14 Manganese concentrations

Manganese concentrations were determined by quantitative ICP-MS. The samples were prepared for analysis as described in section A.9. For some of the samples the dilution factor was increased from 10 to 100 times.

A. 15 Zinc concentrations

Zinc concentrations were determined by quantitative ICP-MS. The samples were prepared for analysis as described in section A.9.

A. 16 Phosphorus concentrations

Ortho-phosphate concentration of the sample was determined according to the Ascorbic Acid Method 4500-P E in Standard Methods. Acid-washed glassware was used to prevent phosphate contamination of the samples.

A. 16.1 Principle

Ammonium molybdate and potassium antimonyl tartrate was added to the sample. The two reagents complex with orthophosphate, in an acid medium, to form a heteropoly acid that is reduced with ascorbic acid to produce a molybdenum blue colour in solution. Red light passing through the solution is absorbed depending on the concentration of phosphate present.

8.0 ml of combined reagent, 50 mL 5 N H_2SO_4; 5 mL K antimonyl tartrate solution; 15 mL ammonium molybdate solution; 30 mL ascorbic acid solution, was added to 50 ml of sample. After 10 min. the absorbance was measured at 880 ηm with a reagent blank as the reference solution (Standard Methods, 1989). A calibration curve was prepared using six standards treated in the same way as the samples. The minimum detectable concentration is ~10 µg P/L and with a lightpath of 1.0 cm the approximate P concentration range is 0.15-1.30 mg/L (Standard Methods, 1989).

A. 16.2 Results

A Sequoia-Turner model 340 Spectrophotometer with a lightpath of 1 cm was used to measure absorbance, at a wavelength of 880 ηm, of the standards and samples. The ortho-phosphate concentrations were calculated using the formula from the calibration curve.

This formula was determined by plotting the concentrations of the standards against their absorbance values. The concentration values obtained were inputted into the formula below to obtain the concentration in mg/L.

$$\text{mg P/L} = \frac{\text{µg P}}{\text{mL sample}}$$

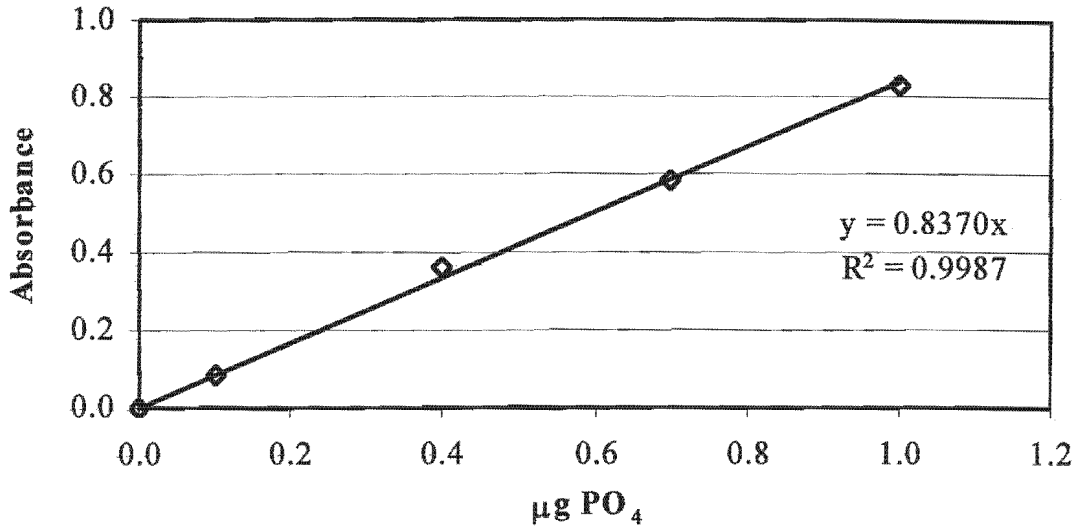

Figure A–2. Calibration curve for ortho-phosphate determinations

A. 17 Water quality guidelines

In Table 4.5, the livestock watering guidelines are those that apply to ruminants and the irrigation guidelines are applicable to Class 1 waters. Class 1 water is defined as " water that can be used for even the most sensitive crops and soils without any reduction in yield or the need for special management practices" (DWAF, 1993).

Table A–7. Water quality guidelines for domestic, irrigation and livestock water.

Constituent	Domestic Use mg/L[1]	Irrigation mg/L[1]	Livestock mg/L[1]
pH	6.0 - 9.0	6.5 - 8.4	ns
EC (mS/m)	<70	<40	<154
SAR ($mmol/L^{0.5}$)	ns	<1.5	ns
Major Anions (mg/L)			
F^-	<1.0	<20	<6
Cl^-	<200	<105	<3000
Br^-	ns	ns	ns
NO_3^-+NO_2^- as N	<10	<5.0	<10
PO_4^{3-}	ns	ns	ns
SO_4^{2-}	<400	ns	<1000
Major cations (mg/L)			
Na^+	<200	<70	<2000
K^+	<50	ns	ns
Mg^{2+}	<70	ns	<500
Ca^{2+}	<80	ns	<1000

Table A-7 continued...

Trace elements (mg/L)			
Al	<0.15	<5.0	<5.0
As	<0.05	<0.1	<0.5
B	ns	<0.2	<5.0
Be	ns	<0.1	ns
Cd	<0.005	<0.01	<0.01
Co	ns	<0.05	<1.0
Cr	<0.05	<0.1	<1.0
Cu	<1.3	<0.2	<5.0
Fe	<1.0	<5.0	<10
Hg	<0.005	ns	<0.002
Li	ns	<2.5	ns
Mn	<0.4	<0.2	<10
Mo	ns	<0.01	<0.01
Ni	ns	<0.2	<1.0
Pb	ns	<0.2	<0.1
Se	<0.02	<0.02	<0.05
U	ns	<0.01	ns
Zn	<10	<1.0	<20

ns = not specified

[1] from Department of Water Affairs and Forestry (1995)

Livestock as applied to cattle and irrigation as applied to class 1 water (DWAF, 1993, Vol. 4). Domestic use DWAF (1999), Vol. 1.

APPENDIX B

Analytical methods used for precipitate samples

B. 1 Introduction

Samples of precipitate were collected from either the clogged pipes found on the surface or from the wells (i.e. fresh), where possible. A sample was not obtained from 5, as there is no precipitation occurring in this well and from well 9, as there was no precipitate available at the time of sampling. Well 9 had been previously sampled as this sample was used for the analysis. Table B-1 lists how many samples were taken from each well.

Table B–1. Precipitate samples

Well number	No. of precipitate samples
1	2 (1A and 1B)
2	2 (2A and 2B)
3	1
4	1
5	0
6	1
7	3 (7A, 7B and 7C)
8	1
9	0

Fresh samples were stored in water from the well and dry precipitates were stored in airtight bottles. Samples were kept in the bottles until required for analysis.

B. 2 XRFS major and trace element concentrations

A portion of precipitate was dried at 110 °C overnight and then crushed in a Seibtechnik carbon-steel swing mill. Some of the samples, 4; 7A; 7B, 7C and 9, were ground down in an agate mortar as there was not enough sample to go in the swing mill.

A portion of sample was then pressed under 10 t pressure into pellet with a Boric acid prepressed backing. Mixing 4-6 g of precipitate with 6 drops of 4% moviol solution to form a powder briquette. The boric acid was AR-grade and the moviol is a polyvinyl alcohol. The briquettes were placed in a desiccator until the analysis was done. Three scans were done on each sample using three different crystals (LiF200, PET and PX1) to obtain readings from U through to Sc.

Fusion disks were prepared by accurately weighing out 6 g of Sigma AR-grade lithium tetraborate ($Li_2B_4O_7$) X-ray flux, 0.15 g of acid washed silica and 0.55 g of sample. The sample-silica-flux mixture was then heated in the automated Claisse Fluxy using program 7 for 8 mins. Six drops of releasing agent (LiBr at 2.5 g/10 ml) was added in order to ensure release of the fusion disk from the disk mould.

The system is usually under vacuum to prevent intensity loses caused by the absorption of long wavelength X-rays by the air and window materials and detection limits for trace elements lie in the 1 to 10 ppm range under routine operating conditions (Potts, 1987).

The fusion disks and pellets were analysed using a Phillips X'Unique Π PW1480 X-ray fluorescence spectrometer (XRFS) in the department of Geological Sciences at the University of Cape Town, which was calibrated using international standards, blanks and specpure compounds (silica and oxides).

The detection limits calculated by:

$$LLD\ (ppm0 = 6/m * (I_b / T_{total})^{½}$$

Where, m = net peak/concentration, I_b = background count rate under the peak in cps and T_{total} = $T_p + T_b$ where T_p = counting time for peak in seconds and T_b = total counting time for background in seconds. Precision (counting statistics) depends on the concentration of the elements being measured but is generally ≤2 ppm (1σ) for most elements.

Four Spectrosil glass standards were analysed with the samples in order to calculate the background and tube correction factors for Zn, Cu, Ni, Co, Mn, Cr, V, Fe and Ti. Nine internal standards were analysed in conjunction with the samples to allow for the calculation of the interference factors (Cu, Zn, Ti-2%, Ti-4%, Cr, Ni, Fe-10% and Fe-5%).

Table B–2. Table of major element lower limits of detection (LLD)

Element	Sensitivity (kcps/%)	LLD (wt%)
Ni	2.206	4.33
Mn	1.084	13.65
Ti	0.741	22.60
K	4.501	3.13
P	1.040	7.71
Al	0.323	73.91
Na	0.116	167.56
Fe	1.219	18.50
Cr	0.894	7.65
Ca	6.107	4.04
S	0.957	23.76
Si	0.316	51.87
Mg	0.309	101.97

Table B–3. Average lower limits of detection for trace elements (the LLD for each element is individually calculated for each sample)

Element	LLD (ppm)
Zn	2.77
Cu	3.33
Ni	4.56
Co	5.18
Mn	3.19
Cr	3.19
V	3.13
Mo	1.58
Nb	1.50
Zr	1.63
Y	1.81
Sr	1.70
U	3.78
Rb	1.84
Th	3.93
Pb	5.22
Pb	8.05
Br	5.30
Se	4.44
Bi	13.64
As	4.66
Ba	1.72
Sc	0.58

B. 3 XRD mineral analysis

The mineralogy of the precipitates was analysed using Phillips PW3890 diffractometer in the Department of Geological Sciences at the University of Cape Town. A portion of the sample was ground using an agate mortar and pestle and pressed into an aluminium frame that was placed in the spectrometer for analysis. The instrument was set to scan over a 2θ range from 5° to 75°, continuously in 0.05^0 steps of 2.8 sec. duration. Samples are irradiated by means of monochromatic x-rays emitted by a Cu X–ray tube (Cu Kα = 1.542 Å). The diffractometer is operated at an accelerating voltage of 40kv and a beam current of 25mA.

Cornell and Schwertmann (1996) X-ray powder diffractograms for Fe^3 oxides (Figure 7.24. in textbook) were scanned in as an image and then converted to a bitmap. The bitmap was digitised using a digitising package, WinDIG 2.5 © D.Lovy 1994-1996. WinDIG allows the user to define three points in space with X and Y co-ordinates and then assigns XY co-ordinates to each pixel of the bitmap line you choose to digitise. In this case an arbitrary vertical scale was assigned, as there is no vertical scale in the original figure. The data was then exported to excel and plotted on the relevant graphs.

B. 4 SEM mineral analysis

Precipitate samples were vacuum–air–dried in a dessicator overnight and then mounted using a carbon–based glue onto metal stubs. The samples were then returned to the dessicator and were carbon–coated prior to analysis. A Lecia Stereoscan 440 scanning electron microscope (SEM), located in the Electron Microprobe Unit of the Physics Department of the University of Cape Town, was used and was operated at an accelerating voltage of 20kV with the samples maintained under a vacuum of between 10^{-4} and 10^{-6} torr. Energy dispersive spectrometry (EDS) was used to obtain spot semi-quantitative chemical analyses of the precipitate forms and high–resolution morphological images were obtained using a secondary electron detector. The instrument used is housed in the Electron Microprobe Unit of the Physics Department of the University of Cape Town.

B. 5 FTIR mineral analysis

Samples were air–dried and crushed to a fine powder using an agate mortar and pestle. Approximately 2 mg of sample was weighed out and mixed with 200 mg of oven-dried (110 ^{0}C) KBr. The sample–KBr mixture was then ground in an agate mortar and pestle to a fine powder and pressed in a dye under 10 tonnes pressure for 1 min. The discs were then placed in the spectrometer and were analysed form a range of 400 to 4000 cm^{-1} at a step rate of 4 scans per 4.0 cm^{-1}.

Analyses were performed on a Paragon 1000 FT-IR that has a single-beam, purgeable, sample compartment and a maximum OPD resolution of 1 cm^{-1}. The mid-infrared detector is either a DTGS (deuterated triglycine sulphate) or a LITA (lithium tantalate) and the system is operated using a Motorola 68340 integrated processor housed in the Department of Chemistry at the University of Cape Town.

The infrared spectra obtained are a result of the interactions of the iron oxides with electromagnetic radiation in a wavelength range of 1-300 μm (wavenumbers 10000-33 cm^{-1}). The interactions lead to the excitation of vibrations or the rotation of molecules in their ground electronic state. This is associated with stretching of interatomic bonds and bending of the interbond angles. The infrared spectrum is a plot of percent radiation absorbed vs. the frequency of the incident radiation (cm^{-1}). FT-IR gives increased resolution and an improved signal to noise ratio compared to conventional IR spectroscopy (Cornell and Schwertmann, 1996).

B. 6 Transmission electron microscopy (TEM) mineral analysis

Samples 6, 7C, 8 and 9 were viewed by TEM in order to view the microcrystalline structure of the precipitates. The precipitate sample was sprinkled onto a drop of distilled water that allowed all the heavier particles to drop to the bottom leaving the smaller particles on the surface. The surface of the drop was then touched with the carbon coated Cu-grid to pick up all the small particles. The grid was dried on filter paper, under a heat lamp, to remove all the water.

The Cu-grids were analysed using a JEOL Jem-200CX transmission electron microscope using an electron beam current of 200 kV. The sample preparation and analysis was performed in the Electron Microprobe Unit of the Department of Physics at the University of Cape Town.

B. 7 Organic carbon determination

The organic carbon content of the samples was determined using the Walkley-Black method as detailed in SSSSA (1990) (Table B-6). The precipitate was ground in a mortar and pestle and then transferred to an Erlenmeyer flask to which 10 cm^3 potassium dichromate is added. This is followed by sulphuric acid. This digests the soil and an indicator, barium dipheylamine sulphonate, is added. The mixture is then titrated with iron (II) ammonium sulphate until the colour changes to green. The percentage organic carbon is then calculated using the following formula:

$$\text{Organic C \%} = \frac{[mc^3\ Fe(NH_4)_2(SO_4)_2 - cm^3 Fe(NH_4)_2(SO_4)_2\ \text{sample}] \times M \times 0.3 \times f}{\text{precipitate mass (g)}}$$

Where M = concentration of the $Fe(NH_4)_2(SO_4)_2$ in mol dm^{-3}

Table B–4. Organic carbon data

Sample number	% Organic Carbon	Amount of sample used (g)
1A	9.04	0.25
1B	4.40	0.25
2A	1.26	0.25
2B	2.77	0.25
3	0.55	0.50
4	0.98	0.25
6	0.95	0.50
7A	0.50	0.50
7B	0.41	0.50
7C	0.16	0.50
8	1.30	0.50
9	0.53	0.50

APPENDIX C

Geological log and water data from previous studies

C. 1 Summary of historical water data for wells

Table C–1. Historical data for wells 2, 5, 6, 7, 8 and 9

Sample number	**2** [1]	**5** [2,3]	**6** [3]	**7** [2,3]	**8** [2,3]	**9** [2,3]
Well	G40118	VR6	VG2	DG110	DP28	DL17
Date	96	94/98	98	91/98	98/99	90/98
EC (mS/m)	114	9.4	32	21	29	36
pH	6.0	5.9	6.4	5.9	4.6	6.6
Alkalinity as $CaCO_3$	22	4	26	4	5	43
TDS (calc. mg/L)	730	55	206	108	185	261
Total hardness as $CaCO_3$ mg/L	117	10	51	11	31	76
Major elements (mg/L)						
K	6.0	0.3	10	1.3	1.4	15
Na	165	11.5	31.0	21.0	11.5	40.0
Ca	13	1.9	13	3.5	4.2	13
Mg	21	1.8	4.2	3.6	4.3	10
NH_3^- as N	<0.1	<0.04	nd	<0.04	nd	0.025
$NO_3^- + NO_2^-$ as N	<0.1	0.135	<0.1	<0.1	<0.1	<0.1
SO_4^{2-}	30	4.6	26	8.0	84	15
PO_4^{3-}	nd	0.044	nd	0.013	nd	0.05
F^-	nd	0.2	nd	0.2	nd	nd
Cl^-	299	23	60	46	35	89
Fe	9	0.14	0.2	8.4	2.5	5.8
Mn	nd	0.03	3.7	3.3	1.5	0.65
Si	nd	3.6	nd	4.9	nd	nd
DOC	nd	Nd	nd	Nd	nd	2.6

nd = not determined

1 – GCS (1996)

2 – Mulder, M.P. (1995)

3 – Engelbrecht, P. and Jolly, J. (1999)

C. 2 Geological logs of wells 2 (G40118), 7 (DG110) and 9 (DL17)

Well Log: Lithology & Construction

Well Ident	Name
G40118	Production Borehole - Albertinia Project

Drill. Method	Mud rotary and Air Percussion	Drill. Dates	9 February 1996

X	Y	Z	Meas. Pt. Elev.

All measurements are in metres. Hole and casing diameters in mm.

Scales (1: xxx)

Water Level (m bc)	Vertical	Horizontal
0.29		

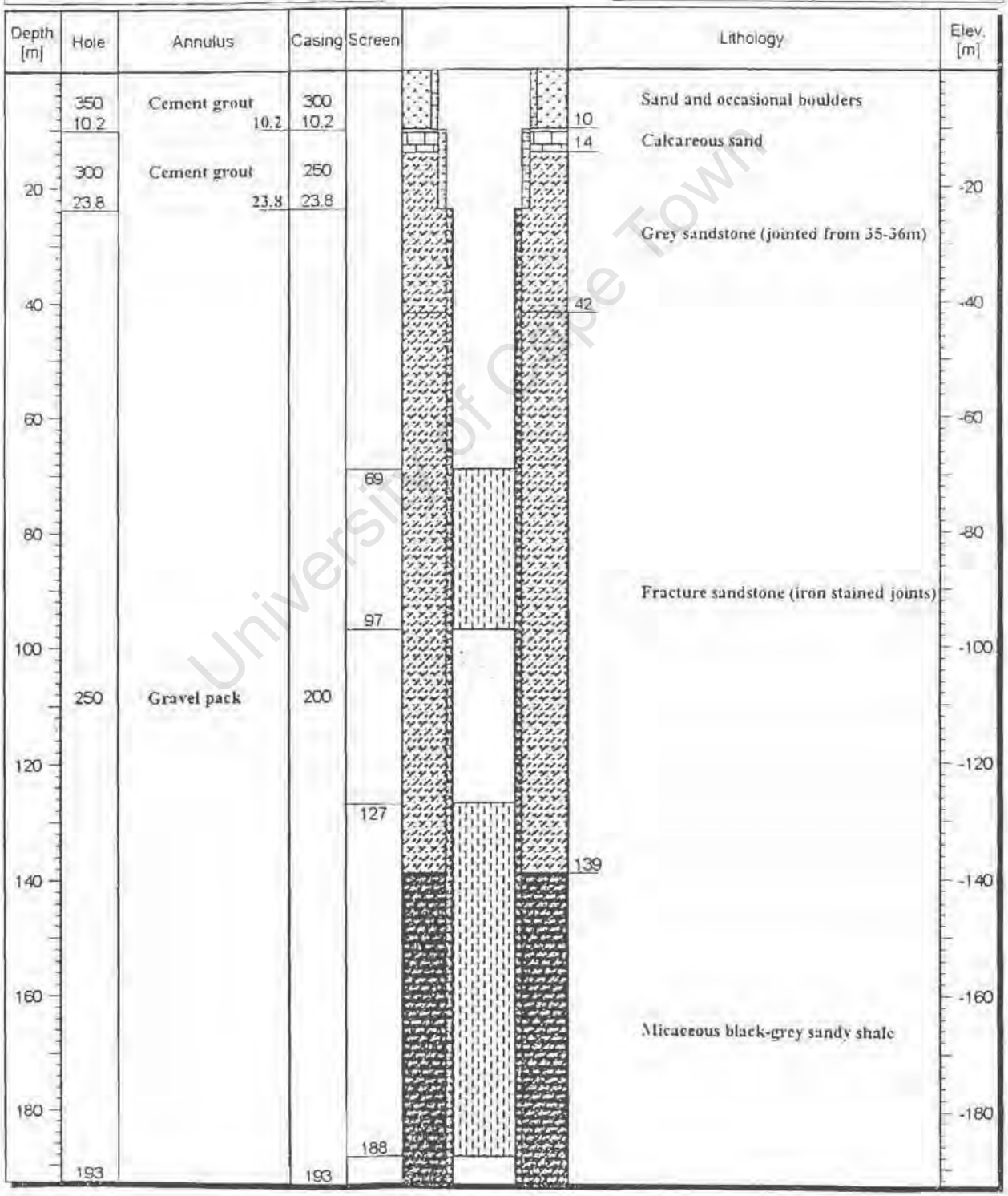

Boorgat Nr DG 110 Status Produksie

Posisie Gebied Oos (Kammanassie)
Plaas Dyselsberg 123
Lokaliteit Droekloof
X 3 715 403,7
Y 49 135,5
h 488,5m

Geboor DWW 02.11.1990
Oorspronklike (blaas)lewering 10 l/s
Hidrologies getoets 02.10.1991 Bedryfspomptoets 26.04.1993, 8,6 l/s
Aanbevole onttrekking (04.1992) 3,5 l/s 300 m³/d
In voltydse bedryf vanaf Sep. 1992
Gem. onttrekking (04.1994) 6,4 l/s 163 m³/d
Gem. onttrekking (11.1994) 2,7 l/s 155 m³/d
Probleme met ysterneerslag

KONSTRUKSIE

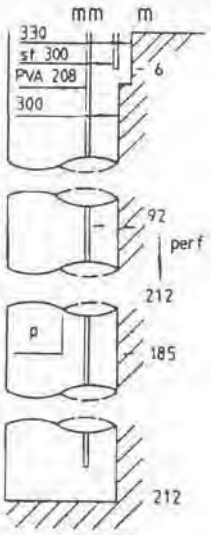

WATER

GEOLOGIE

m		
0-3,5	Kwartsietklippe in sand	
3,5-216	Kwartsiet met enkele skaliebande	Formasie Baviaanskloof Groep Tafelberg
40	Geel klei	
101	Kleierig	
	Genaat met oksidasie (water) 114-117, 137, 200-203	
	Genaat 147, 156	
216-(228)	Soliede kwartsiet	Formasie Skurweberge Groep Tafelberg

perf : Voering is geperforeer
p-185 : Pomp met inlaatdiepte
▽ : Grondwatervlak met diepte en datum
W... : Water invloei met l/s en diepte (s)

LOKALITEITSPLAN
LOCALITY PLAN

Boorgat Nr. DL 17 Status : Produksie

Posisie : Gebied : Wes (Calitzdorp)
Plaas : Daniels Kraal
Lokaliteit
X 3 715 773,1
Y 58 698,3
h 291,7 m

Geboor : Masterbore - Prinsloo 24.09.1989
Oorspronklike (blaas) lewering : 15 l/s
Hidrologies getoets 10.08.90 Bedrytspamptoets 16.05.1994 16 l/s
Aanbevole onttrekking (04.1992) 15 l/s 1300 m^3/d (afhanklik van rehabilitasie)
In (voltydse) bedryf vanaf Feb. 1994 (slegs 1-2 ure per dag a.g.v. ysterneerslag
Gem. onttrekking (04.1994) 11,7 l/s 75 m^3/d
Aanbeveling 05.1994: 8,5 l/s en 300 m^3/d

KONSTRUKSIE

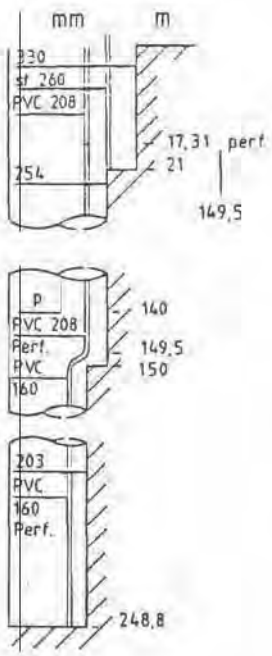

WATER

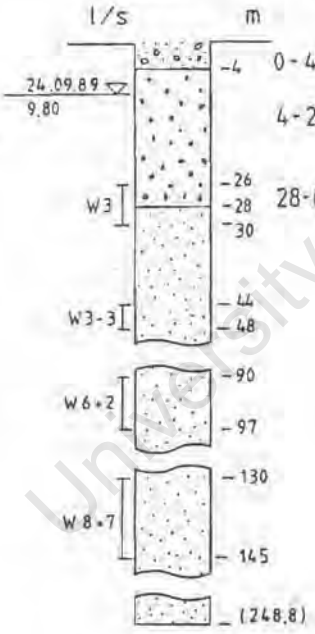

GEOLOGIE

0-4	Kwartsietklippe in sand	
4-28	Sagte verweerde sandsteen	
28-(249)	Kwartsitiese sandsteen Skalie-agtig 70, 128, 150 m naatvlakke 93, 163, 195 en 237 m	Formasie Baviaanskloof Groep Tafelberg

perf. = Voering is geperforeer
p = Pomp met inlaatdiepte
▽ = Grondwatervlak met diepte en datum
W..... = Water invloei l/s met diepte

LOKALITEITSPLAN
LOCALITY PLAN